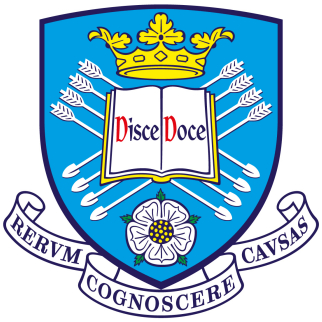

The University Of Sheffield.

Performance Analysis of Indoor Small-Cell Networks with Interior Wall Blockages

Yunbai Wang

Department of Electronic and Electrical Engineering
The University of Sheffield

Supervisor: Prof. Xiaoli Chu
Thesis submitted to the University of Sheffield for the degree of
Doctor of Philosophy

September 2022

To my beloved family.

Declaration

This thesis, submitted in fulfillment of the requirements for the degree of Doctor of Philosophy, is the original work of the author, unless otherwise stated, while enrolled in the School of Electronic & Electrical Engineering at the University of Sheffield. The content presented in this thesis has not been previously submitted for the award of any other academic qualification in any other university or educational institution. All sources and references used in this thesis have been duly acknowledged and cited.

Acknowledgements

I would like to begin by expressing my heartfelt gratitude to my supervisor, Professor Xiaoli Chu, for her unwavering support and guidance throughout my PhD journey. Her expertise, patience, and encouragement have been instrumental in shaping me into an independent and skilled researcher. I am truly fortunate to have had her as my mentor.

I am also deeply grateful to my dear parents, Mr. Zhusheng Wang and Mrs. Runrong Liu, for their constant love and support. Their belief in me and their sacrifices have been a driving force behind my pursuit of higher education and research.

Furthermore, I want to extend my sincere appreciation to my beloved husband, Dr. Yufeng Lai, and my lovely daughter, Miss Yitong Lai. Their unwavering encouragement, understanding, and love have been my pillar of strength during this challenging journey. Especially, my husband, he is the one always encourage and help me to conquer the difficulties in all aspects of my life. His long-term company, encouragement and love give me courage to keep pursuing a better me. I am incredibly blessed to have such a wonderful and supportive family.

Lastly, I would like to thank my colleagues, Dr. Chen Chen and Dr. Hui Zheng, for their valuable technical discussions and camaraderie during my PhD studies. Their insights and feedback have been invaluable in shaping my research and enriching my knowledge.

To all those who have supported and encouraged me along the way, I offer my deepest

gratitude. Your belief in me has been a constant source of motivation, and I am truly grateful for your presence in my life.

Abstract

The performance of indoor small-cell networks (SCNs) is greatly influenced by the indoor environment, particularly the presence of interior walls and blockages. This thesis extensively investigates the impact of interior walls on the downlink coverage probability of an indoor SCN.

To achieve this, the thesis develops a comprehensive distance-dependent indoor channel model that takes into account both line-of-sight (LOS) and non-line-of-sight (NLOS) links, incorporating the effects of interior wall penetration loss. The spatial distribution of interior walls is accurately modelled using the random shape theory, while the distribution of indoor base stations (BSs) is represented by a homogeneous Poisson point process (HPPP). The channel model also includes path loss, Rayleigh fading, and wall attenuation, all of which are crucial factors in indoor SCN performance.

By deriving analytical expressions for the downlink coverage probability under three different user association strategies (UASs), namely the closest LOS BS UAS, the closest NLOS BS UAS, and the smallest path-loss BS UAS, the thesis provides valuable insights into the performance of indoor SCNs in various scenarios. Furthermore, the probability distribution function (PDF) of the distance from a typical user equipment (UE) to its serving BS is derived, enabling the derivation of numerically tractable expressions for the downlink coverage probability while accounting for the effects of interior wall penetration losses.

To validate the analytical results, extensive Monte Carlo simulations are conducted un-

der diverse parameter settings and three typical interior wall layouts: random layout, binary orientation layout, and Manhattan grid. The close agreement between the analytical and simulation results demonstrates the accuracy and reliability of the proposed model in capturing the coverage probability performance of indoor SCNs.

The thesis goes on to explore the impact of various factors, such as BS density, wall density, wall attenuation, and average wall length, on the coverage probability. The results highlight the sensitivity of coverage probability to these factors, providing valuable guidance for network designers and researchers in optimizing indoor SCNs for different deployment scenarios.

In conclusion, this thesis represents a significant contribution to the understanding of how interior walls affect the performance of indoor SCNs. By providing accurate analytical expressions and validating them through simulations, it equips network designers and researchers with powerful tools to analyze and optimize indoor wireless communication systems. The insights gained from this work have the potential to lead to improved coverage and overall performance in practical indoor SCN deployments.

List of Publications

1. Y. Wang, H. Zheng and X. Chu, "Impact of Wall Blockage on LOS User Association Strategy in Indoor Small Cell Networks," 2020 International Symposium on Antennas and Propagation (ISAP), 2021, pp. 579-580, doi: 10.23919/ISAP 47053.2021.9391246.

2. Y. Wang, H. Zheng, C. Chen and X. Chu, "The Effect of Wall Blockages on Indoor Small Cell Networks with LOS/NLOS User Association Strategies," 2021 IEEE 93rd Vehicular Technology Conference (VTC2021-Spring), 2021, pp. 1-6, doi: 10.1109/VTC2021-Spring 51267.2021.9448638.

3. Y. Wang, C. Chen, H. Zheng and X. Chu, "Performance of Indoor Small-Cell Networks under Interior Wall Penetration Losses," in IEEE Internet of Things Journal, vol. 10, no. 12, pp. 10907-10915, 15 June15, 2023, doi: 10.1109/JIOT. 2023. 3241759.

4. Y. Wang, C. Chen and X. Chu, "Performance Analysis for Hybrid mmWave and THz Networks with Downlink and Uplink Decoupled Cell Association," Submitted to the IEEE Transactions on Wireless Communications in July 2023.

Table of Contents

List of Tables

List of Figures

List of Abbreviations

2-D	Two-dimensional
3GPP	the 3rd Generation Partnership Project
5G	Fifth-generation wireless system
AWGN	Additive white Gaussian noise
ASE	Area spectral efficiency
BPP	Binomial point process
BS	Base station
bps	bits per second
CDF	Cumulative distribution function
CCDF	Complementary cumulative distribution function
EE	Energy efficiency
GBSM	Geometry-based stochastic model
HPPP	Homogeneous Possion point process
LOS	Line-of-sight
MIMO	multiple-input multiple-output
mmWave	millimeter-wave
NLOS	Non-line-of-sight
PGFL	Probability generating functional
PDF	Probability distribution function
SCN	Small cell network

SIR	Signal-to-interference ratio
SINR	Signal-to-interference-plus-nois ratio
SNR	Signal-to-noise ratio
UE	User equipment
UAS	User association strategy

List of Symbols

Greek Letters

α	Path loss distance exponent
β	Variable of $\frac{2\lambda L}{\pi}$, cf. (3.11)
Δ	Set of l_k, cf. (3.4)
Γ	HPPP set of wall centres
η_0	Path loss at the reference distance of 1 m
θ	Angle between the i-th link and the horizontal axis
λ	Density of walls
Ξ	Set of ξ_{ik}, cf. (3.4)
ξ	Angle between the wall $\lvert EF \rvert$ and the link YX, cf. Fig. 3.3
ξ_{ik}	Angles between the i-th link and the intersecting k-the wall, cf. (3.3)
ψ_k	Orientation of walls
Φ	HPPP set of the BSs
Φ_{L}	Set of the LOS BSs, cf. (**??**)
Φ_{N}	Set of the NLOS BSs, cf. (**??**)
μ	Density of BSs
ω	Wall attenuation ratio

ω_k	Wall attenuation ratio of the k-th wall intersecting with the ith link, cf. (3.2)

Roman Letters

A	The size of indoor area
C	Round area
$\overline{C}$	Ergodic capacity
C^{L}	distance between the UE and its serving LOS BS
d_i	Distance between the UE and the i-th BS
D	Maximum length of links in the indoor scenario
E_1	Event that there are n BSs in round area $C(O,r)$
E_2	Event that all the BSs are NLOS to the UE in round area $C(O,r)$
E_3	Event that all the BSs are LOS to the UE in round area$C(O,r)$
E_4	Event that the nearest BS located at the distance r has a LOS path to the typical UE
E_5	Event that the UE is associated with a BS at distance d_{LOS_j}
E_6	Event that the nearest BS located at the distance r has a NLOS path to the typical UE
E_7	Event that the UE is associated with a BS at distance d_{NLOS_j}, where $d_{NLOS_j} = r$
$E[K_i]$	the average number of interior walls intersected with the i-th link, cf. (3.4), (3.7) and (3.8)
$f_L(l_k)$	PDF of the length of walls
$f_{\mathrm{L}}(r)$	PDF of event E_4, cf. (5.6)
$\hat{f}_{\mathrm{L}}(r)$	PDF of d_{LOS_j}, cf. (5.10) and (5.11)

$f_{\mathrm{N}}(r)$	PDF of event E_6, cf. (5.12)
$\hat{f}_{\mathrm{N}}(r)$	PDF of d_{NLOS_j}, cf. (5.16)
$\hat{f}^a_{\mathrm{N}}(r)$	PDF of the typical UE connecting to nearest NLOS BS at distance r, where its range is within $(0, r_D]$, cf. (5.17)
$\hat{f}^b_{\mathrm{N}}(r)$	PDF ofthe typical UE connecting to nearest NLOS BS at distance r, where its range is within (r_D, D), cf. (5.18)
$f_{R^{\mathrm{L}}}(r)$	PDF of R^{L}, cf. (3.18)
$f_{R^{\mathrm{N}}}(r)$	PDF of R^{N}, cf. (4.5)
$f_{R^{\mathrm{N}}_s}(r)$	PDF of R^{N}_s, cf. (4.10)
$F_{R^{\mathrm{L}}}(r)$	CDF of R^{L}, equal to $\mathbb{P}[R^{\mathrm{L}} \leq r]$
$F_{\mathrm{L}}(r)$	CDF of event E_4, cf. (5.5)
$F_{R^{\mathrm{N}}}(r)$	CDF of R^{N}, equal to $\mathbb{P}[R^{\mathrm{N}} \leq r]$
$F_{R^{\mathrm{N}}_s}(r)$	CDF of R^{N_s}, equal to $\mathbb{P}[R^{\mathrm{N}}_s \leq r]$
$\overline{F}_{d_{\mathrm{LOS}_j}}(r)$	CDF of C^{L}, cf. (5.9)
$\overline{F}_{d_{\mathrm{NLOS}_j}}(r)$	CDF of C^{N}, cf. (5.15)
h_i	Power gain of Rayleigh fading
I_{L}	Total interference power received by the UE via LOS interference links, cf. (**??**)
I_{N}	Total interference power received by the UE via NLOS interference links, cf. (**??**)
K_i	Number of walls intersecting with the i-th link, cf. (3.3)
l_k	Length of walls
L	Average length of walls
$L(d_i)$	Path losscf. (5.1) and (5.2)
$M(r)$	Variable of $\frac{1-(\beta r+1)e^{-\beta r}}{\beta^2}$, cf. (3.16)
n	The number of BSs
N_0	AWGN power

O	Centre of the round area and location of the typical UE
p_i	Typical UE received power from the i-th BS, cf. (3.1)
p_T	Transmission power of a BS
$P_c(T)$	Downlink coverage probability under the smallest path-loss user association strategy, cf. (5.4)
$P_c^{\mathrm{L}}(T)$	Downlink coverage probability under LOS user association strategy, cf. (3.13)
$P_c^{\mathrm{N}}(T)$	Downlink coverage probability under NLOS user association strategy, cf. (4.2)
$P_{c,s}^{\mathrm{N}}(T)$	Downlink coverage probability under NLOS user association strategy, cf. (4.12)
$\hat{P_c^{\mathrm{L}}}(T)$	LOS serving case, cf. (5.4)
$\hat{P_c^{\mathrm{N}}}(T)$	NLOS serving case, cf. (5.4)
r	Length of the serving link
r_1	The minimum distance between the UE and the NLOS BSs, cf. (5.7)
r_2	The minimum distance r_2 between the UE and the LOS BSs, cf. (5.13)
R^{L}	Length of the serving link between the UE and the closest LOS BS in LOS UAS case, cf. (3.14)
R^{N}	Length of the serving link between the UE and the closest NLOS BS in NLOS UAS case, cf. (4.2)
R_s^{N}	Length of the serving link between the UE and the closest BS in NLOS UAS case under a High Density of Interior Walls, cf. (4.9)
S_i	Interior wall penetration loss caused by blockage walls along the i-th link, cf. (3.2)

SIR_j	SIR of the j-th link, cf. (**??**)
SINR_j	SINR of the j-th link, cf. (4.1) and (**??**)
T	Minimum required SIR threshold
X	The BS, cf. Fig. 3.3
Y	The UE, cf. Fig. 3.3
YX	The i-th link with length d_i, cf. Fig. **??**

Superscripts

L	Type of LOS
N	Type of NLOS

Subscripts

i	Index of the links, $i \in \Phi$
j	Index of the serving link, $j \in \Phi$
k	Index of the walls, $k \in \Gamma$
m	Index of the links, $m \in \Phi_{\mathrm{L}}$
n	Index of the links, $n \in \Phi_{\mathrm{N}}$
s	Notation of the NLOS UAS case under a high density of interior walls

Other Symbols

$\mathbb{E}$	Expectation
$\mathbb{E}[K_i]$	Average number of interior walls intersecting with the i-th link, cf. (3.4)
$EFPQ$	Parallelogram, cf. Fig. 3.3

$\|EF\|$	Wall with the length l, cf. Fig. 3.3
$\|E'F'\|$	Length of the wall $E'F'$, cf. Fig. 3.3
$\|PQ\|$	Wall with the length l, cf. Fig. 3.3
$\mathbb{N}$	Set of natural number.
$\mathbb{P}$	Probability
$\mathbb{P}(E_1)$	Probability of event E_1, cf. (3.15)
$\mathbb{P}(E_2\|E_1)$	Probability of event E_2 conditioned on the event E_1, cf. (3.16)
$\mathbb{P}(E_3\|E_1)$	Probability of event E_3 conditioned on the event E_1, cf. (4.3)
$\mathbb{P}(E_2)$	Probability of event E_2, cf. (3.17)
$\mathbb{P}[E_5\|d_{\mathrm{LOS}_j} = r]$	Probability of event E_5 conditioned on $d_{\mathrm{LOS}_j} = r$, cf. (5.8)
$\mathbb{P}[E_7\|d_{\mathrm{NLOS}_j} = r]$	Probability of event E_7 conditioned on $d_{\mathrm{NLOS}_j} = r$, cf. (5.14)
$\mathbb{P}\{R^{\mathrm{L}} > r\}$	CCDF of R^{L}, cf. (3.17)
$\mathbb{P}\{R^{\mathrm{N}} > r\}$	CCDF of R^{N}, cf. (4.4)
$\mathbb{P}\{R_s^{\mathrm{N}} > r\}$	CCDF of R_s^{N}, cf. (4.9)
$\mathbb{P}[\mathrm{SIR} > T\|R^{\mathrm{L}}]$	Coverage probability conditioned on the shortest LOS link in LOS UAS case, cf. (3.19)
$\mathbb{P}[\mathrm{SINR} > T\|R^{\mathrm{N}}]$	Coverage probability conditioned on the shortest NLOS link in NLOS UAS case, cf. (4.6)
$\mathbb{P}[\mathrm{SINR} > T\|R_s^{\mathrm{N}}]$	Coverage probability conditioned on the shortest NLOS link in NLOS UAS case under a high density of interior walls, cf. (4.11)
$\mathbb{P}[\mathrm{SINR} > T\|d_{\mathrm{LOS}_j}]$	Coverage probability conditioned on the shortest LOS link in the smallest path-loss UAS case, cf. (5.19)

$\mathbb{P}[\text{SINR} > T \mid d_{\text{NLOS}_j}]$	Coverage probability conditioned on the shortest NLOS link in the smallest path-loss UAS case, cf. (5.21) and (5.22)
$\mathbb{R}$	Set of real numbers.
$\mathbb{Z}$	Set of integer numbers.

Chapter 1

Introduction

This chapter provides an introduction to the background and objectives of the research conducted in this thesis. Small cell technology is recognized as a promising solution to meet the growing demand for high-data services in the context of fifth-generation (5G) wireless systems. The main focus of this study is to explore the characteristics of small cell technology through the application of stochastic geometry, which serves as a powerful tool for conducting in-depth analysis of indoor wireless communication.

The chapter begins by discussing the motivation behind this research and the specific objectives that I aim to accomplish. The primary goal is to gain a comprehensive understanding of small cell technology and its implications for indoor wireless communication. By leveraging stochastic geometry, I can analyze the performance and deployment of small cells in indoor scenarios.

Furthermore, the chapter highlights the contributions made by this thesis. These contributions include the development of analytical models, the formulation of mathematical strategies, and the evaluation of network performance metrics. These efforts are aimed at shedding new insights into the practical deployment of indoor small cells and en-

hancing the capacity and efficiency of indoor wireless networks.

Lastly, the chapter provides an overview of the structure of the thesis, outlining the organization of subsequent chapters and how they contribute to addressing the research objectives and fulfilling the research aims.

1.1 Background

Over the past few decades, the widespread use of smartphones and other smart devices has led to a substantial surge in wireless data traffic, particularly in urban and indoor settings. As the demand for high-data services continues to grow, there is a need for specialized technologies to cater to the unique requirements of urban and indoor wireless communication scenarios. In response to these challenges, small-cell networks (SCNs) have emerged as a noteworthy solution.

SCNs involve the deployment of small base stations (BSs) in close proximity to users to improve network capacity and coverage. These small cells are typically deployed in densely populated areas, such as shopping malls, office buildings, and public venues, to enhance network performance and provide better user experiences. Unlike traditional macrocell networks, SCNs offer several advantages, including increased data rates, reduced interference, and improved indoor coverage.

The deployment of SCNs brings about new challenges and considerations, especially in indoor environments where factors like interior walls, blockages, and multipath fading can significantly impact network performance. To address these challenges, researchers and engineers have been working on developing sophisticated channel models and analytical techniques to accurately analyze and optimize the performance of indoor SCNs.

1.1.1 Small-Cell Networks

A small cell refers to a low-power, short-range radio access node that can be controlled by operators and deployed in hotspot areas. The advantages of small cells have been summarized in [6] and include:

- High spatial spectrum reuse: Small cells have a limited coverage range, allowing for the allocation of spatial spectrum in a repetitive manner within a specific area. This leads to efficient spectrum utilization and high spectrum reuse.
- Effective handling of unexpected data traffic: Small cells are capable of handling sudden increases in data traffic. By offloading traffic from macrocell base stations (BSs), small cells help distribute network resources more fairly.
- Improved quality of service: Small cells serve a smaller number of user equipment (UE), enabling them to provide better quality of service to individual UEs. This ensures a more reliable and satisfactory user experience.

With the possession of numerous small cells, the wireless radio backhaul between small-cell BSs and the core network for mobile devices may contribute to data traffic, emphasizing the need to minimize signal load from the core network.

The increasing demands for network traffic have prompted the formation of SCNs consisting of a large number of small cells. SCNs are designed to improve network capacity and reduce energy consumption. In fact, SCNs have been identified as the most promising approach to meet the requirements of 5G cellular networks and future generations of networks, as stated in [7]. The current standardization efforts for 5G technology further emphasize the significance of SCNs, positioning them as the leading force in the evolution of cellular networks in the upcoming era.

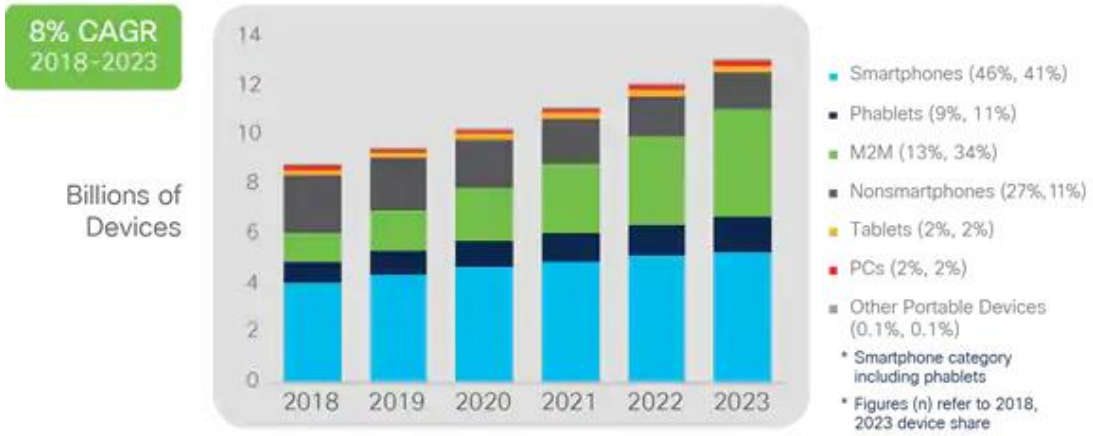

Figure 1.1: Global mobile device and connection growth [1].

1.1.2 Requirements of Wireless Communication for Indoor Scenarios

It is projected that by 2030, mobile traffic requirements will experience an annual data inflation rate of 47%, due to the growing use of mobile phones, tablets, portable laptops, and smart furniture [3], as shown in Figure 1.1. This exponential growth in data consumption is predominantly observed in indoor scenarios, accounting for approximately 80% of the total traffic demand. This trend can be attributed to modern lifestyles characterized by extensive time spent working in offices, shopping in malls, and engaging in domestic activities [4]. Furthermore, as depicted in Figure 1.2, the demand for diversified work styles and entertainments, including augmented and virtual reality technologies, is further stimulating the massive growth in the need for high-quality data services, especially in indoor environments. One crucial solution to this escalating traffic demand is network densification, which can be achieved by increasing the number of small cells.

The capacity of indoor wireless can be tremendously improved through the deployment of small cells with high spatial spectrum reuse, as they can enhance existing networks [5]. In this thesis, my primary objective is to conduct an analytical evaluation of the

Figure 1.2: Significant demand for bandwidth and video in the connected home of the future [1].

coverage performance of indoor SCNs using stochastic geometry. A key aspect of my analysis involves considering the impact of interior walls on network performance. By employing stochastic geometry as a mathematical tool, I aim to gain valuable insights into the practical deployment of indoor small cells and improve my understanding of their coverage capabilities.

1.1.3 Indoor Small-Cell Networks

The demand for data services in indoor environments is rapidly increasing, surpassing the capabilities of traditional outdoor networks and Wi-Fi access points [8]. Moreover, connections from outdoor networks to indoor areas face significant challenges due to the high penetration losses of building walls. To address these issues, indoor SCNs have emerged as a promising solution to cater to the specific demands of indoor mobile traffic.

In recent years, indoor SCNs have been widely deployed in various settings, including residential and enterprise scenarios. However, the deployment of small cells without proper planning and coordination can result in severe inter-cell interference, especially

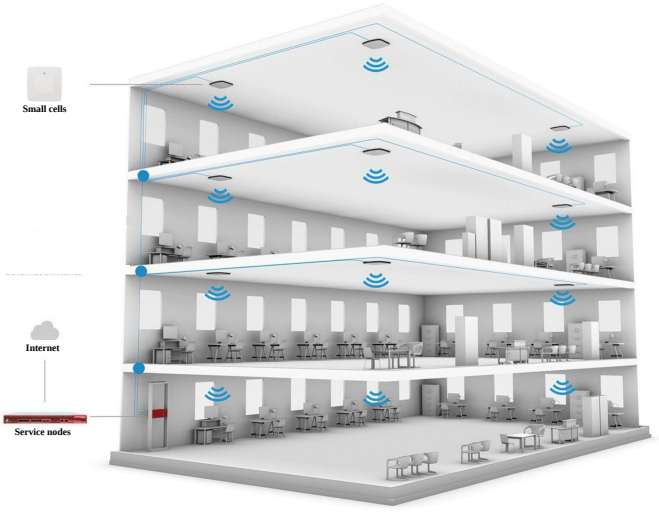

Figure 1.3: An illustration of an indoor small-cell network.

as the number of small cells increases. To overcome this challenge, a more centralized deployment strategy has been introduced. This strategy aims to optimize the performance of the overall network by carefully coordinating the placement and configuration of small cells [9]. Such a centralized approach can effectively mitigate interference issues and ensure better network performance in indoor environments.

In contrast to outdoor SCNs, the performance of indoor SCNs is susceptible to various obstacles and blockages present in indoor environments, including human bodies, building structures, and interior walls. To accurately analyse and evaluate the performance of indoor SCNs, stochastic geometry has emerged as a widely used mathematical tool. Stochastic geometry provides a mathematically tractable approach to modelling the spatial distributions of Base Stations (BS) and blockages within indoor environments.

By employing stochastic geometry, researchers can effectively capture the impact of interior walls and other performance-impacting parameters in indoor SCNs. This approach enables a comprehensive analysis of network performance by considering the distribution and arrangement of BSs, as well as the presence of blockages. With the

ability to incorporate interior walls and other relevant factors, stochastic geometry facilitates a thorough evaluation of the performance of indoor SCNs.

1.2 Motivation and Objectives

As previously mentioned, the emergence of small cells has introduced a mutually complementary aspect to conventional approaches in wireless communication. The architecture of indoor Small Cell Networks (SCNs) has been the subject of extensive study and exploration. However, as the network becomes denser with the deployment of small cells, the structure of the cellular network becomes more complex.

In analyzing the performance of indoor SCNs, it is imperative to consider not only the properties of interferences but also to model parameters that are specific to indoor scenarios. One such crucial parameter is the presence of interior walls. Indoor environments often feature various obstacles, including human bodies, furniture, and building structures. These obstacles, particularly interior walls, significantly impact the propagation of wireless signals and contribute to the overall network performance.

Therefore, when evaluating the performance of indoor SCNs, it is essential to incorporate the effects of interior walls into the analysis. This entails developing models and methodologies that account for the presence of interior walls and their impact on signal propagation, interference, and network performance. By considering these unique parameters and incorporating them into the analysis, a more comprehensive and accurate evaluation of the performance of indoor SCNs can be achieved.

The main challenges addressed in this thesis, considering the aforementioned features of indoor propagation, can be summarized as follows:

- Accurate Analysis of Network Performance: Achieving precise analysis of network performance requires accounting for the complexity of indoor scenarios, including network densification and interior blockages. To address this, a stochastic geometry model based on the line-of-sight (LOS) probability is employed to capture the impacts of these influential factors. This approach allows for a more comprehensive evaluation of network performance metrics.

- Incorporation of Interior Walls in Signal Propagation Models: Previous research on indoor wireless communication has either disregarded the effects of interior walls or focused solely on LOS probabilities of transmission links. To overcome this limitation, it is crucial to differentiate between LOS and non-line-of-sight (NLOS) BS for signal propagation. Additionally, the losses resulting from interior wall penetration need to be incorporated into signal propagation models. By doing so, a more practical mathematical coverage model can be developed to analyse network performance accurately in indoor environments.

- Consideration of User Association Strategies (UAS): In indoor scenarios, with both LOS and NLOS propagation, there are potentially more UAS options to consider for wireless connectivity. Existing UASs, which only consider the nearest BS or the nearest LOS BS as the serving BS, are too simplistic to address the complexities of indoor scenarios adequately. Therefore, it is essential to explore and develop more sophisticated UAS strategies that cater to the specific characteristics of indoor environments.

The main objectives of my research can be summarized as follows:

- Outline the Architecture of Indoor SCNs: The first objective of my research is to provide a comprehensive overview of the architecture of indoor SCNs. This in-

cludes examining the structure, components, and functionalities of indoor SCNs to establish a clear understanding of the design and operation.

- Propose a Path-Loss Model for Signal Propagation: I aim to develop a path-loss model that distinguishes between LOS and NLOS BSs for signal propagation. This model will incorporate the LOS probability to accurately capture the variations in signal strength and coverage in indoor environments.

- Analytically Evaluate the Coverage Performance of Indoor SCNs: Utilizing stochastic geometry, I will conduct analytical evaluations of the coverage performance of indoor SCNs. This analysis will consider the effects of interior walls, which can significantly impact signal propagation and network performance. By incorporating these factors, I aim to provide valuable insights into the practical deployment of indoor small cells.

- Construct Mathematical Coverage Models with Different User Association Strategies: To adapt to the complexities of indoor scenarios, I will develop mathematical coverage models that incorporate various UASs. By considering factors such as proximity, LOS/NLOS differentiation, and other relevant parameters, I aim to optimize network performance and connectivity in indoor environments.

- Create and Validate Analytical Models through Simulations: I will create analytical models based on the proposed path-loss model, coverage models, and UAS strategies. These models will be validated through extensive simulations using appropriate scenarios and network configurations. The simulations will provide empirical evidence of the performance and effectiveness of the proposed models.

By achieving these objectives, my research aims to contribute to the understanding and improvement of indoor SCNs, providing valuable insights into their deployment, performance optimization, and network management.

1.3 Contributions

The major contributions of this thesis can be summarized as follows:

- Incorporation of interior wall penetration losses into a path-loss model that takes into account both Line-of-Sight (LOS) and Non-Line-of-Sight (NLOS) BSs for signal propagation. This also involves formulating a mathematical strategy for assessing network performance, using stochastic geometry under the nearest LOS BS User Association Strategy (UAS). The derived expression for unconditional downlink coverage probability enables the evaluation of network performance metrics. Detailed content can be found in Chapter 3.

- Formulation of a tractable mathematical strategy for assessing network performance based on stochastic geometry under the nearest NLOS BS UAS or the nearest BS in areas with high wall density. This strategy utilizes the path loss model that differentiates LOS and NLOS BSs for signal propagation, as proposed in Chapter 3. To evaluate network performance metrics, expressions for unconditional downlink coverage probability are derived. Detailed content can be found in Chapter 4.

- Proposal of a path-loss model that includes the penetration loss of interior walls, using the model of LOS probability. This is followed by the construction of a tractable mathematical SCN model based on stochastic geometry under the smallest path loss UAS. The derived expression for unconditional downlink coverage probability enables the evaluation of network performance metrics. Detailed content can be found in Chapter 5.

These contributions enhance the understanding and analysis of indoor SCNs by considering the effects of interior walls and optimizing network performance in complex

indoor scenarios. The proposed models and strategies provide valuable insights for the practical deployment and performance optimization of indoor small cells.

1.4 Thesis Outline

The following component parts of this thesis are cogitated along these lines:

Chapter 2: Literature Review

In this chapter, a comprehensive review of the literature related to the research topic is presented. The chapter begins by introducing the fundamental knowledge of SCNs, including cellular network concepts, channel models, evaluation metrics, validation metrics, and the role of stochastic geometry in SCNs. The significance of stochastic geometry as a mathematical tool for modeling and analyzing cellular networks is emphasized.

Furthermore, the chapter explores the development and advancements in the field of SCNs, with a specific focus on stochastic geometry, the LOS probability model, and indoor SCNs. The application of stochastic geometry in SCNs allows for precise and tractable analysis of network performance by capturing the spatial distribution of BSs and obstacles. The LOS probability model plays a crucial role in understanding the characteristics of signal propagation in SCNs.

Overall, this chapter provides a comprehensive overview of the relevant literature, highlighting the key concepts and research advancements in the field of SCNs and stochastic geometry. It serves as a foundation for the subsequent chapters, setting the stage for the research conducted in this thesis.

Chapter 3: The Effect of Interior Wall Penetration Losses on Indoor

Small-Cell Networks under LOS BS User Association Strategy

In this chapter, I delve into the investigation of the impact of interior wall penetration losses on Indoor SCNs under the nearest LOS BS UAS. The chapter begins by proposing a system model for indoor scenarios based on random shape theory, specifically focusing on a two-dimensional (2-D) indoor SCN. To generate the small-cell BSs, a Homogeneous Poisson point process (HPPP) is employed.

Subsequently, a comprehensive path-loss model is developed, taking into account both the blockage and distance factors. This model provides a detailed characterization of the signal propagation in the indoor environment, considering the presence of interior walls and their impact on the transmission. To analyse the network performance, the expressions for downlink coverage probability are derived, incorporating the interior wall penetration loss caused by possible blockage walls. These expressions enable the evaluation of the coverage performance of the considered indoor SCN under the nearest LOS BS UAS.

The analytical results obtained from the derived expressions are validated through Monte Carlo simulations, providing empirical evidence of the model's accuracy and effectiveness. Additionally, various parameter scenarios are examined and discussed, shedding light on the behaviour and performance of the indoor SCN under different conditions. By investigating the effect of interior wall penetration losses and analysing the downlink coverage probability, this chapter provides valuable insights into the performance of indoor SCNs under the LOS BS UAS. The findings contribute to the understanding of network performance in indoor environments and guide the practical deployment of indoor small cells.

Chapter 4: The Effect of Interior Wall Penetration Losses on Indoor Small-Cell Networks under NLOS BS User Association Strategy

In this chapter, I focus on investigating the impact of interior wall penetration losses on Indoor SCNs under the nearest NLOS BS UAS. The system model and path-loss model proposed in Chapter 3 are utilized in this analysis. The chapter begins by introducing the system model, which is based on random shape theory and specifically designed for indoor scenarios. The small-cell BSs are generated using an HPPP.

Building upon the path-loss model developed in Chapter 3, the expressions for downlink coverage probability are derived, considering the nearest NLOS BS UAS. These expressions enable the evaluation of the coverage performance of the indoor SCN, incorporating the effects of interior wall penetration losses. Furthermore, a simplified model for nearest NLOS connectivity under dense interior walls is presented, taking into account the unique characteristics of these scenarios. This model provides a simplified yet effective representation of the network connectivity under such conditions.

To validate the analytical downlink coverage probability of the proposed SCN model, extensive Monte Carlo simulations are conducted. The simulation results serve as empirical evidence and provide a comprehensive understanding of the model's performance. Additionally, the findings from the simulations are discussed, shedding light on the behavior and performance of the indoor SCN under different parameter scenarios.

By examining the effect of interior wall penetration losses and analyzing the downlink coverage probability under the nearest NLOS BS UAS, this chapter enhances my understanding of network performance in indoor SCNs. The validated analytical model and the insights gained from simulations contribute to the practical deployment and optimization of indoor small cells in complex indoor scenarios.

Chapter 5: The Effect of Interior Wall Penetration Losses on Indoor Small-Cell Networks under the Nearest Path-Loss User Association Strategy

In this chapter, I explore the impact of interior wall penetration losses on the downlink coverage probability of an indoor SCN under the nearest path-loss UAS. The system model incorporates interior walls using random shape theory, providing a realistic representation of the indoor environment. The indoor small-cell BSs are distributed following an HPPP. The channel model takes into account various factors, including the distance-dependent indoor path loss, LOS probability, Rayleigh fading, and wall penetration loss. These factors collectively contribute to the characterization of signal propagation in the indoor SCN.

Using the mathematical analysis framework of the SCN model, the expression for coverage probability is derived. This expression enables the assessment of the network performance in terms of downlink coverage. By incorporating the effects of interior wall penetration losses, the derived expression provides valuable insights into the impact of these losses on the downlink coverage probability.

To validate the analytical model and gain further understanding, simulations are conducted. Specifically, the coverage probability of SCNs under three typical interior wall layouts, including random layout, binary orientation, and Manhattan grid, is compared. These simulations provide valuable insights into the effect of interior wall penetration losses on the downlink coverage probability and help evaluate the performance of SCNs in different scenarios.

By investigating the effect of interior wall penetration losses and analyzing the downlink coverage probability, this chapter contributes to my understanding of indoor SCNs. The validated analytical model and simulation results provide valuable guidance for optimizing network performance and deployment strategies in indoor environments with varying interior wall layouts.

Chapter 6: Conclusion and Future Work

In this final chapter, a comprehensive summary of the research conducted in this thesis is presented. The key findings, contributions, and outcomes of the study are summarized, highlighting their significance and implications for the field of indoor SCNs.

The chapter presents the conclusions drawn from the research findings. These conclusions are based on the analysis, evaluation, and validation of the proposed models and strategies. The implications of these conclusions for the practical deployment and optimization of indoor SCNs are discussed.

Furthermore, the chapter outlines plans for future work in this area of study. It identifies potential avenues for further research and development, addressing the limitations and gaps identified during the course of the study. These suggestions for future work aim to extend and enhance the existing knowledge and understanding of indoor SCNs, paving the way for further advancements in this field.

Chapter 2

Literture Review

The research topics addressed in this thesis are reviewed and summarized as follows. Firstly, a comprehensive explanation is provided for the fundamental concepts of wireless networks, channel models, evaluation metrics, validation metrics, and the application of stochastic geometry in the context of SCNs. This section establishes the necessary theoretical foundation for understanding the subsequent research work.

Next, the literature review delves into related research on SCNs, with a specific focus on stochastic geometry, the LOS probability model, and SCNs in indoor scenarios. The review examines existing studies and identifies gaps in the current literature, paving the way for the original contributions of this thesis. By exploring these topics, a deeper understanding of the current state of research is gained and the groundwork for our own investigations is laid.

2.1 Fundamentals of Small-Cell Networks

This section serves as an introduction to the fundamental knowledge of SCNs and stochastic geometry, both of which are central to this thesis. To gain a comprehensive understanding of SCNs and the stochastic geometry method employed in our research, it is essential to familiarize ourselves with the basic characteristics of SCNs and the principles of stochastic geometry.

Therefore, in this section, I cover the fundamental concepts related to wireless networks, including the architecture and operation of SCNs. I also delve into the channel model used for analyzing signal propagation in SCNs. Additionally, I explore the evaluation metrics commonly employed to assess the performance of SCNs and the validation metrics used to verify the accuracy of analytical models.

Furthermore, I provide an overview of how SCNs can be modelled and analysed using the stochastic geometry approach. This mathematical framework enables me to analyse the spatial distributions of BSs and their impact on network performance.

By thoroughly understanding these fundamental concepts, I establish a solid foundation for the subsequent chapters, where I apply and extend this knowledge to address specific research objectives.

2.1.1 Wireless Networks

In the field of communication networks, wireless networks play a crucial role as they provide connectivity without the need for physical cables [10]. With the continuous advancement of wireless communication, various types of wireless networks have been developed to cater to different scenarios and environments. These networks are becom-

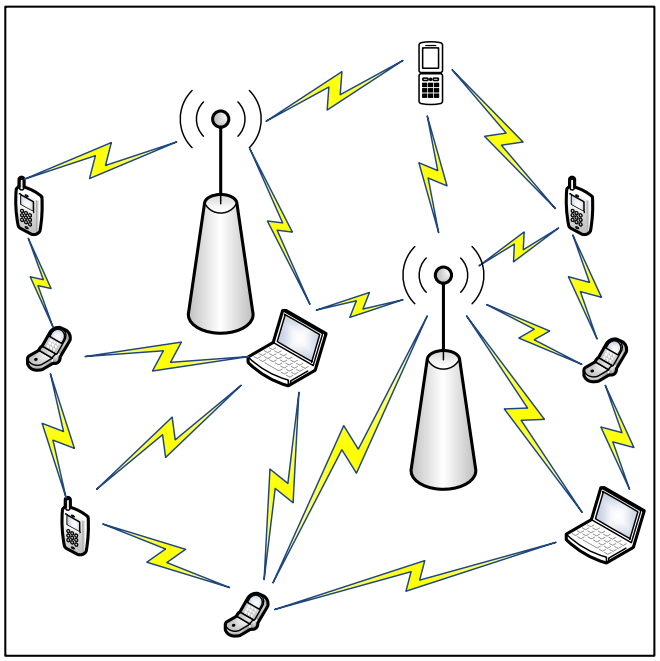

Figure 2.1: An illustration of mobile ad hoc network.

ing increasingly heterogeneous and decentralized, and one of the major challenges they face is interference, which can significantly impact network performance. In this section, we will discuss three trending wireless network types based on stochastic geometry and the Poisson Point Process (PPP): ad hoc networks, SCNs, and heterogeneous networks.

- **Ad hoc networks**: Ad hoc networks are self-organizing networks that operate without relying on a pre-existing infrastructure. Examples include wireless networks with access points and routing in wired networks. In ad hoc networks, each node participates in routing by transmitting data to other nodes. The connectivity of the network and the routing algorithm dynamically select the nodes for data transmission. Ad hoc networks are suitable for scenarios where main nodes are not reliable, such as mobile ad hoc networks for smartphones and vehicular ad hoc networks for vehicles [11]. Ad hoc networks are also advantageous in emergency situations, as they can be intelligently deployed and require minimal

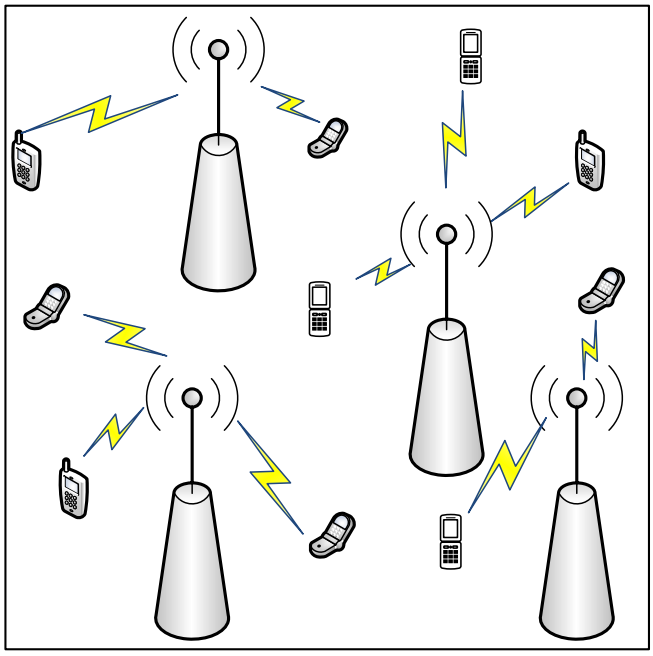

Figure 2.2: An illustration of SCN.

configuration, as shown in Figure 2.1.

- **Small-cell networks**: Small-cell networks consist of small-cell BSs, which are low-power cellular radio access nodes. These networks are designed to provide enhanced capacity and coverage in urban areas. Compared to traditional wireless networks, SCNs offer higher capacity, larger coverage areas, and utilize higher frequency signals, all while consuming less power. These networks are capable of meeting the increasing demands of wireless communication in densely populated areas, as illustrated in Figure 2.2.

- **Heterogeneous networks**: Heterogeneous networks integrate different access technologies, allowing UE to seamlessly switch between services from wireless LANs to SCNs. A typical heterogeneous network combines macrocells and small cells, where macrocells provide umbrella coverage for UEs and small cells act as capacity enhancers and fill coverage gaps, as depicted in Figure 2.3.

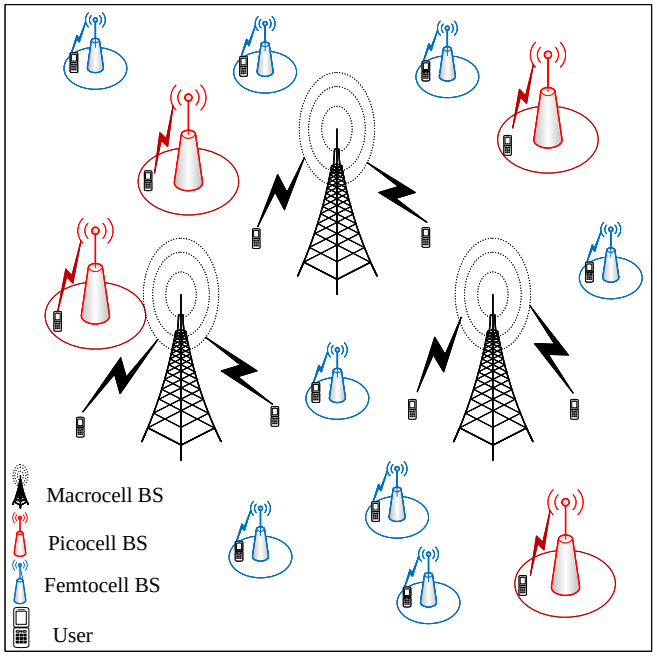

Figure 2.3: An illustration of heterogeneous network.

These three types of wireless networks demonstrate the versatility and adaptability of wireless communication in various scenarios. Understanding the characteristics and capabilities of each network type is essential for designing efficient and robust communication systems.

2.1.2 Channel Model

The channel in wireless communication refers to the distance between the antenna of the transmitter and the antenna of the receiver, the signal propagation of the link path, and the scatterers to the link path. According to the feature of the channel model, it is simple to derive the attributes of the signal propagation between the transmitter and receiver. The channel model can be determined from a mathematical model describing the channel behaviour between the transmitter and the assigned receiver. Generally, a channel model is mainly composed of path loss along the link, shadowing from block-

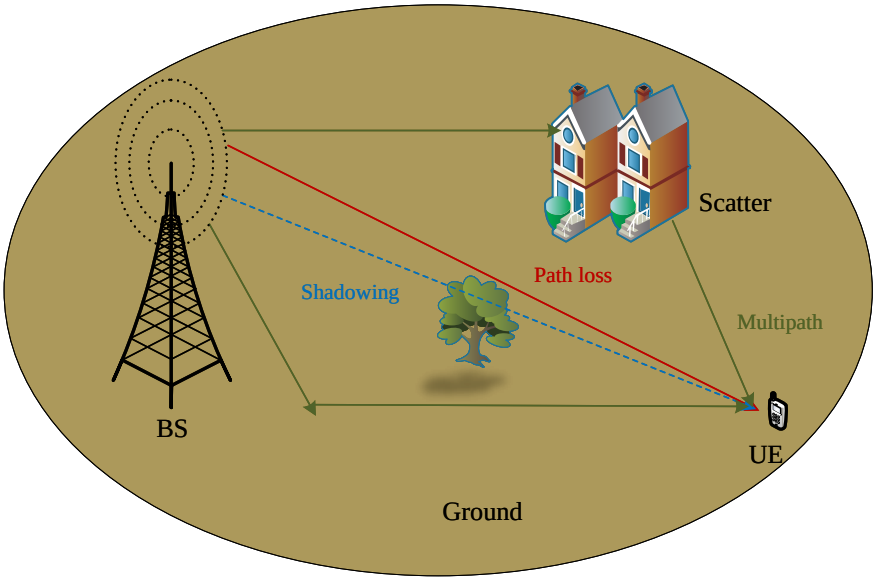

Figure 2.4: Channel model.

age and multipath from scatters, exhibited in Figure 2.4.

- **Path loss**

  Path loss accounts for the attenuation of the signal power as it travels through the channel. It is influenced by factors such as distance, frequency, and environmental conditions. The path loss component of the channel model enables us to estimate the signal strength at different distances from the transmitter.

  The wavelength of the signal is inversely proportional to its frequency. In general, higher frequency signals have shorter wavelengths, while lower frequency signals have longer wavelengths. As the wavelength decreases, the signal is more prone to attenuation and scattering by objects in the environment, resulting in increased path loss.

  The distance between the transmitter and receiver also plays a significant role in path loss. As the distance between the two increases, the signal spreads out over a larger area, leading to a decrease in signal power at the receiver. This phenomenon is known as free-space path loss and follows the inverse square

law, which states that the power of the signal diminishes with the square of the distance.

Therefore, path loss increases as the wavelength of the signal decreases and as the distance between the transmitter and receiver increases. These factors need to be taken into account when designing wireless communication systems to ensure that the signal power at the receiver is sufficient for reliable communication.

- **Shadowing**

  Shadowing refers to the attenuation or loss of signal strength caused by obstacles or blockages in the propagation path of wireless signals. These obstacles can include buildings, trees, terrain features, or other objects that obstruct the direct LOS between the transmitter and the receiver.

  When a signal encounters a blockage, it experiences additional path loss due to the obstruction. This results in a decrease in signal strength at the receiver compared to a scenario with a clear line-of-sight. The amount of shadowing can vary depending on the size, shape, and material properties of the obstructing object.

  Shadowing is typically modeled as a random variable with a log-normal distribution. This statistical model accounts for the variability in signal attenuation caused by different environmental conditions and the randomness of the blockage positions and properties. The log-normal distribution is often used because it provides a good fit to the observed data and captures the statistical characteristics of shadowing.

  By considering shadowing in the channel model, we can account for the impact of obstacles and blockages on the signal propagation in wireless communication systems. This helps in understanding and predicting the signal strength variations and designing robust wireless networks that can handle shadowing effects.

- **Multipath**

  Multipath refers to the phenomenon where the transmitted signal reaches the receiver through multiple paths due to reflections, diffractions, and scattering. It occurs when the signal encounters obstacles or objects in the environment that cause the signal to take different paths before reaching the receiver antenna.

  There are several causes of multipath propagation. One common cause is reflection, where the signal bounces off surfaces such as walls, buildings, or the ground. These reflected signals can take different paths and arrive at the receiver antenna with different delays and angles, resulting in multiple copies of the signal arriving at different phases.

  Diffraction is another cause of multipath propagation, where the signal bends around obstacles or edges, leading to the formation of secondary wavefronts. This can result in additional signal paths and variations in signal strength at the receiver.

  Scattering occurs when the signal encounters small objects, such as trees or vegetation, that scatter the signal in different directions. The scattered signals can interfere with the direct signal path and create additional signal paths with different delays and angles.

  Multipath propagation can cause constructive or destructive interference at the receiver antenna, depending on the phase relationship between the different signal components. This can result in signal fading, fluctuations in signal strength, and distortion of the received signal.

  To mitigate the effects of multipath propagation, various techniques are employed in wireless communication systems, such as equalization, diversity techniques, and antenna design. These techniques aim to combat the fading and distortion caused by multipath propagation and improve the reliability and quality of wire-

less communication.

Overall, multipath propagation is a common phenomenon in wireless communication, and understanding its causes and effects is crucial for designing robust wireless systems that can cope with the challenges posed by multipath propagation.

Figure 2.4 provides a visual representation of these components in the channel model, illustrating the path loss, shadowing, and multipath effects on the signal propagation between the transmitter and receiver.

By incorporating these components into the channel model, we can analyze and predict the signal strength, quality, and reliability of wireless communication systems. This knowledge is crucial for designing and optimizing wireless networks, ensuring efficient and robust communication between transmitters and receivers.

2.1.2.1 Physical Channel Models

The channel model is able to be classified based on the different properties. In physical channel models, the focus is primarily on the propagation of electromagnetic waves, and the antenna configuration has limited influence on these models. Therefore, double-directional multipath propagation occurs between the antennas of the serving transmitters and the assigned receiver [12]. Physical channel models provide a means to characterize the wave propagation parameters in such scenarios.

Physical channel models can exhibit various characteristics, including scattering clusters and time-varying scenes, in more sophisticated models [13]. These models aim to capture the complexities of real-world propagation environments and provide a detailed representation of the wave propagation phenomena.

By analysing and modelling these wave propagation phenomena, physical channel models provide insights into the behaviour of the wireless channel, enabling the evaluation and optimization of wireless communication systems. These models play a crucial role in designing and deploying wireless networks, predicting signal coverage and quality, and optimizing system performance in various environments and scenarios.

Based on their properties, physical channel models can be classified into three main types: deterministic models, geometry-based stochastic models (GBSMs), and non-geometrical stochastic models.

- **Deterministic models**

  In deterministic channel models, there is no randomness involved in predicting future states. These models aim to reproduce the physical propagation parameters in a completely deterministic manner. The parameters are typically obtained by considering factors such as the signal path between the serving transmitters and the assigned receiver, the electromagnetic characteristics of the environment, and geometric features.

  Deterministic models provide a high level of accuracy in predicting the behavior of the channel. However, they often require detailed and precise information about the environment, making them challenging to apply in practical measurements or real-world scenarios.

  One representative example of a deterministic model is ray tracing. Ray tracing involves tracing the path of individual rays as they interact with the environment, including reflections, diffractions, and scattering. By considering the geometric details and material properties of objects in the environment, ray tracing can accurately predict the propagation characteristics of the channel.

  For example, the works in [14] demonstrate the application of deterministic mod-

eling in predicting system capacity. They show that the system capacity decreases significantly with the presence of a single wedge obstruction and improves as more wedges are added to the environment.

While deterministic models offer high accuracy, their practical application is often limited due to the need for detailed environment information and computational complexity. Therefore, they are primarily used in specific scenarios where a precise understanding of the channel is required, such as in designing complex wireless systems or analyzing the performance of specific communication links.

- **Geometry-based stochastic models**

  geometry-based stochastic models (GBSMs) consider the statistical properties of the environment and take into account the random nature of wave interactions with scatterers. In contrast to deterministic models, GBSMs introduce randomness by incorporating a predefined random probability distribution of effective scatterers for wave propagation [15].

  In GBSMs, the propagation environment is characterized by a set of statistical parameters that describe the distribution, correlation, and scattering properties of the scatterers. These parameters are typically obtained from measurements or statistical analysis of real-world environments.

  By incorporating randomness into the model, GBSMs allow for a more realistic representation of the variability and unpredictability of the channel. They capture the statistical variations in signal strength, delay, and other propagation parameters that result from the interaction between the electromagnetic waves and the random distribution of scatterers in the environment.

  One advantage of GBSMs is their ability to capture the spatial and temporal variations of the channel. They can account for the effects of multipath propagation, shadowing, and other phenomena that arise from the random distribution of scat-

terers. GBSMs are widely used in various applications, including system-level simulations, performance analysis, and optimization of wireless communication systems.

It is important to note that while GBSMs introduce randomness into the model, they still rely on predefined probability distributions and statistical parameters. The randomness is constrained within the framework of the model and does not capture all possible real-world variations.

- **Non-geometrical stochastic models**

  In non-geometrical stochastic models, the focus is on the statistical characteristics of the links between serving transmitters and assigned receivers, without explicitly considering the physical environment's geometry. These models rely on statistical data and parameters to capture the statistical behaviour of the channel without incorporating detailed geometric information.

  Non-geometrical stochastic models are typically based on statistical analysis of measured data or simulations that capture the statistical variations of the channel. They aim to characterize the statistical properties of the channel, such as the statistical distribution of signal strength, fading, and other channel parameters.

  While non-geometrical stochastic models provide a simplified approach to capturing statistical channel behaviour, they may not accurately capture the impact of the physical characteristics of the environment. The lack of consideration for the geometric details and physical properties of the channel can lead to limitations in analysing network performance accurately.

  The study in [16] highlights the importance of considering the physical characteristics of the channel when analyzing network performance. The results indicate that non-geometrical stochastic models, which solely rely on statistical data

without considering the physical environment, may not provide an accurate representation of the network's performance.

Therefore, while non-geometrical stochastic models offer a simplified approach to modeling the channel, it is important to consider the limitations and ensure that the models are validated against real-world scenarios or supplemented with additional information to capture the physical characteristics of the environment accurately.

The choice of channel model depends on the specific requirements of the wireless communication system and the available information about the propagation environment. Deterministic models are suitable for detailed analysis but may be computationally demanding, while GBSMs and non-geometrical stochastic models provide a balance between accuracy and complexity.

2.1.3 Evaluation Metrics

Evaluation metric is a crucial step for assessing the performance of SCNs with constructing a tractable metric. Specifically, for the SCNs by utilizing stochastic geometry, the critical ability of the mathematical model is to synthesize a realistic path-loss model which is included the characteristics of BSs for SCNs under variant scenarios. Generally, there are four evaluation metrics which are widely used for the performance analyses of networks: coverage probability, spectral efficiency, area spectral efficiency and ergodic capacity.

- **Coverage probability**

  In wireless communication, the coverage probability is a metric used to assess the ability of a typical UE to achieve a certain threshold of signal quality, such as

signal-to-interference-plus-noise ratio (SINR), signal-to-interference ratio (SIR), or signal-to-noise ratio (SNR). It represents the probability that the UE's signal quality exceeds a predefined threshold. The coverage probability can be expressed as

$$P_c = \mathbb{P}[\text{SINR}(x) > T], \tag{2.1}$$

where SIR can be replaced by SINR/SNR depending on the defined networks.

The coverage probability is particularly useful in evaluating the performance of wireless networks, as it provides insights into the extent of coverage and the probability of achieving satisfactory signal quality. By determining the coverage probability, network operators can assess the network's ability to provide reliable and satisfactory connectivity to users across different areas of the network. It enables network operators to make informed decisions and optimizations to enhance the network's performance and ensure a better user experience.

Furthermore, the coverage probability is influenced by various factors, including path loss, interference, fading, and the density and distribution of BSs. Analyzing the coverage probability helps in understanding the impact of these factors on the network's overall performance and identifying areas that may require optimization or improvement.

- **Ergodic capacity**

  The ergodic capacity is a metric used to evaluate the average capacity of a wireless communication channel over an infinite time interval, taking into account the statistical variations caused by fading. It provides an upper bound on the achievable capacity of the channel.

  The ergodic capacity is typically expressed in bits per second (bps) or a similar unit, representing the average data rate that can be reliably transmitted over the

channel. Higher ergodic capacity values indicate better channel performance and the ability to achieve higher data rates on average. It can be derived as [17]

$$C_{\text{erg}} = \mathbb{E}[\log_2(1 + \text{SINR})], \tag{2.2}$$

where SIR can be replaced by SINR/SNR depending on the defined networks.

In wireless communication, the channel conditions can vary due to factors such as multipath fading, shadowing, and interference. These variations result in fluctuations in the signal quality, which in turn affects the capacity of the channel. The ergodic capacity takes into consideration these statistical variations and provides an average capacity value that can be achieved over a long period of time.

Mathematically, the ergodic capacity is calculated as the average of the instantaneous capacity of the channel over an infinite time interval. It is derived by considering the probability distribution of the fading channel and integrating the capacity over all possible channel realizations.

The ergodic capacity provides a measure of the average data rate that can be reliably achieved over the channel, accounting for the effects of fading. It is an important metric for assessing the performance of wireless communication systems, particularly in scenarios where fading is significant.

- **Spectral efficiency**

  In wireless communication, spectral efficiency is a metric that measures the efficiency of transmitting information data within a given bandwidth or spectrum in a specific communication network. It evaluates how effectively the available frequency spectrum is utilized by the physical layer protocol and the channel access protocol [18].

  In SCNs, spectral efficiency refers to the maximum amount of data that can be

transmitted to a specified number of UE per second while maintaining an acceptable level of service quality. It is a key performance metric that reflects the network's ability to utilize the available spectrum resources efficiently. The spectral efficiency can be expressed as

$$\eta_s = \frac{R_b}{B_s}, \tag{2.3}$$

where R_b notes the system bit rate, B_s is the system bandwidth.

The spectral efficiency of an SCN is influenced by various factors, including the number of simultaneous UEs accessing the network, the modulation and coding schemes employed, the interference from neighbouring cells, and the deployment of advanced techniques like multiple-input multiple-output (MIMO) systems with beamforming.

To improve spectral efficiency, network operators can employ strategies to mitigate potential interference, such as using interference coordination techniques or optimizing resource allocation algorithms. Additionally, deploying MIMO systems with beamforming techniques can enhance spectral efficiency by allowing multiple spatial streams to be transmitted simultaneously.

By maximizing spectral efficiency, SCNs can achieve higher data rates and support more concurrent users within the available spectrum, leading to improved network capacity and overall performance.

It is worth noting that spectral efficiency is an important consideration in the design and optimization of wireless communication systems, as it directly impacts the network's ability to accommodate increasing data demands and deliver high-quality services to users.

- **Area spectral efficiency**

In wireless communication, it is a method to measure the number of UEs or simultaneous services provided with restricted bandwidth of radio frequency in a defined area . The main influences on the area spectral efficiency are the single UE technique, multiple access schemes and the utility of radio resource management.

The area spectral efficiency is a metric used to evaluate the efficiency of wireless communication systems in terms of the number of UE or simultaneous services that can be supported within a given area, while utilizing a limited bandwidth of radio frequency [18]. It quantifies the system's ability to maximize the utilization of available spectrum resources and serve multiple users effectively. The formula for area spectral efficiency can be expressed as:

$$ASE = \frac{R_t}{A}, \tag{2.4}$$

where R_t is the total throughput in bits per second, A denotes the total area in square meters. The total throughput in bits per second is determined by factors such as the number of simultaneously served UE, the achievable data rate per UE, and the utilization of multiple access schemes. The total area represents the coverage area where the wireless communication system provides service.

To improve the area spectral efficiency, various techniques can be employed, including efficient resource allocation, advanced multiple access schemes (e.g., orthogonal frequency-division multiple access, time-division multiple access), beamforming, and interference management strategies. These techniques aim to maximize the number of supported UEs and increase the data rates within the given area while maintaining acceptable quality of service levels.

- **Energy efficiency**

Energy efficiency is an important metric that reflects the trade-off between achieving high spectral efficiency and minimizing power consumption in wireless communication networks. The spectral efficiency can be expressed as

$$EE = \frac{D}{P}, \tag{2.5}$$

where the D represents the amount of data transmitted, and P denotes the total power consumed by the wireless communication system. It takes into account the power consumed by the BSs, access points, transmission equipment, and other components of the network.

The energy efficiency is defined as the ratio of the area spectral efficiency (ASE) to the power consumption per unit area. By dividing the ASE by the power consumption per unit area, the energy efficiency metric provides an indication of how efficiently the network utilizes its power resources to achieve a certain level of spectral efficiency. A higher energy efficiency value indicates that the network is able to achieve a greater spectral efficiency while consuming less power per unit area, which is desirable from an energy-saving perspective.

Improving energy efficiency in wireless communication networks is crucial for reducing operational costs, minimizing carbon footprint, and prolonging battery life in mobile devices. Various techniques can be employed to enhance energy efficiency, such as optimizing transmit power, implementing energy-saving algorithms, adopting advanced modulation and coding schemes, and deploying energy-efficient hardware components.

Different performance metrics serve different purposes and have different assumptions. The choice of performance metrics depends on the specific research goals, system requirements, and the aspects of network performance that need to be evaluated. It is

important to carefully select the appropriate performance metrics to ensure they accurately capture the desired aspects of network performance and support the research objectives.

2.1.4 Validation Metrics

In wireless communication, it is necessary to confirm the mathematical framework is an effective method for investigating the network performance. Generally, the Monte Carlo method is widely engaged to validate the result of the proposed mathematical model on the predefine networks. The Monte Carlo method is a panoramic category of computing schemes for deriving numerical results by repeated random sampling. Its underlying objective is to verify the physical and mathematical problems, which is difficult or impossible to use other approaches, with repeated random experiments under the deterministic principle [20]. Besides, it is mostly deployed for three physical and mathematical areas: optimization, numerical integration, and generating draws from a probability distribution [20].

The basic pattern of the Monte Carlo methods:

1. Determine the principle of input generating: Define the rules or principles for generating input values that will be used in the simulation or calculation. These input values can represent various parameters or variables relevant to the problem being studied.

2. Produce the inputs probability distribution under the principle: Generate the input values according to a specified probability distribution that reflects the characteristics of the problem. The probability distribution can be uniform, normal (Gaussian), exponential, or any other suitable distribution.

3. Repeat the calculation with inputs which are updated each time: Perform the desired calculations or simulations using the generated input values. The calculations are typically repeated a large number of times to obtain a statistically significant sample of results. In each iteration, the input values are updated according to the defined probability distribution.

4. Aggregate the results: Collect and analyse the results obtained from the repeated calculations. This may involve calculating statistical measures such as means, variances, confidence intervals, or other relevant metrics. The aggregated results provide insights into the behaviour and performance of the system or phenomenon under study.

By using the Monte Carlo method, the proposed mathematical models can be validated and reliable numerical results can be obtained. This enhances the credibility of their studies by providing a robust validation approach that is suitable for addressing complex physical and mathematical problems in wireless communication.

2.1.5 Stochastic Geometry for Small-Cell Networks

In this section, I will first summarize the steps involved in deriving systematic expressions for performance metrics in SCNs. These expressions are crucial for evaluating the performance of SCNs and understanding their behaviour. Then, an overview of the concept of modelling SCNs using stochastic geometry is provided, which is a powerful mathematical tool for analysing the spatial characteristics and performance of wireless networks.

2.1.5.1 The Process for SCN Performance Analysis

The systematic derivation of performance metric expressions for SCNs involves several key steps.

A. System model

The system model plays a crucial role in analyzing and evaluating the performance of wireless networks. In this section, we will discuss the key components of the system model that need to be defined for further investigations and analyses.

1. Scenarios of targeted environment: It is important to clearly define the scenarios or environments in which the network will be deployed and studied. This could include indoor environments, outdoor environments, or specific types of locations such as urban areas, residential buildings, or office spaces. The characteristics of the environment, such as the presence of obstacles or blockages, can have a significant impact on the network performance.

2. Distributions of the BSs: The placement of BSs in the network has a direct influence on the coverage, capacity, and interference levels. The distribution of BSs can be modelled using various techniques, such as PPP or grid-based models. Generally, the locations of BSs can be represented by the points generated by PPP, and this approach is able to preserve most essential characteristics of networks [21]. The choice of distribution model should align with the characteristics of the targeted environment.

3. Distributions of blockages: In indoor environments, blockages such as walls, furniture, or human bodies can significantly affect the wireless signal propagation. It is important to model the distribution of these blockages to accurately assess

the impact on network performance. The distribution can be based on the layout of the indoor environment or statistical models that capture the presence and characteristics of blockages.

4. Locations of user equipment (UEs): The positions of UEs in the network can have a significant impact on the received signal quality, interference levels, and overall network performance.

5. Selection of appropriate channel model: The channel model defines the characteristics of the wireless channel, including path loss, shadowing, and fading effects. The choice of channel model depends on the targeted environment and the specific frequency band being considered.

By defining these components in the system model, a realistic representation of the network can be created under investigation. This enables the analysis and evaluation of various network performance metrics and facilitates the design and optimization of wireless communication systems.

B. Mathematical framework

Formulating the mathematical framework is a crucial step in analysing the behaviour and performance of SCNs. It involves developing mathematical models and equations that accurately capture the key aspects of the networks. Some of the important components of the mathematical framework include:

1. Path loss models: Path loss models describe the attenuation of the wireless signal as it propagates through the environment. These models take into account factors such as distance, frequency, and the presence of obstacles or blockages. Different path loss models can be used depending on the specific characteristics of the SCN, such as indoor or outdoor environments.

2. Interference models: Interference models capture the impact of interference from other BSs in the network. The interference can degrade the signal quality and affect the performance of UEs. The mathematical models for interference consider factors such as the proximity of BSs, their transmit power, and the channel conditions.

3. Fading models: Fading models account for the variations in signal strength due to multipath propagation, where the signal arrives at the receiver through multiple paths with different delays and attenuations. These models capture the statistical properties of fading, such as Rayleigh fading or Nakagami fading, and are used to analyze the performance of the network under fading conditions.

By formulating the mathematical framework, researchers can use these models and equations to analyse the performance of SCNs, predict network behaviour, and optimize system parameters. This mathematical framework serves as a basis for conducting simulations, analytical derivations, and performance evaluations, leading to valuable insights and guidelines for network design and optimization.

C. Network performance

In the network performance analysis in SCNs, stochastic geometry is a powerful tool for evaluating various performance metrics. Stochastic geometry provides a mathematical framework for analysing the random spatial distribution of network elements, such as BSs and UE, and their interactions.

To assess network performance metrics, two important techniques in stochastic geometry are commonly used: Campbell's theorem and probability generating functional (PGFL).

1. Campbell's theorem: Campbell's theorem allows for the calculation of the ex-

pected value of a random sum over a point process. It provides a way to evaluate performance metrics that involve the aggregation of random variables associated with the locations of BSs or UEs. By applying Campbell's theorem, the expected values of key network performance metrics, such as coverage probability or interference level, can be determined.

2. Probability generating functional (PGFL): PGFL is a powerful tool for analyzing point processes and their characteristics. It provides a way to calculate the probability distribution or moments of a function of a point process. By utilizing PGFL, network performance metrics can be expressed as functions of the underlying point process, enabling the evaluation of metrics such as SIR or throughput.

By applying Campbell's theorem and PGFL in stochastic geometry, researchers can analytically describe and evaluate network performance metrics of interest, such as coverage probability, interference, capacity, and other statistical measures. These techniques enable a comprehensive analysis of the network behaviour and assist in optimizing system design and performance in SCNs.

In the next section, I will provide a detailed explanation of Campbell's theorem and PGFL and demonstrate their applications in network performance analysis.

D. Validation

Finally, to validate the analytical results obtained from the defined SCN (SCN) model, the Monte Carlo method is often employed. The Monte Carlo method is a powerful tool for numerical simulations and provides a means to validate the mathematical model and assess its performance under realistic conditions.

By running a large number of Monte Carlo simulations, statistical properties of the network performance metrics, such as coverage probability, spectral efficiency, or energy

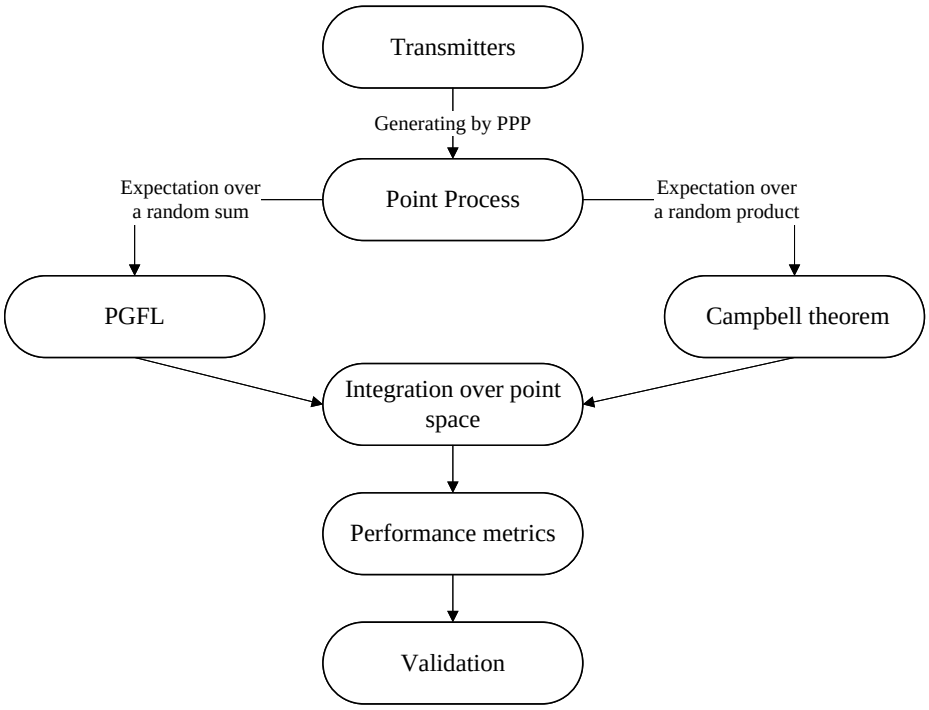

Figure 2.5: The procedure of stochastic geometry analysis by PPP.

efficiency, can be estimated. These simulation results can then be compared to the analytical results obtained from the mathematical model. If the simulation results closely match the analytical results, it provides evidence of the validity and accuracy of the mathematical model.

The combination of analytical techniques and Monte Carlo simulations helps ensure the robustness and reliability of the SCN model and its predictions, providing valuable insights into network performance and facilitating the design and optimization of SCNs.

The process of modelling the SCNs by using stochastic geometry is concluded in Figure 2.5.

2.1.5.2 A Point Process

In the following sections, we will further explore the properties and applications of point processes in the context of SCNs and network performance analysis.

The point process is encompassed in this section. First of all, a definition of point process is introduced: a point process in $\mathbb{R}^d$ is a random variable that takes a value in space $\mathbb{N}$ and any bounded set $A \subset \mathbb{R}^d : \Phi(A)$ [22]

$$\Phi = \sum_i \delta x_i, \tag{2.6}$$

where Φ is the point process. According to the properties of the point process, it can be classified into five different types:

- **Translated point process** It is the point process that $\Phi \triangleq \{x_i + x, x_2 + x, ...\}$, translating $x \in \mathbb{R}^d$.
- **Stationary point processes** It is the point process that the distribution of points is translation-invariant, thus the point process is defined as a stationary process, $\Phi \stackrel{d}{=} \Phi_x$.
- **Isotropy point process** It is the point process that the point distribution is a rotational invariant depending on the point of origin o, thus the point process is defined as isotropy, as $\Phi \stackrel{d}{=} r\Phi_x$ and r is rotational invariant of the original point o.
- **Motion-invariance point process** It is the point process that the distribution of point is defined as not only a stationary process but also an isotropic process.
- **Thinning point process** It is the point process that removing selected points follow a regulation. Moreover, according to the property of the regulation, it is

categorized as independent thinning and dependent thinning with the condition that if the removed points have no correlation with other points.

A. Distance

The distance of the point process is an essential factor in the point process. In the following part, the distances among the points generated by the point process and the functions of its properties will be introduced. First of all, the notion of the closest-neighbour operator is defined as, if a set of points ϕ contains at least two points,

$$NN_{\Phi}(x) \stackrel{\triangle}{=} \underset{y \in \phi / \{x\}}{\arg\min} \{||y-x||\}, \qquad x \in \phi. \tag{2.7}$$

If more than one closest neighbour exists, the one will be randomly selected from them. The operator is able to be utilized to an arbitrary location $v \in \mathbb{R}^d$. Then, the definition of the shortest distance between the point x and the set A is derived as

$$||v-A|| \stackrel{\triangle}{=} \min\{||y-x||\}, \qquad v \in \mathbb{R}^d, A \in \mathbb{R}^d, y \in A. \tag{2.8}$$

furthermore, the contact distance can further describe the characteristic of the distances of the point process.

Definition 2.1. *With a point process Φ, at position v, the contact distance is set as $||v-\Phi||$.*

Definition 2.2. *The distribution of contact distance is set as F^v, the the cumulative distribution function (CDF) of $||v-\Phi||$, is defined as*

$$F^v(r) \stackrel{\triangle}{=} \mathbb{P}(||v-\Phi|| \leq r) = \mathbb{P}(N(b(v,r)) > 0). \tag{2.9}$$

For the stationary point process, this function is not limited by the location v, thus it can be indicated as F. In SCNs, it is usually employed as its ability of the shortest distance between the serving BS and the typical UE.

Definition 2.3. *In the point process, the distance of the closest neighbour, from a point to its closest neighbour, is defined as*

$$||x - NN_{\Phi}(x)|| = ||x - \Phi/\{x\}||, \qquad x \in \Phi. \tag{2.10}$$

Definition 2.4. *The function of the closest-neighbour distance distribution is defined as*

$$G^{x}(r) = \mathbb{P}(||x - NN_{\Phi}(x)|| \leq r). \tag{2.11}$$

Similarly, for the stationary point process, this function is not limited by x, thus it can be denoted as G. With the PPP, the function of contact distance distribution is isotropic as the distribution of closest-neighbour distance, thus it can be written as

$$F^{v}(r) \stackrel{\triangle}{=} G^{v}_{\Phi\cup\{v\}}(r), \tag{2.12}$$

where $G^{v}_{\Phi\cup\{v\}}(r)$ is the distribution of closest-neighbour distance of the point process $\Phi\cup\{v\}$ at location v.

B. Poisson point process

The Poisson point process (PPP) is an important point process and is widely applied in SCNs. In the following part, it will be introduced in the instance of a 2-D PPP.

Definition 2.5. *A PPP Φ of density λ, where the amount of points in a bounded set*

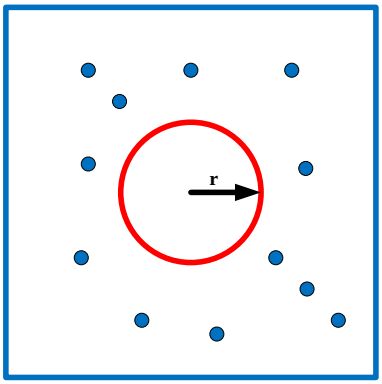

Figure 2.6: An illustration of PPP.

$B \cup \mathbb{R}^2$ has a Poisson distribution with mean $\lambda|B|$, is characterized by

$$\mathbb{P}(\Phi(B) = n) = \exp(-\lambda|B|)\frac{(\lambda|B|)^n}{n!}. \tag{2.13}$$

It can be seen that a stationary PPP is completely characterized by the density λ. Then, the distance properties of a PPP will be introduced.

Theorem 2.1. *The complementary cumulative distribution function (CCDF) of the distance of two closest point for the process from the origin denoted by G is $\mathbb{P}(G \geq r) = \exp(-\lambda\pi r^2)$, shown in Figure 2.6.*

Proof.

$$\begin{aligned}\mathbb{P}(G \geq r) &= \mathbb{P}(C(o,r) \quad \text{has} \quad \text{no} \quad \text{point}) \\ &= \exp(-\lambda|C(o,r)|) \\ &= \exp(-\lambda\pi r^2)\end{aligned} \tag{2.14}$$

□

Thus, the probability distribution function (PDF) $f(r) = 2\pi r\lambda\exp(-\lambda\pi r^2)$, as the CDF of r is $1-\mathbb{P}(G \geq r)$ and the PDF of r is $f(r) = \frac{\mathrm{d}(1-\mathbb{P}(G \geq r))}{\mathrm{d}r}$.

Then, the calculations of sums over PPP ((Campbells' theorem) and products over PPP (PGFL) are introduced in detail.

(i) Campbells theorem

Theorem 2.2. *For the PPP set Φ with the density λ, $f(x):\mathbb{R}^2\to\mathbb{R}^+$, then sums over PPP can be*

$$\mathbb{E}\left[\sum_{x\in\Phi} f(x)\right] = \lambda \int_{\mathbb{R}^2} f(x)\mathrm{d}x. \tag{2.15}$$

Proof. As known that

$$\mathbb{E}\left[\sum_{x\in\Phi} f(x)\right] = \lim_{R\to\infty} \mathbb{E}\left[\sum_{x\in\Phi\cap C(o,r)} f(x)\right], \tag{2.16}$$

Conditioning on the number of points n, $n=\Phi(C(o,r))$,

$$\mathbb{E}\left[\sum_{x\in\Phi\cap C(o,r)} f(x)\right] = \mathbb{E}_n\left[\mathbb{E}\left[\sum_{x\in\Phi\cap C(o,r)} f(x)\middle| n\right]\right]. \tag{2.17}$$

As conditioned on the number of points, it can be written as

$$\mathbb{E}\left[\sum_{x\in\Phi\cap C(o,r)} f(x)\middle| n\right] = n\int_{C(o,r)} \frac{f(x)}{|C(o,r)|}\mathrm{d}x. \tag{2.18}$$

Averaging over n

$$\mathbb{E}\left[\sum_{x\in\Phi\cap C(o,r)} f(x)\right] = \mathbb{E}[n]\int_{C(o,r)} \frac{f(x)}{|C(o,r)|}\mathrm{d}x, \tag{2.19}$$

as $\mathbb{E}[n]=\lambda|C(o,r)|$, and the trend of $r\to\infty$, the result can be obtained. □

(ii) Probability generating functional

Theorem 2.3. *For the PPP set Φ with the density λ, $f(x):\mathbb{R}^2\to[0,1]$ be a real-valued function, thus products over PPP can be*

$$\mathbb{E}\left[\prod_{x\in\Phi} f(x)\right] = \exp\left(-\lambda\int_{\mathbb{R}^2}(1-f(x))\mathrm{d}x\right). \tag{2.20}$$

Proof. The result of $\Psi_r = \Phi\cap C(o,r)$ will be proved. Ψ_r is a PPP set with the quantities of points n distributed following a Poisson random variable with average value $\lambda\pi r^2$,

$$\begin{aligned}\mathbb{E}\left[\prod_{x\in\Psi_r} f(x)\right] &= \mathbb{E}_n\left[\mathbb{E}\left[\prod_{x\in\Psi_r} f(x)\middle| n\right]\right]\\ &= \mathbb{E}_n\left[\mathbb{E}\left[f(x)\right]\right]^n.\end{aligned} \tag{2.21}$$

Besides, $\mathbb{E}[f(x)] = \frac{1}{\pi r^2}\int_{C(o,r)} f(x)\mathrm{d}x$, thus

$$\mathbb{E}\left[\prod_{x\in\Psi_r} f(x)\right] = \mathbb{E}_n\left[\left(\frac{1}{\pi r^2}\int_{C(o,r)} f(x)\mathrm{d}x\right)^n\right]. \tag{2.22}$$

Let $z>0$, and n is a Poisson random variable with average value w, therefore $\mathbb{E}[z^n] = \exp(-w(1-z))$, so

$$\begin{aligned}\mathbb{E}\left[\prod_{x\in\Psi_r} f(x)\right] &= \exp\left(-\lambda\pi r^2\left(1-\frac{1}{\pi r^2}\int_{C(o,r)} f(x)\mathrm{d}x\right)\right)\\ &= \exp\left(-\lambda\int_{C(o,r)}(1-f(x))\mathrm{d}x\right).\end{aligned} \tag{2.23}$$

□

Furthermore, the PGFL can be applied to the interference characterization of SCNs by PPP.

Definition 2.6. *The function of path loss $\ell : \mathbb{R}^2 \to \mathbb{R}$, the BSs are distributed by a PPP Φ. The location of UE is at distance r, then the power of interference can be formed as*

$$I(r) = \sum_{x \in \Phi} h_x \ell(x - r), \qquad r \in \mathbb{R}^2 \tag{2.24}$$

where h_x represents the path loss multiplying attenuation coefficient between the BS and UE, and it is assumed independently.

Hence, the Laplace transform of interference is able to be described in the statistical characterization. In agreement with the PGFL of PPP, it is derived as

$$\begin{aligned}
\mathscr{L}(s) &= \mathbb{E}[\exp(-sI(r))] \\
&= \mathbb{E}\left[\exp\left(-s \sum_{x \in \Phi} h_x \ell(x - r)\right)\right] \\
&= \mathbb{E}\left[\prod_{x \in \Phi} \exp(-s h_x \ell(x - r))\right] \\
&\overset{(a)}{=} \exp\left(-\lambda \int_{\mathbb{R}^2} \left(1 - e^{-s h_x \ell(x-r)}\right) \mathrm{d}x\right),
\end{aligned} \tag{2.25}$$

where step (a) is the PGFL of PPP. Substituting $x - r \to x$, it is denoted as

$$\mathscr{L}_I = \exp\left(-\lambda \int_{\mathbb{R}^2} \left(1 - e^{-s h_x \ell(x)}\right) \mathrm{d}x\right) \tag{2.26}$$

2.2 Related Works of Small-Cell Networks

With rapid global urbanization, mobile traffic has increased significantly in urban areas, where 80% of mobile traffic is generated indoors [23], [24], and will surpass a half zettabyte globally by 2021 [25]. According to [2] and [5], traditional outdoor networks

and Wi-Fi access points can barely satisfy the increasing indoor wireless service demand. The small cell is a potential technology to satisfy future mobile traffic through spatial reused [26]. As a newly designed network, SCNs can supply the diverse solutions of cost-efficiency and energy-efficiency to handle the forecast traffic growth [27]. As a result, indoor SCNs have gained prominence as a promising solution to the increasing demand for indoor wireless services. With their ability to address the challenges of indoor mobile traffic and provide cost-effective and energy-efficient solutions, SCNs offer a viable approach to meet the growing connectivity needs in indoor environments.

2.2.1 Stochastic Geometry

For assessing the performance of SCNs, stochastic geometry is widely utilized to form the SCNs model and analysis its performance [28–32].The main objective of employing stochastic geometry is to assess the average performance of SCNs and statistically evaluate them using metrics such as coverage probability, ergodic capacity, spectral efficiency, area spectral efficiency, and probability of system error [21, 33]. With stochastic geometry, it becomes possible to analyse various parameters of SCNs based on the derived expressions of these metrics. This provides valuable insights into the practical deployment of small cells. In actuality, it is known that SCNs are widely deployed for a specific environment or certain geographical layout. Besides, in the method of stochastic geometry, the deterministic character of SCNs is replaced by the probabilistic spatial distribution of BSs [34]. Based on stochastic geometry, we are able to investigate a general mathematical model for an uncertain scenario and analysis the average of overall small cells. The stochastic geometry not only is able to characterize the spatial randomness of SCNs, but also is able to incorporate some factors in signal propagation.

From the late 90s, stochastic geometry was first attempted to model SCNs, as its natural

ability to capture the randomness [35, 36]. Then, the author in [34, 37, 38] successfully disclosed the randomness of realistic SCNs and the irrationality of the hexagonal grid model. In [34], the distribution of BSs was generated following a homogeneous Poisson point process (HPPP) on a 2-D plane, and the mathematical expression of downlink coverage probability was acquired. With a contrast between the model of the hexagonal grid and realistic networks, the model of SCNs affords a strict lower bound for the performance of SCNs, whereas the traditional model of hexagonal grid supplies the upper bound. The authors in [37] examined the rationality of the PPP model by comparing the practical layouts of BSs in the various factors. Thus, the mathematical tractability characteristics of the PPP model can be verified.

After the success of deploying the PPP model, the downlink system of SCNs was characterized. In [39], single-layer networks were discussed. In [40–45], multi-tier heterogeneous networks were modelled using stochastic geometry where BSs in each tier were distributed following an independent HPPP. In [46–50], MIMO was incorporated into SCNs to scrutinize the impact of antenna quantities and schemes of beamforming on the performance of networks. Besides, the authors in [51, 52] further applied the PPP model and stochastic geometry to analyse massive MIMO. In [53–57], millimeter-wave SCNs were modelled and analysed taking into account the effects of blockages.

With further study of the PPP model and stochastic geometry, the authors in [58–62] encompassed the methods of corresponding analytical interference management and BS cooperation strategies as the densification of networks. In [63–66], the Coverage probability was enhanced by deploying the relaying nodes in SCNs, where both the BSs' location and the relay nodes were generated by the PPP model. Furthermore, due to the dense BSs applied in networks, energy efficiency (EE) is also considered a decisive theme in SCNs. In [67–71], the authors investigated EE under dense SCNs. Besides, in order to improve the SCNs EE, the authors in [72–74] incorporated nodes

with energy harvesting functions into the PPP model to analyse the energy utilization of SCNs.

In summary, stochastic geometry is a powerful tool for analysing SCNs, providing insights into their performance and aiding in the practical deployment of small cells. By characterizing the spatial randomness and incorporating relevant propagation factors, stochastic geometry facilitates a comprehensive analysis of SCNs and contributes to the advancement of wireless communication systems.

2.2.2 LOS Probability Model

Based on the conventional metrics for analysing the performance of SCNs, the path-loss models with standard power-law were deployed by the authors in [34, 75, 76] without differentiating links between the LOS and NLOS BSs to the typical UE. Besides, the BSs were generated by an HPPP, and the channel model was combined with the models of path loss including the Rayleigh fading. Furthermore, the authors concluded that incorporating the effect of blockage in the path-loss models significantly improves the investigation of network performance in practical propagation environments. By considering the impact of blockages, such as buildings or obstacles, the models can more accurately represent the signal propagation characteristics in real-world scenarios. This allows for a more realistic analysis of network performance and aids in the optimization and deployment of SCNs.

By considering the blockage in the SCNs, differentiating LOS and NLOS BS to the assigned typical UE is an analytical method to make the performance evaluation of SCNs accurate. The LOS probability model is designed to exactly differentiate the LOS and NLOS BSs to the assigned typical UE, and is a decisive factor to construct the piratical signal propagation path and tractably analyse the network performance. This

model provides a tractable method to o describe signal propagation and build a channel model for SCNs [77]. In [78–83], by differentiating LOS and NLOS BSs, the authors examined the effect of LOS/NLOS propagation on the outdoor SCNs performance. In [80, 81], the model of path loss constructed with a piece-wise function and LOS probability function were applied. Furthermore, the linear LOS propagation function led to more tractable results in [81]. The authors in [84, 85] discussed if both altitudes of BS and idle mode of BS affect the SCNs performance. The works in [86] revealed that the power of the signal is attenuated significantly for NLOS links in millimetre-wave SCN. In the MIMO system, it is in favour of improving the SNR, while the NLOS link still can significantly affect the network performance [87]. The LOS probability function was also incorporated in the Third Generation Partnership Project (3GPP) to improve the evaluation of networks performance [88–90].

Overall, the studies highlighted the importance of incorporating blockage effects in path-loss models to capture the true performance of SCNs in practical propagation environments.

2.2.3 Indoor Small-Cell Networks

For indoor environments, the performance of SCNs is considerably affected by complex blockages including moving blockages (e.g. moving human bodies) and stationary blockages (e.g. building structure, wall, ceiling, furniture) [91, 92]. Conventionally, the impact of multifarious wall blockages on the propagation of wireless signals is represented by the log-normal shadowing model [91–94]. The ray tracing is also deployed to characterize indoor scenarios [95–99]. However, these models have limitations, as they often ignore important characteristics of blockages, such as size and density, and require empirical calibration for specific wireless environments. To overcome these

limitations and avoid reliance on specific environment knowledge, random shape theory was used to generate blockages [100]. This approach allows for the investigation of blockage effects in SCNs without the need for detailed information about the specific environment. In previous studies, the effects of outdoor blockages on random SCNs and urban SCNs were examined using random shape theory [78, 101]. Outdoor blockages were modeled as random rectangles with uncertain directions and sizes. The use of random shape theory provides a general framework for investigating the influence of blockages in SCNs, considering their inherent randomness and variability.

The authors in [4, 102–104] studied the performance of SCNs considering the modelling of building structures. The authors in [102] developed a spatial model of in-building SCNs and investigated the correlated shadowing model among the links passing through the walls and ceilings. In [103], the LOS probability was derived for practical indoor layouts with interior walls and ceilings. This study focused on characterizing the spatial correlation of shadowing caused by building structures, which can significantly affect the performance of indoor SCNs. In [4], the authors developed a tractable SCN model conditioned on multi-story construction and investigated the influence of ceilings on the network coverage and capacity. This study recognized the impact of ceilings in indoor environments and analyzed how their presence affects the overall network performance. In [104], the cross-floor connection was studied by an idealistic assumption of blockages. However, these studies ignored the effects of interior walls on indoor wireless coverage.

Several papers [2, 105–109] addressed the effects of interior walls within a single floor on the performance of indoor SCNs. The different wall layouts were discussed in [2]. The authors in [105] analysed the effect of wall-angle distributions on indoor wireless communications. However, only the specific placements of BSs were considered in [2], [105]. In [106], the authors derived the coverage probability in indoor SCNs with

wall blockages based on the horizontal or vertical orientations of walls, but the interior walls were simply considered impenetrable blockages. The interior wall penetration loss was studied in [107], where the wall layouts were only modelled as regular grids and the expressions of coverage probability were not investigated. In [108], [109], the authors incorporated the wall penetration loss into the path-loss model under the closest LOS and NLOS BS UASs for indoor SCN models constructed by stochastic geometry. However, the UASs considered in these papers, namely the closest LOS and NLOS BS UASs, do not guarantee that the typical user is served by the BS providing the strongest signal power. Overall, while these studies have contributed to understanding the effects of interior walls on indoor SCNs, there are still aspects to be explored, such as incorporating more realistic wall layouts and considering UASs that optimize the signal power for the typical user.

2.2.4 Summary

In the existing works, the field of SCNs have addressed various aspects of network performance, including coverage probability, interference management, and capacity optimization. However, there are some limitations and gaps in the current research that motivated the present work.

One of the main limitations is the lack of comprehensive consideration of interior wall penetration losses in indoor SCNs. While some studies have focused on blockages and their impact on signal propagation, they often treated interior walls as impenetrable obstacles or used idealized assumptions. This overlooks the realistic scenario where signals can penetrate walls with certain losses, affecting the coverage and performance of indoor SCNs.

Another limitation is the reliance on specific placements or orientations of BSs and

walls in the models. Some studies have considered specific wall layouts or assumed regular grid-like arrangements, which may not capture the diversity and complexity of real-world indoor environments. This restricts the generalizability of the findings and their applicability to different deployment scenarios.

Furthermore, existing works often overlook the influence of different user association strategies on network performance. Most studies have focused on the nearest BS UAS, neglecting the impact of other strategies that could provide stronger signal power to the typical user.

These limitations and gaps in the existing literature motivated the present work to develop a comprehensive analysis of the effect of interior wall penetration losses on the performance of indoor SCNs. The aim was to incorporate realistic models for wall penetration losses, consider diverse and arbitrary wall layouts, and investigate the influence of different user association strategies on coverage probability of SCNs. By addressing these gaps, this work contributes to a more accurate and practical understanding of the performance of indoor SCNs and informs the design and optimization of such networks in real-world scenarios.

2.3 Conclusions

In this chapter, it is combined with two major parts: the basic concept section of wireless networks, channel model, evaluation metrics, validation metric and stochastic geometry for SCNs; the section of related works in stochastic geometry, LOS probability model and indoor SCNs.

In the basic concept section, In the basic concept section, I first encompass three trending wireless networks: ad hoc networks, SCNs and heterogeneous networks, then con-

clude the features of these three types. The channel model describes how wireless signals propagate and includes factors such as path loss, blockage, and fading. Evaluation metrics, such as coverage probability and spectral efficiency, are used to measure the performance of SCNs. Validation metrics help verify the accuracy of mathematical models and simulation results. Stochastic geometry provides a mathematical framework for analyzing the spatial distribution of BSs and UEs in SCNs, allowing for statistical analysis of network performance.

In the review section, this section discusses the related works in stochastic geometry, LOS probability models, and indoor SCNs. Stochastic geometry has been widely used to model and analyse the performance of SCNs, taking into account factors such as random BS locations, blockages, and interference. LOS probability models capture the likelihood of having a line-of-sight connection between a BS and a UE, which is crucial for determining the quality of wireless communication. Indoor SCNs are specifically designed for indoor environments and require considering factors such as interior wall penetration loss and the impact of blockages on signal propagation.

By combining these sections, this chapter provides a comprehensive overview of the key concepts, models, techniques relevant to the analysis of SCNs using stochastic geometry. Furthermore, the chapter reviews existing research work in the field, identifying the limitations and gaps in the literature.

Chapter 3

The Effect of Interior Wall Penetration Losses on Indoor Small-Cell Networks under LOS BS User Association Strategy

3.1 Introduction

In this chapter, we present a system model for an indoor single floor SCN using random shape theory. The wall blockages are represented as straight lines distributed according to an HPPP, and the locations of BSs follow another independent HPPP. Besides, the LOS and NLOS links to the typical UE are differentiated in the subsequent calculations. I incorporate penetration loss caused by possible interior wall blockages along every link between a BS and a UE into the path-loss model.

To account for the presence of interior wall blockages, I derive expressions for the downlink coverage probability in the considered indoor SCN, specifically under the assumption of the nearest LOS BS UAS. I analyse the impact of wall attenuation and BS density on the downlink coverage probability through numerical simulations.

By considering the spatial distribution of walls, the differentiation of LOS and NLOS links, and the effect of wall attenuation, our proposed system model provides insights into the performance of indoor SCNs. The derived expressions and numerical results contribute to understanding the coverage probability in such networks and can guide the design and optimization of indoor SCN deployments.

The rest of this chapter is organised as follows. In Section 3.2, I present the system model that incorporates interior wall blockages in the indoor SCN. I describe the assumptions and parameters used in the model. In Section 3.3, I derive the analytical expression for the indoor downlink coverage probability under the assumption of LOS UAS. We explain the methodology used to calculate the coverage probability and provide the mathematical formulation for its determination. In Section 3.4, numerical and simulation results are analysed and discussed. Finally, in Section 3.5, we summarize the main findings of this chapter and draw conclusions based on the analysis and results presented.

3.2 System Model

In this section, we present a comprehensive system model for an indoor SCN that incorporates the effects of interior wall blockages. We use random shape theory to generate the wall blockages, taking into account their random shapes and distributions within the network. To analyse the performance of the SCN, we focus on the SINR, which is

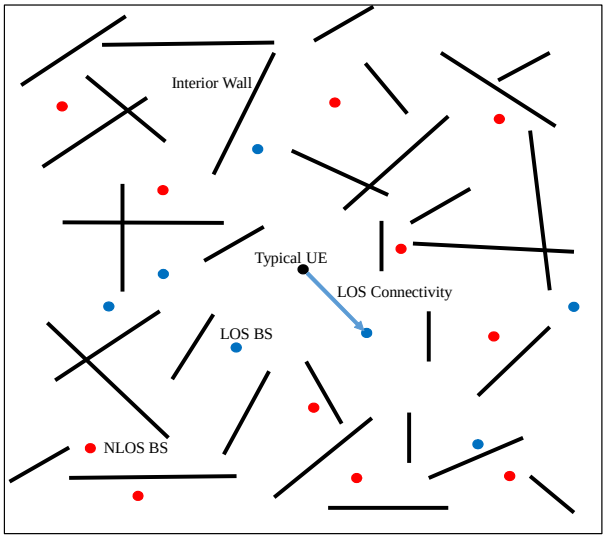

Figure 3.1: An indoor scenario. The red and blue point represent the SC BS, and black point represents the typical UE located at the centre of the indoor scenario. Black solid lines represent the wall blockages, the blue points and red points denote the LOS BSs and the NLOS BSs, respectively, the blue solid line represents the serving link between the UE and the closest LOS BS.

a key metric for evaluating the quality of the wireless communication links. We derive the SINR expression by considering the penetration loss caused by the interior wall blockages.

Additionally, we determine the average number of interior walls intersecting with a link. This information is crucial for accurately assessing the impact of wall blockages on the network performance. By quantifying the number of walls that obstruct a given link, we can better understand the extent of signal degradation and interference caused by the blockages.

By incorporating these factors into our system model, we aim to provide a more realistic representation of indoor SCNs and enable a more accurate analysis of their performance.

3.2.1 An Indoor Scenario

In our system model, we consider an indoor area represented as a 2-D plane. The focus of our analysis is on the UE of interest, which is positioned at the centre of the indoor area. This allows us to establish a central reference point for evaluating the network performance.

Figure 3.1 provides an example of the indoor scenario, illustrating the presence of wall blockages in the indoor environment. In this representation, the wall blockages are depicted as straight lines. The centers of these wall blockages are generated according to an HPPP denoted as Γ with a density of λ. The orientations of the walls, denoted as ψ_k, are randomly chosen within the range of $[0, \pi)$, where k corresponds to the points in Γ. The lengths of the walls, denoted as l_k, follow an arbitrary PDF $f_L(l_k)$ with an average length of L. It is important to note that the width of the walls is neglected in this model, as it has limited influence on the spatial representation of wall blockages, as discussed in previous works [105, 106].

On the other hand, the small-cell BSs are randomly distributed following another HPPP denoted as Φ with a density of μ. The locations of these BSs within the indoor scenario are independent of the wall blockages. This random distribution of BSs allows for the realistic modeling of their spatial arrangement within the indoor environment.

3.2.2 The Signal-to-Interference Ratio

The channel model incorporates several factors that affect the received power at the UE. These include distance-dependent path loss, Rayleigh fading, and wall penetration loss caused by the presence of wall blockages. The received power from the i-th BS, where $i \in \Phi$, can be expressed as

$$p_i = \frac{p_T h_i S_i}{d_i^{\alpha}}, \tag{3.1}$$

where p_T represents the transmission power of a BS assuming all BSs have the same transmission power, h_i denotes the power gain of Rayleigh fading, which follows the exponential distribution with a unit mean, i.e., $h_i \sim \exp(1)$, d_i is the distance between the UE and the i-th BS, α is the path loss distance exponent, and S_i is the penetration loss caused by wall blockages along the i-th link (i.e., the link between the UE and the i-th BS). In an interference-limited dense indoor network, the impact of thermal noise on connectivity is limited. Therefore, for the purposes of this chapter, we neglect the influence of thermal noise on the network performance and focus on analysing the effects of path loss, fading, and wall penetration loss.

Denoting the number of walls intersecting with the i-th link by K_i, the wall penetration loss along the i-th link can be expressed as

$$S_i = \prod_{k=0}^{K_i} \omega_k, \tag{3.2}$$

where ω_k is the wall attenuation ratio of the k-th wall intersecting with the i-th link, defined as the multiplicative factor with the range $[0,1]$. In order to simplify the calculation, the wall attenuation ratios are assumed to be the same, i.e., $\omega_k = \omega$. Then, the total wall penetration loss along the i-th link can be expressed as $S_i = \omega^{K_i}$.

3.2.3 Wall Blockage Models

The three typical wall layouts depicted in Figure 3.2 are representative of common indoor scenarios and provide a realistic depiction of wall configurations in indoor environments. The ability to quantify the average number of interior walls intersecting

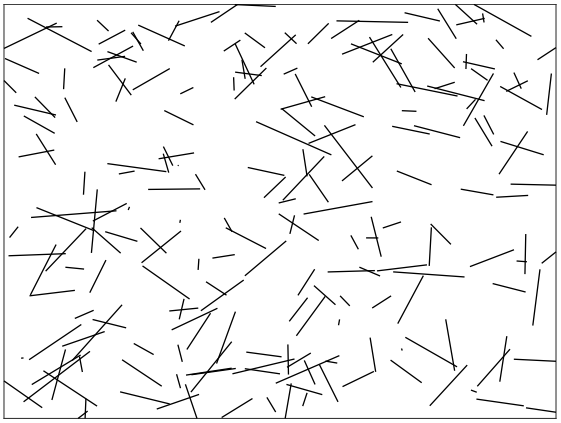

(a)

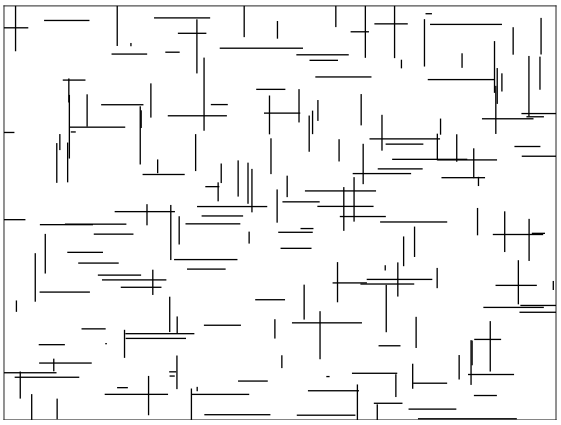

(b)

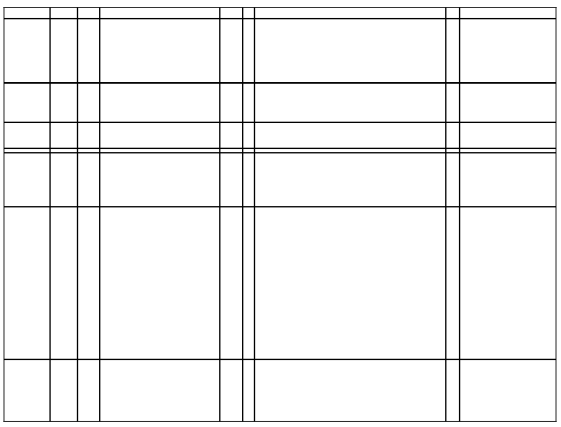

(c)

Figure 3.2: Three typical wall layouts: (a) Random layout: the wall orientation ψ_k are randomly chosen in the range $[0, \pi)$, (b) Binary orientation layout: the wall orientation ψ_k are randomly chosen from $\left\{0, \frac{\pi}{2}\right\}$, and (c) Manhattan grid. These three scenarios were created with parameters that lead to the same average wall volume[2].

with links is crucial for understanding the interference and path loss characteristics in indoor SCNs. With this information, network designers and researchers can optimize the placement and density of SC BSs to improve coverage and capacity while minimizing interference. The analytical model presented in this work offers a powerful tool for predicting the average number of interior walls and provides important guidance for efficient indoor SCN design and deployment.

To generate the interior walls in Figure 3.2 (a) Random layout and (b) Binary orientation layout, we use the random shape theory to model the wall blockages. The centres of the wall blockages are distributed on the 2-D plane according to an HPPP Γ with density λ. The width of each wall, denoted as l_k, follows an arbitrary PDF $f_L(l_k)$ with mean L. In this model, we neglect the thickness of the walls [2]. The orientation of each wall is represented by ψ_k, where k belongs to the set Γ.

3.2.3.1 The Average Number of Walls in Random Layout

In Figure 3.3, the plot illustrates that the wall represented by $|E'F'|$ intersects with the link YX because its centre falls within the parallelogram $EFPQ$. The area of the parallelogram $EFPQ$ is $ld_i|\sin(\xi)|$, where l is the length of the walls, d_i is the distance between the UE and the i-th BS, and ξ is the angle between the link and the walls. Similarly, the determination of walls intersecting with the i-th link is based on the condition that their central points fall within the corresponding parallelogram region.Thus, the number of walls intersecting with the i-th link can be expressed as [101]

$$K_i = \lambda l_k d_i |sin(\xi_{ik})|, \tag{3.3}$$

where ξ_{ik} is the angles between the i-th link and the intersecting k-th wall ranging at $[0, \pi)$. Therefore, the average number of interior walls intersecting with the i-th link,

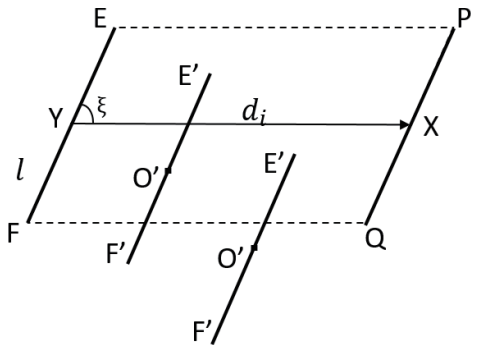

Figure 3.3: An example of how the link intersect with the wall blockages in random layout. YX is the i-th link with length d_i, where Y and X denote the UE and BS, respectively. $|EF|$ and $|PQ|$ denote the walls with the length l and ξ is the angle between the wall $|EF|$ and the link YX.

denoted as $\mathbb{E}[K_i]$, can be obtained by taking the expectation of K_i, which yields

$$\begin{aligned}\mathbb{E}[K_i] &= \int_{\Delta}\int_{\Xi} \lambda l_k d_i |sin(\xi_{ik})| f_L(l_k) \mathrm{d}l \frac{1}{\pi} \mathrm{d}\xi \\ &= \frac{2\lambda L}{\pi} d_i,\end{aligned} \tag{3.4}$$

where Δ is the set of l_k which following an arbitrary PDF $f_L(l_k)$ with an average length L, Ξ is the set of ξ_{ik} which ranges at $[0,\pi)$. This expression provides the average number of interior walls that intersect with the link based on the given densities of wall blockages and BSs.

3.2.3.2 The Average Number of Walls in Binary Orientation Layout

In Figure 3.4, the link between the UE and the i-th BS is blocked by the walls randomly selected form $\{0, \frac{\pi}{2}\}$, where $\psi \in \{0, \frac{\pi}{2}\}$. The angle γ_i between the wall and the link is defined, and it is uniformly distributed in the range $[0,\pi]$. Similarly, the angle θ_i between the link and the horizontal axis is also uniformly distributed in the range $[0,2\pi]$.

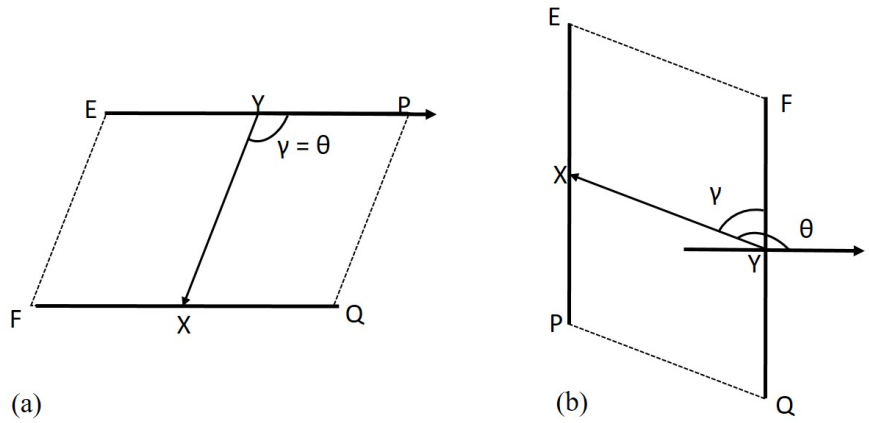

Figure 3.4: An example of how the link intersect with the wall blockages in binary orientation layout. YX is the i-th link with length d_i, where Y and X denote the UE and BS, respectively. $|EF|$ and $|PQ|$ denote the walls with the length l and ξ is the angle between the wall $|EF|$ and the link YX.

The relationship of θ_i and γ_i can be derived as

$$\gamma_i = \begin{cases} \frac{\pi}{2} - \theta_i, & \psi = \frac{\pi}{2}, \\ \theta_i, & \psi = 0. \end{cases} \tag{3.5}$$

Thus, for $\theta_i \in (0, \frac{\pi}{2}]$, the PDF of γ_i can be calculated as

$$f_\Gamma(\gamma_i) = \frac{1}{2}\delta[\gamma_i - (\frac{\pi}{2} - \theta_i)] + \frac{1}{2}\delta[\gamma_i - \theta_i] \tag{3.6}$$

where δ is Dirac function. As for $\theta_i \in (\frac{\pi}{2}, 2\pi]$, the PDF $f_\Gamma(\gamma_i)$ is the same as (3.6).

Similarly, the link is intersected with the walls only if the centres of walls are located in the parallelogram which is shaped by the walls and the link. For the wall orientation $\psi_k \in \{0, \frac{\pi}{2}\}$, the average number of interior walls intersected with the i-th link is given by [106]

$$\begin{aligned} E[K_i] &= \int_\Delta \int_\Gamma \lambda l_k d_i |sin(\gamma_{ik})| f_L(l_k) \mathrm{d}l f_\Gamma(\gamma_i) \mathrm{d}\gamma \\ &= \frac{\lambda L}{2}(|\sin(\theta_i)| + |\cos(\theta_i)|)d_i, \end{aligned} \tag{3.7}$$

where θ represents the angle between the i-th link and the horizontal axis.

3.2.3.3 The Average Number of Walls in Manhattan Grid

In Figure 3.2 (c) Manhattan grid, the Manhattan grid can be obtained by two independent Manhattan Poisson line processes. The centres of the interior walls are distributed according to HPPP along each axis with density λ', the average number of interior walls intersected with the i-th link is given by [2]

$$\begin{aligned} E[K_i] &= \int_{\Gamma} \lambda' d_i |sin(\gamma_{ik})| f_{\Gamma}(\gamma_i) \mathrm{d}\gamma \\ &= \lambda'(|sin(\theta_i)| + |cos(\theta_i)|) d_i. \end{aligned} \tag{3.8}$$

For the comparability among the Manhattan grid and the other two layouts of the interior walls, the density λ' is defined as $\lambda' = \frac{\lambda L}{2}$.

For the purpose of mathematical tractability, the actual number of interior walls K_i can be replaced by the average number of interior wall $E[K_i]$, thus the wall penetration loss for the i-th NLOS link can be derived as $S_i^{\mathrm{N}} = \omega^{E[K_i]}$. This means that the wall penetration loss of NLOS links can be obtained by the length of links, not from the scenario.

3.2.4 LOS and NLOS Links

According to (3.1)-(3.4), the SINR can be expressed as

$$\mathrm{SINR}_j = \frac{\eta_0 p_T h_j S_j d_j^{-\alpha}}{\sum\limits_{i \in \Phi / j, d_i \in (0,D)} \eta_0 p_T h_i S_i d_i^{-\alpha} + N_0}, \tag{3.9}$$

where the j-th BS is the serving link and D is the maximum length of links in the indoor scenario, η_0 is the path loss at the reference distance of 1 m, N_0 is the additive white Gaussian noise (AWGN) power.

In the indoor scenario with wall blockages, the links can be classified into two types: LOS links and NLOS links. Considering the difference between LOS and NLOS links, the SINR can be rewritten as

$$\begin{aligned}\mathrm{SINR}_j &= \frac{h_j S_j d_j^{-\alpha}}{\sum\limits_{m\in\Phi_\mathrm{L}/j} h_m S_m d_m^{-\alpha} + \sum\limits_{n\in\Phi_\mathrm{N}/j} h_n S_n d_n^{-\alpha} + \frac{N_0}{\eta_0 p_T}} \\ &= \frac{h_j S_j d_j^{-\alpha}}{I_\mathrm{L} + I_\mathrm{N} + \frac{N_0}{\eta_0 p_T}},\end{aligned} \tag{3.10}$$

where I_L and I_N denote the total interference power received by the UE via LOS interference links and NLOS interference links, respectively, Φ_L denotes the set of LOS BSs, Φ_N denotes the set of NLOS BSs, and $\Phi = \Phi_L + \Phi_N$. The value of S_m^L can be taken as 1, as the m-th LOS link experiences no wall attenuation. The value of S_n^N is determined by the number of walls intersected with the n-th link K_n and each wall attenuation ω_{n_k}.

Depending on the indoor scenario and assumptions, I consider the LOS probability model as the exponential model, which assumes that the LOS probability decays exponentially with distance. This model is often used in scenarios where there are minimal obstacles. In the exponential LOS probability model, the LOS probability $P_\mathrm{L}(d_i)$ as a function of distance d_i is given by:

$$\begin{aligned}P_\mathrm{L}(d_i) &= \exp(-\beta d_i) \\ &= \exp(-\frac{2\lambda L}{\pi} d_i),\end{aligned} \tag{3.11}$$

where β is a parameter that controls the rate of decay. A higher value of β indicates a faster decay of the LOS probability with distance, implying a higher likelihood of LOS at shorter distances. It is important to note that the specific value of β depends on the characteristics of the environment and the propagation conditions. It can be determined through measurements or calibrated based on empirical data. In this case, we assume that the wall blockages follow an HPPP with density λ and an average wall length L. The β is considered as $\beta = \frac{2\lambda L}{\pi}$, where derived from $\mathbb{E}[K_i]$, the average number of walls intersecting with the i-th link, [100].

The LOS and NLOS probability follows a Bernoulli distribution. Similarly, the probability of the i-th link being an NLOS link, denoted as $P_{\mathrm{N}}(d_i)$, can be calculated as the complement of the LOS probability:

$$P_{\mathrm{N}}(d_i) = 1 - P_{\mathrm{L}}(d_i) = 1 - \exp\left(-\beta d_i\right). \tag{3.12}$$

3.3 Downlink Coverage Probability

In this section, we introduce the inclusion of penetration loss caused by wall blockages in the analysis of the downlink coverage probability for the LOS UAS. This addition allows us to more accurately assess the performance of the downlink coverage in indoor SCN scenarios by accounting for the impact of wall blockages on signal propagation. We make the assumption that the wall blockages along each link are independent, which simplifies the analysis while still capturing the essential effects of wall penetration loss.

The downlink coverage probability $P_c(T)$ is defined as

$$P_c(T) = \mathbb{P}(\mathrm{SINR} > T), \tag{3.13}$$

where SINR is given in (3.10), and T is the minimum required SINR threshold.

3.3.1 The Typical UE Association with the Closest LOS BS

In this section, we consider the scenario where the typical UE, located at the center of the indoor area, is served by the closest LOS BS. The serving link between the UE and the closest LOS BS is represented by the red solid line in Figure 3.1. If there are multiple BSs with the same shortest LOS distance to the typical UE, the UE randomly selects one of them as its serving BS. The signals from all other BSs are treated as interference to the typical UE. Based on this model, the coverage probability can be calculated as

$$P_c^{\mathrm{L}}(T) = \int_0^D \mathbb{P}\left[\mathrm{SINR} > T | R^{\mathrm{L}}\right] f_{R^{\mathrm{L}}}(r)\mathrm{d}r, \tag{3.14}$$

where R^{L} is the length of the serving link between the UE and the closest LOS BS, $f_{R^{\mathrm{L}}}(r)$ is the PDF of R^{L} and $\mathbb{P}[SINR > T|R^{\mathrm{L}}]$ denotes the coverage probability conditioned on the shortest LOS link with the length R^{L}.

3.3.1.1 PDF of the Distance between the Closest LOS BS and the Typical UE

Define the event E_1 as follows: $E_1 = \{$there are n BSs in round area $C(O,r)\}$, where O represents the location of the typical UE and r is the radius of the round area, with r ranging from 0 to R^{L}.The number of BSs distributed following an HPPP in the round area is given by $\pi r^2\mu$ [100]. Therefore, the probability of event E_1 can be expressed as

$$\mathbb{P}(E_1) = \frac{e^{-\pi r^2\mu}(\pi r^2\mu)^n}{n!}, \tag{3.15}$$

where n is the number of BSs.

Next, we define the event $E_2 = \{$ all the BSs are NLOS to the UE in round area $C(O,r)\}$. Based on the event E_1, the conditional probability of event E_2 is calculated by

$$\begin{aligned}
\mathbb{P}(E_2|E_1) &= \left[\int_0^r P_{\mathrm{N}}(t)\frac{2t}{r^2}\mathrm{d}t\right]^n \\
&= \left[\int_0^r (1-\exp(-\beta t))\frac{2t}{r^2}\mathrm{d}t\right]^n \\
&= \left[\frac{2}{r^2}\int_0^r (1-\exp(-\beta t))t\mathrm{d}t\right]^n \\
&= \left[\frac{2}{r^2}\left(\frac{r^2}{2}-\frac{1-e^{-\beta r}(1+\beta r)}{\beta^2}\right)\right]^n \\
&= \left[1-\frac{2M(r)}{r^2}\right]^n, \qquad (3.16)
\end{aligned}$$

where $M(r) = \frac{1-(\beta r+1)e^{-\beta r}}{\beta^2}$.

Furthermore, the complementary cumulative distribution function (CCDF) of R^{L} is calculated by

$$\begin{aligned}
\mathbb{P}\{R^{\mathrm{L}} > r\} &= \mathbb{P}(E_2) \\
&= \sum_{n=0}^{\infty} \mathbb{P}(E_2|E_1)\mathbb{P}(E_1) \\
&= \sum_{n=0}^{\infty} \left[1-\frac{2M(r)}{r^2}\right]^n \frac{e^{-\pi r^2\mu}(\pi r^2\mu)^n}{n!} \\
&= e^{-\pi r^2\mu\left[1-(1-\frac{2M(r)}{r^2})\right]} \\
&= e^{-2\pi\mu M(r)}. \qquad (3.17)
\end{aligned}$$

Therefore, the CDF of R^{L} is $\mathbb{P}[R^{\mathrm{L}} \le r] = F_{R^{\mathrm{L}}}(r) = 1-\mathbb{P}\{R^{\mathrm{L}} > r\}$ and the PDF is

calculated as

$$f_{R^{\mathrm{L}}}(r) = \frac{\mathrm{d}F_{R^{\mathrm{L}}}(r)}{\mathrm{d}r} = 2\pi r\mu e^{-[\beta r + 2\pi\mu M(r)]}. \tag{3.18}$$

3.3.1.2 Coverage Probability

The coverage probability is formulated under the conditions of the closest LOS link between the UE and the serving BS. Specifically, the coverage probability can be expressed as

$$\begin{aligned}
&\mathbb{P}\left\{\frac{p_T h_j d_j^{-\alpha}}{I_{\mathrm{L}} + I_{\mathrm{N}} + \frac{N_0}{\eta_0 p_T}} > T \middle| R^{\mathrm{L}} = r\right\} \\
&= \mathbb{P}\left\{h_j > \left(\sum_{m\in\Phi_{\mathbb{L}}/j, d_m\in(r,D)} h_m S_m d_m^{-\alpha} + \sum_{n\in\{\Phi_{\mathbb{N}}\}, d_n\in(0,D)} h_n S_n d_n^{-\alpha} + \frac{N_0}{\eta_0 p_T}\right) T r^{\alpha} S_j^{-1}\right\} \\
&= \mathbb{E}\left[\exp\left(-\left(\sum_{m\in\Phi_{\mathbb{L}}/j, d_m\in(r,D)} h_m S_m d_m^{-\alpha} + \sum_{n\in\Phi_{\mathbb{N}}, d_n\in(0,D)} h_n S_n d_n^{-\alpha} + \frac{N_0}{\eta_0 p_T}\right) T r^{\alpha} S_j^{-1}\right)\right] \\
&\overset{(a)}{\approx} \mathbb{E}\left[\prod_{m\in\Phi_{\mathbb{L}}/j, d_m\in(r,D)} \mathbb{E}_{h_m}\left[\exp\left(-h_m d_m^{-\alpha} T r^{\alpha}\right)\right] \times \right. \\
&\qquad \left. \prod_{n\in\Phi_{\mathbb{N}}, d_n\in(0,D)} \mathbb{E}_{h_n}\left[\exp\left(-h_n d_n^{-\alpha} T r^{\alpha} \omega^{\mathbb{E}[K_n]}\right)\right] \times \exp\left(-\frac{N_0}{\eta_0 p_T} T r^{\alpha}\right)\right] \\
&= \mathbb{E}\left[\prod_{m\in\Phi_{\mathbb{L}}/j, d_m\in(r,D)} \frac{d_m^{\alpha}}{d_m^{\alpha} + T r^{\alpha}}\right] \times \mathbb{E}\left[\prod_{n\in\Phi_{\mathbb{N}}, d_n\in(0,D)} \frac{d_n^{\alpha}}{d_n^{\alpha} + T r^{\alpha}\omega^{\mathbb{E}[K_n]}}\right] \times \\
&\quad \exp\left(-\frac{N_0}{\eta_0 p_T} T r^{\alpha}\right) \\
&\overset{(b)}{=} \exp\left(-2\pi\left[\int_r^D \mu P_{\mathrm{L}}(t)\left[1 - \frac{t^{\alpha}}{t^{\alpha} + T r^{\alpha}}\right] t\,\mathrm{d}t + \int_0^D \mu P_{\mathrm{N}}(t)\left[1 - \frac{t^{\alpha}}{t^{\alpha} + T r^{\alpha}\omega^{\beta t}}\right] t\,\mathrm{d}t\right]\right) \\
&\quad \times \exp\left(-\frac{N_0}{\eta_0 p_T} T r^{\alpha}\right) \\
&= \exp\left(-2\pi\mu\left[\int_r^D e^{-\beta t}\left[1 - \frac{t^{\alpha}}{t^{\alpha} + T r^{\alpha}}\right] t\,\mathrm{d}t + \int_0^D (1 - e^{-\beta t})\left[1 - \frac{t^{\alpha}}{t^{\alpha} + T r^{\alpha}\omega^{\beta t}}\right] t\,\mathrm{d}t\right]\right)
\end{aligned}$$

$$\times \exp\left(-\frac{N_0}{\eta_0 p_T} T r^{\alpha}\right). \tag{3.19}$$

In step (a), the assumption is made that the wall attenuation ω_{n_k} is the same for all walls, denoted as ω. Therefore, the expression for S_n^{N} simplifies to $S_n^{\mathrm{N}} = \omega^{K_n}$. To further simplify the calculations in step (a), the average number of walls intersecting with the n-th link, denoted as $\mathbb{E}[K_n]$, is used instead of K_n according to (3.4). This allows us to write $S_n^{\mathrm{N}} = \omega^{\mathbb{E}[K_n]}$. The value of $\mathbb{E}[K_n]$ is a function of the link length d_n and the given wall density λ. In step (b), the PGFL is used for the PPP to calculate the densities of the LOS and NLOS BSs. The densities of the LOS and NLOS BSs in the PGFL process are determined by incorporating the probability of LOS and NLOS links, respectively, with the BS density μ. This allows us to analyze the network performance considering both the LOS and NLOS scenarios.

Based on (3.18) and (3.19), the unconditional coverage probability of the LOS serving link is computed by

$$\begin{aligned}
&P_c^{\mathrm{L}}(T) \\
&= \int_0^D \left\{ \mathbb{P}\left[\frac{p_T h_j d_j^{-\alpha}}{I_{\mathrm{L}} + I_{\mathrm{N}}} > T \right] f_{R^{\mathrm{L}}}(r) \right\} \mathrm{d}r \\
&= \int_0^D 2\pi\mu \exp\big(-[\beta r + 2\pi\mu M(r)] \big) \times \exp\left(-\frac{N_0}{\eta_0 p_T} T r^{\alpha}\right) \times \\
&\quad \exp\left(-2\pi\mu \left[\int_r^D e^{-\beta t} \left[1 - \frac{t^{\alpha}}{t^{\alpha} + T r^{\alpha}} \right] t \mathrm{d}t + \int_0^D (1 - e^{-\beta t}) \left[1 - \frac{t^{\alpha}}{t^{\alpha} + T r^{\alpha} \omega^{\beta t}} \right] t \mathrm{d}t \right] \right) r \mathrm{d}r.
\end{aligned} \tag{3.20}$$

Table 3.1: Parameters for Numerical Simulations and Analysis in Chapter 3

Parameter	**Value**
maximum link length	20 m
Transmit power	$p_T = 24$ dBm
AWNG power	$N_0 = -95$ dBm
Path loss at reference distance	$\eta_0 = -38.5$ dB
BSs density	$\mu = 0.01$ m^{-2}
Wall density	$\lambda = 0.05$ m^{-2}
Wall Orientation	$\psi_k \in [0, \pi)$
Wall attenuation	$\omega = 3, 7, 10, 15$ dB
Average width of walls	$L = 3$ m
Path-loss exponent	$\alpha = 2$
Simulation times	10^5

3.4 Numerical Evaluation

In this section, the proposed analytical results for the closest BS UAS with different wall attenuation are validated through Monte Carlo simulations. Table I presents a summary of the parameters used in the simulations [106]. These parameters provide important input values for the simulations and ensure that the results are consistent with the proposed analytical model.

Figure 3.5 presents the comparison between the analytical and simulation results of the average number of interior walls intersecting with the i-th link. The analytical result is obtained using equation (3.4), while the simulation results are obtained through Monte Carlo simulations with 10^5 repetitions. The close match between the analytical and simulation curves indicates the accuracy of the proposed analytical model in capturing the behaviour of the average number of interior walls intersecting with a link in the indoor SCN. Furthermore, the figure reveals an interesting relationship between the average number of interior walls and the average length of interior walls for a given link length. Specifically, the average number of interior walls exhibits a linear increase

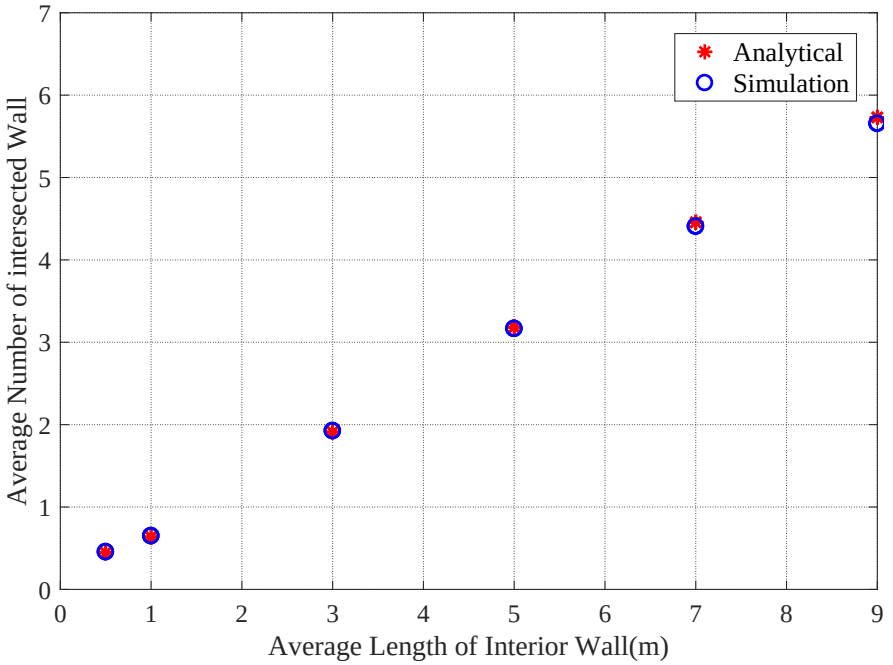

Figure 3.5: The analytical and simulation results of the average number of interior walls intersecting with the i-th link for the different average wall lengths under the random layout. The validation of analytical models is investigated by Monte Carlo simulations. The length of Links is 20 m.

with the average length of interior walls. This relationship provides valuable insights into the impact of wall length on the number of walls intersecting with a link in the indoor SCN scenario.

Figure 3.6 illustrates the comparison between the analytical and simulation results of the average number of interior walls intersecting with the i-th link under the binary orientation layout and Manhattan grid. The analytical result is obtained using (3.7) and (3.8), while the simulation results are obtained through Monte Carlo simulations with 10^5 repetitions. The close match between the curves of the analytical results and the Monte Carlo simulations indicates the accuracy of the analytical model. Furthermore, the figure reveals that the angle between the link and the horizontal axis has a significant effect on the average number of interior walls intersecting with the i-th link. This demonstrates the importance of considering the orientation of the interior walls in the

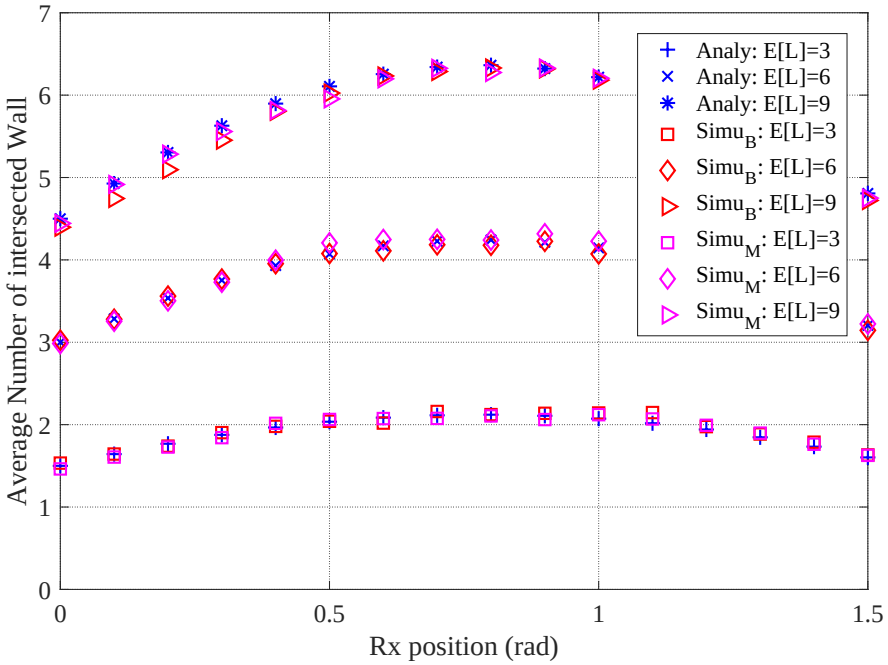

Figure 3.6: The analytical and simulation results of the average number of interior walls intersecting with the i-th link for the different average wall lengths under the binary orientation layout and Manhattan grid. The validation of analytical models is investigated by Monte Carlo simulations. The length of Links is 20 m.

indoor SCN model, as it can have a substantial impact on the network performance and coverage probability.

Figure 3.7 presents the comparison between the analytical and simulation results of the coverage probability with a SINR threshold, considering different wall attenuations (ω) of 3, 7, 10, and 15 dB. The analytical results are obtained using equation (3.14), while the simulation results are based on 10^5 Monte Carlo repetitions. From the figure, we can observe a slight gap between the two sets of results is attributed to the approximation of replacing the factor K_i with its expectation $E[K_i]$ in the derived expressions of coverage probability. Furthermore, it is evident that the coverage probability is influenced by the wall attenuation. As the wall attenuation increases, the coverage probability also increases. This is because higher wall attenuation results in reduced interference from NLOS links, leading to improved coverage. Therefore, increasing the wall attenuation

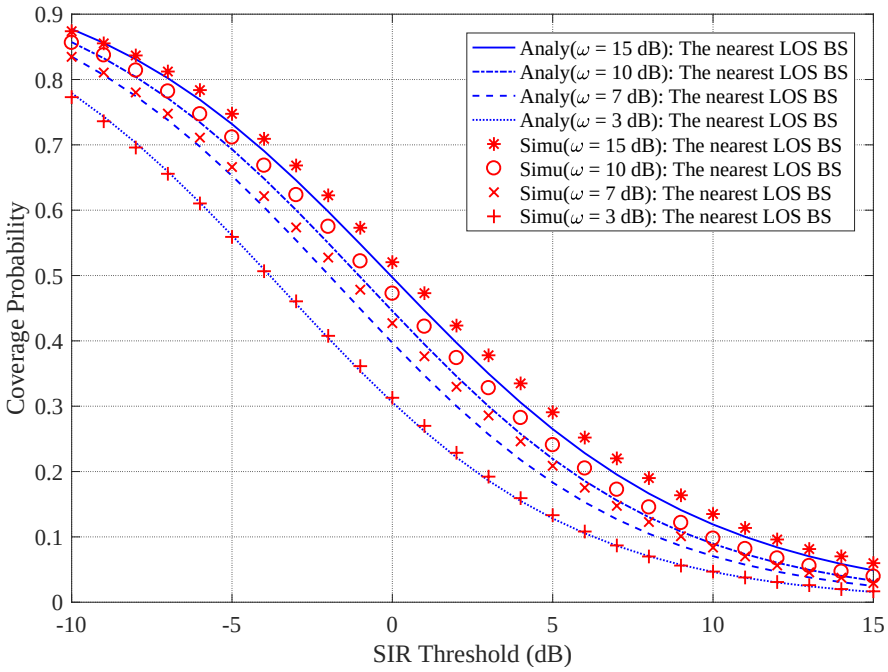

Figure 3.7: The analytical and simulation results of coverage probability under nearest LOS connectivity case with the SINR Threshold, for different wall attenuation taken as 15 dB, 10 dB, 7 dB and 3 dB, respectively.

is beneficial for achieving higher coverage probability in the nearest LOS connectivity scenario.

Figure 3.8 presents the comparison between the analytical and simulation results of the coverage probability with varying wall attenuations under the nearest LOS BS connectivity scenario. The analytical results are obtained using the derived expression of coverage probability, while the simulation results are based on Monte Carlo simulations with 10^5 repetitions. The good fitting between the analytical and simulation results validates the accuracy of our derived expression for the coverage probability. However, it is important to note that there are deviations between the analytical and simulation results. These deviations can be attributed to the approximation made in our analysis, where the average number of walls $E[K_i]$ is used instead of the actual number of walls K_i in the expression of the wall penetration loss (3.2). Furthermore, it can be observed that the deviations between the analytical and simulation results of the cover-

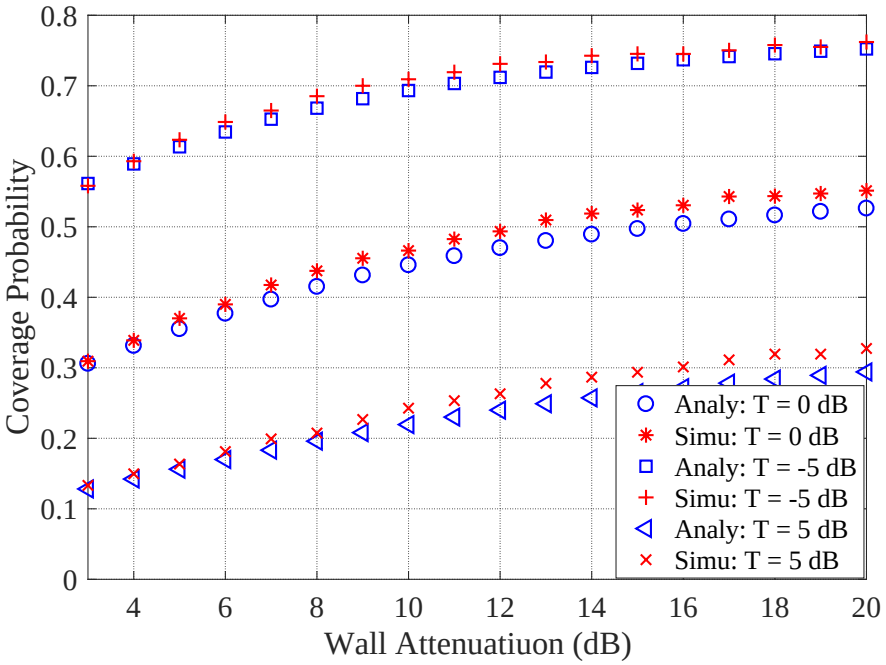

Figure 3.8: The analytical and simulation results of coverage probability under the nearest LOS connectivity case with wall attenuations, for SINR threshold $T = -5, 0, 5$ dB.

age probability increase with higher wall attenuation. This suggests that the accuracy of the analytical model may be slightly compromised as the wall attenuation becomes more significant. Nevertheless, the overall results between the analytical and simulation results demonstrates the effectiveness of our approach in analysing the coverage probability under the influence of wall attenuation in the nearest LOS BS connectivity scenario.

Figure 3.9 presents the comparison between the analytical and simulation results of the coverage probability with a SINR threshold under the three typical layout, considering different wall attenuations (ω) of 3 and 10 dB. The analytical results are obtained using equation (3.14), while the simulation results are based on 10^5 Monte Carlo repetitions. From the figure, we can observe a well match between the two sets of results for random layout and binary orientation layout. However, there is a disparity in the analytical results for the Manhattan grid layout. This indicates that the analytical model

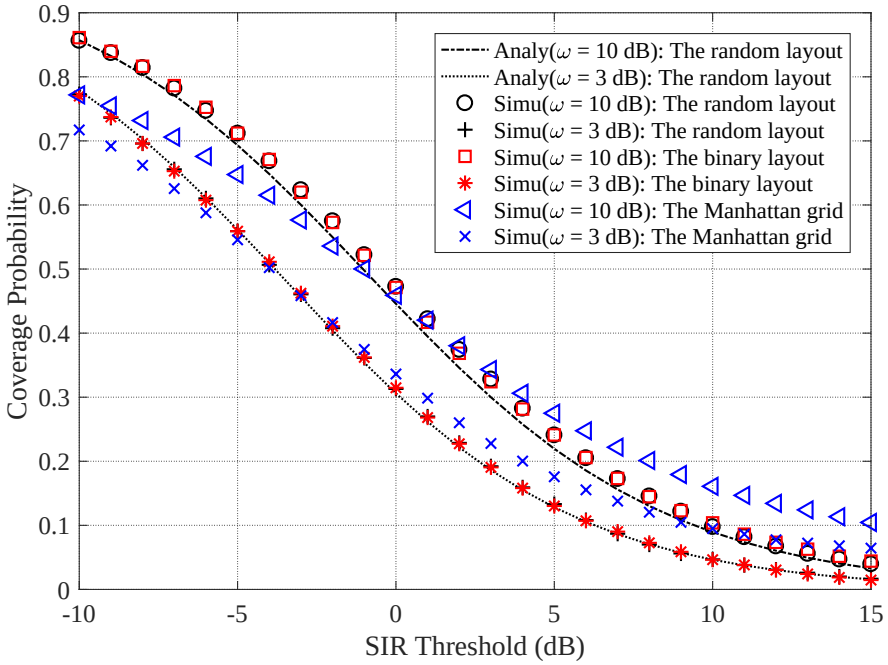

Figure 3.9: The analytical and simulation results of coverage probability for the nearest LOS connectivity case with the SINR Threshold under the three typical wall layout, for different wall attenuation taken as 10 dB and 3 dB, respectively.

may have some limitations or approximations when it comes to accurately capturing the performance of the Manhattan grid layout. Furthermore, it is evident that the coverage probability of these three interior wall layout is influenced by the wall attenuation. The larger wall attenuation leads to a bigger difference between the analytical and simulation results, especially for the Manhattan grid. This suggests that the impact of wall attenuation should be carefully considered in indoor SCN design and analysis, as it can significantly affect the network performance and coverage probability.

Figure 3.10 presents the analytical results of coverage probability with varying threshold for two different interior wall densities $\lambda = 0.05, 0.1, , \mathrm{m}^{-2}$, under the nearest LOS BS connectivity scenario with penetrable walls and the nearest LOS BS connectivity scenario with impenetrable walls. The comparison between the results of these two scenarios reveals interesting insights into the impact of interior wall characteristics on network performance. From the figure, it can be observed that the coverage probability

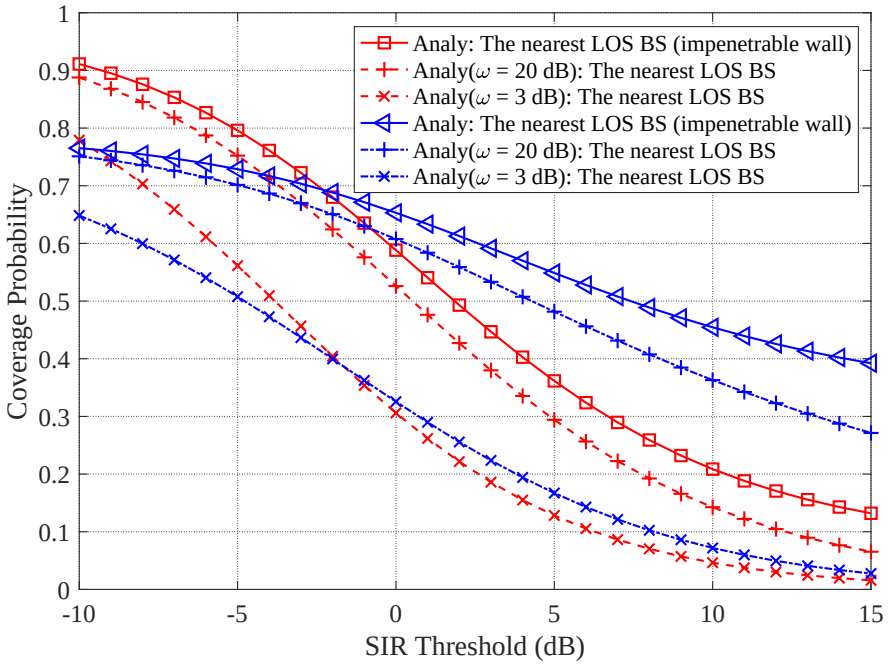

Figure 3.10: The analytical results of coverage probability under the nearest LOS BS connectivity scenario with penetrable wall and the nearest LOS BS connectivity scenario with impenetrable wall, for different BS density taken as $0.05, 0.1$ m^{-2}, respectively.

of the nearest LOS BS connectivity scenario with impenetrable walls is higher than that of the scenario with penetrable walls. This difference is more significant with smaller wall attenuation. The proposed analytical framework, which includes the effect of penetrable wall losses, offers a more accurate representation of the network performance in indoor scenarios. This is because the model with impenetrable interior walls neglects the impact of non-line-of-sight (NLOS) interference, which can be substantial in indoor environments. Moreover, the proposed model with penetrable wall losses is more practical for indoor environments, as it can considers the different materials used for interior walls and SC BS that may lead to different signal penetration characteristics. By incorporating penetrable wall losses, the proposed model captures the complex interactions between LOS and NLOS links, which are critical for accurately analysing indoor SCN performance. The results in Figure 3.10 emphasize the importance of considering the effect of interior wall characteristics on indoor SCN performance. The proposed

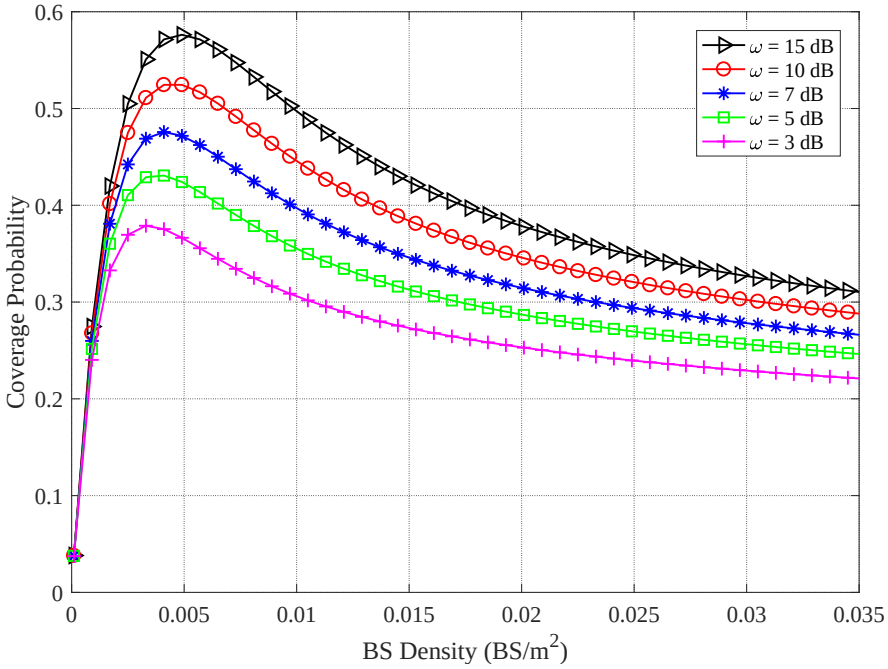

Figure 3.11: The analytical results of coverage probability under nearest LOS connectivity case with BS densities, for the different wall attenuations and SINR threshold T = 0 dB.

analytical framework with penetrable wall losses provides a more comprehensive and practical model for network design and optimization in realistic indoor scenarios.

Figure 3.11 illustrates the analytical results of the coverage probability under the nearest LOS BS connectivity scenario for different wall attenuations ($\omega = 3, 5, 7, 10, 15$ dB) as a function of the BS density. It can be observed that the coverage probability initially increases rapidly with the BS density, indicating that a higher density of BSs improves the coverage probability. However, after reaching a certain turning point, the coverage probability starts to decrease rapidly with further increases in the BS density. This turning point represents the optimal BS density that maximizes the coverage probability. It can be observed that the coverage probability initially increases rapidly with the BS density, indicating that a higher density of BSs improves the coverage probability. However, after reaching a certain turning point, the coverage probability starts to decrease rapidly with further increases in the BS density. This turning point represents

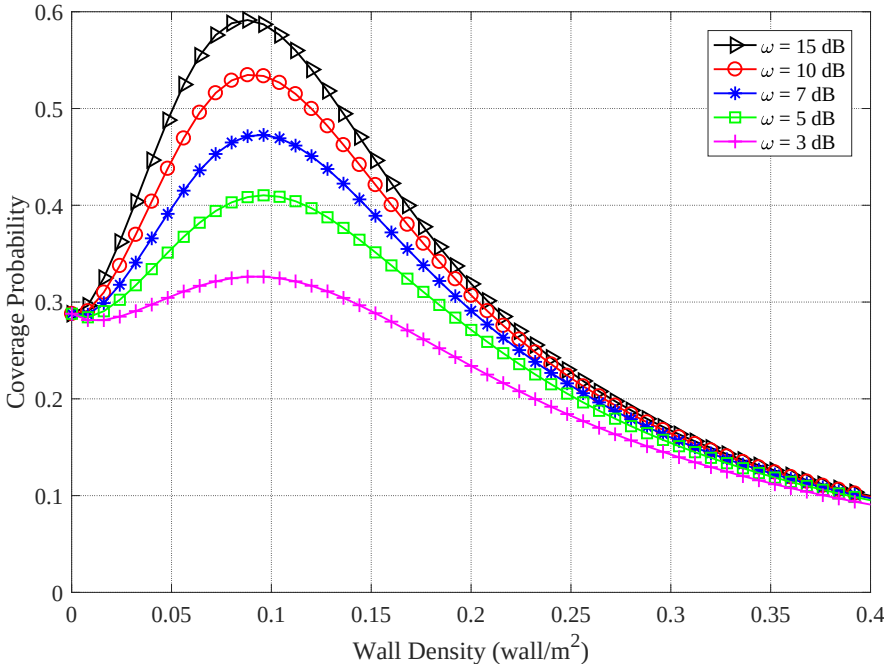

Figure 3.12: The analytical results of downlink coverage probability under nearest LOS connectivity case with different wall density, for the different wall attenuations and SINR threshold T = 0 dB.

the optimal BS density that maximizes the coverage probability. Furthermore, it can be observed that the coverage probability is relatively low when the BS density is much smaller than the density of wall blockages. This is because, in such cases, the typical UE is less likely to be served by the closest LOS BS, resulting in lower coverage probability.

Figure 3.12 illustrates the analytical results of the downlink coverage probability under the nearest LOS BS connectivity scenario for different wall attenuations ($\omega = 3, 5, 7, 10, 15$ dB) as a function of the wall density. It can be observed that the downlink coverage probability initially increases with the increase of the wall density, reaching a maximum value at a certain optimal wall density. This indicates that a higher density of interior walls improves the coverage probability. However, beyond the optimal wall density, the coverage probability starts to decline quickly. This suggests that there is an optimal wall density that maximizes the coverage performance. Furthermore, it can be

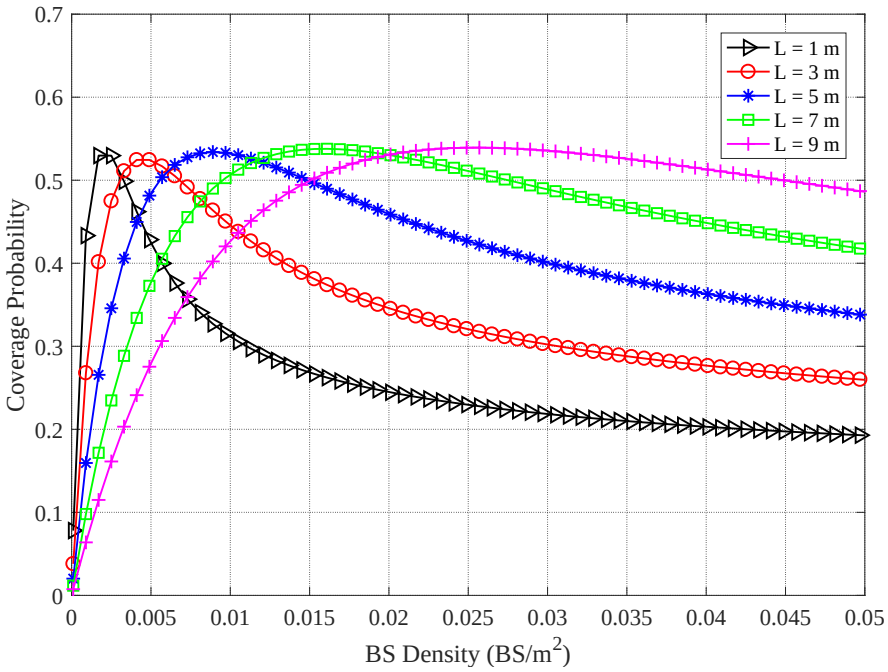

Figure 3.13: The analytical results of coverage probability under nearest LOS connectivity case with BS density, for the different average wall lengths. SINR threshold T = 0 dB and wall attenuation ω = 10 dB.

noted that there is no significant disparity in coverage probability among different wall attenuations when the wall density is sufficiently high. This implies that the impact of wall attenuation on coverage probability diminishes as the wall density increases.

Figure 3.13 illustrates the analytical results of the downlink coverage probability under the nearest LOS BS connectivity scenario for different average wall lengths ($L = 1, 3, 5, 7, 9$ m) as a function of the BS density, with a fixed wall attenuation of $\omega = 10$ dB. It can be observed that the coverage probability initially increases rapidly with the increase of the BS density. However, as the BS density continues to increase, the growth rate of the coverage probability slows down, eventually reaching a saturation point. This indicates that a higher BS density improves the coverage probability, but beyond a certain point, the impact becomes less significant. Furthermore, when comparing the curves for different average wall lengths, it can be seen that the coverage probability exhibits more variability for lower average wall lengths. This suggests that

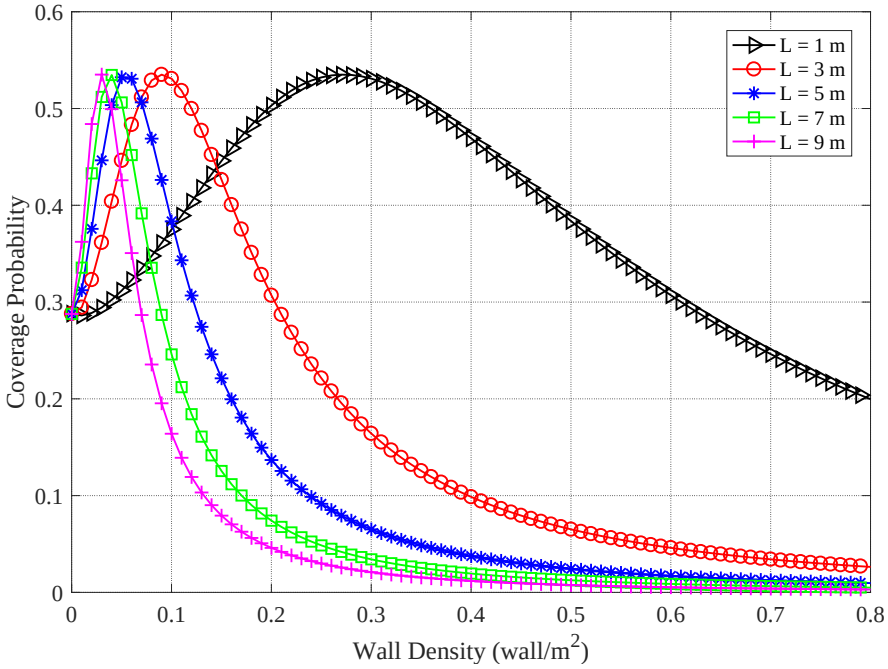

Figure 3.14: The analytical results of coverage probability under nearest LOS connectivity case with wall density, for the different average wall lengths. SINR threshold T = 0 dB and wall attenuation ω = 10 dB.

the average wall length has a significant effect on the performance of the proposed SCN model. The average wall length directly affects the LOS probability, which in turn affects the coverage probability. Therefore, it is important to consider the average wall length when analyzing and designing indoor SCNs.

Figure 3.14 displays the analytical results of the downlink coverage probability under the nearest LOS BS connectivity scenario for different average wall lengths ($L = 1, 3, 5, 7, 9$ m) as a function of the wall density, with a fixed wall attenuation of $\omega = 10$ dB. It can be observed that the coverage probability initially increases rapidly and reaches a peak value with a relatively low wall density. However, as the wall density continues to increase, the coverage probability decreases rapidly. This suggests that a certain level of wall density is necessary to achieve a high coverage probability, but beyond that point, an excessive number of wall blockages can severely degrade the coverage probability. Furthermore, when comparing the curves for different average

wall lengths, it can be seen that the coverage probability exhibits a more pronounced change for lower average wall lengths. This indicates that the average wall length has a significant impact on the sensitivity of the coverage probability to changes in the wall density. In other words, a lower average wall length leads to a more drastic change in the coverage probability with a relatively low wall density.

3.5 Conclusion

In this chapter, I have presented a comprehensive analysis of indoor SCNs considering the effects of blockages. We proposed a system model that incorporates the impact of interior wall blockages into the path loss model and adopts the nearest LOS UAS. By considering stochastic geometry, we developed an analytical framework for evaluating the downlink coverage probability in the presence of interior wall penetration losses. The expression for the downlink coverage probability is derived, taking into account the effects of wall attenuation.

The analytical results were validated through extensive Monte Carlo simulations, and we investigated the reasons for any deviations observed between the analytical and simulation results. Our findings emphasized the significance of wall attenuation in accurately analysing indoor SCNs. The numerical results revealed the sensitivity of the nearest LOS BS connectivity to wall attenuation. We observed that there exists an optimal BS density and wall density that maximize the coverage probability for different wall attenuations under the nearest LOS BS connectivity. These results provide valuable insights for optimizing the deployment and performance of indoor SCNs.

Additionally, our analysis highlighted the impact of the average wall length on the performance of the proposed SCN model. We demonstrated that the average wall length

plays a significant role in shaping the coverage probability and should be carefully considered in network design and optimization.

In conclusion, the analysis in this chapter provides valuable insights into the impact of interior wall blockages and wall attenuation on the performance of small-cell networks under the nearest LOS BS UAS. The derived analytical model offers a deeper understanding of how these factors influence the coverage probability in indoor environments. These insights can guide network planners in making informed decisions and optimizing parameter settings to achieve maximum coverage probability in practical indoor network scenarios. By taking into account the effects of interior walls and wall attenuation, network planners can design more efficient and reliable indoor small-cell networks, meeting the increasing demands for high-quality wireless communication services in indoor environments. The findings of this chapter serve as a foundation for further research and improvements in indoor network design and optimization.

Chapter 4

The Effect of Interior Wall Penetration Losses on Indoor Small-Cell Networks under NLOS BS User Association Strategy

4.1 Introduction

In this chapter, I extend the analysis of the indoor SC network model proposed in Chapter 3 to consider the nearest NLOS BS UAS. I derive the expressions of downlink coverage probability, taking into account the interior wall penetration loss, for this scenario. Additionally, I develop a simplified analysis for the nearest NLOS connectivity under dense interior walls. To validate the analytical coverage probability of the proposed SCN model, I perform Monte Carlo simulations and compare the results. The numerical results provide insights into the performance of the network and allow for a

comprehensive understanding of the impact of various parameters.

Overall, this chapter contributes to a deeper understanding of the performance of the considered indoor SC network model, considering nearest NLOS UAS. The analytical results are supported by simulation results, enhancing the credibility of the proposed model and analysis.

The remaining part of this chapter is organized as follows. Section 4.2 provides a brief introduction to the system model. In Section 4.3, the analytical expressions for the downlink coverage probability under the nearest NLOS BS UAS are derived. Additionally, a simplification of the SCN model and coverage probability is discussed. Section 4.4 presents the numerical and simulation results and provides discussions based on the findings. Finally, in Section 4.5, the chapter concludes with key insights and implications.

4.2 System Model

In this section, we maintain the same indoor scenario as described in Chapter 3. However, in this chapter, we specifically focus on the UAS that serves as the closest NLOS BS. This UAS is represented in Figure 4.1. Unlike in the previous chapter, where we primarily analysed the impact of wall blockages on the downlink coverage probability under the nearest LOS BS UAS, here we consider the power of NLOS links. Consequently, we cannot neglect the effect of thermal noise, and the analysis is based on the Signal-to-Interference-plus-Noise Ratio (SINR). This allows us to more accurately evaluate the performance of the indoor SC network in the presence of NLOS links.

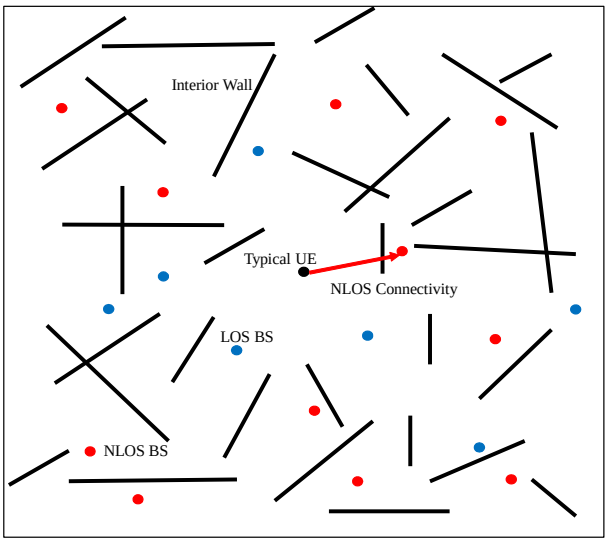

Figure 4.1: The NLOS UAS. The red solid line represents the serving link between the UE and the closest NLOS BS.

4.2.1 The Signal-to-Interference-plus-Noise Ratio

Based on the received power of UE (3.1), the SINR can be rewritten as

$$\begin{aligned}\mathrm{SINR}_j &= \frac{\eta_0 p_T h_j S_j d_j^{-\alpha}}{\sum\limits_{m\in\Phi_\mathrm{L}/j} \eta_0 p_T h_m S_m d_m^{-\alpha} + \sum\limits_{n\in\Phi_\mathrm{N}/j} \eta_0 p_T h_n S_n d_n^{-\alpha} + N_0} \\ &= \frac{h_j S_j d_j^{-\alpha}}{I_\mathrm{L} + I_\mathrm{N} + \frac{N_0}{\eta_0 p_T}}.\end{aligned} \tag{4.1}$$

4.3 Downlink Coverage Probability

In this section, the expressions for the downlink coverage probability under the closest NLOS BS UAS are derived. The assumption is made that the interior walls and links are independent of each other, enabling an analysis of their individual effects on the coverage probability. This approach allows for a comprehensive assessment of the network's performance and provides insights into the impact of NLOS links on coverage

in indoor environments.

4.3.1 The Typical UE Association with the Closest NLOS BS

In this section, the UAS is that the UE is served by the closest NLOS BS, shown as the red solid line in Figure 4.1. Other links are considered interferences to the UE. Moreover, the length of the serving link is defined as R^{N}. Thus, the coverage probability of UE association with the closest NLOS BS can be computed as

$$P_c^{\mathrm{N}}(T) = \int_0^D \mathbb{P}\left[\mathrm{SIR} > T | R^{\mathrm{N}}\right] f_{R^{\mathrm{N}}}(r)\mathrm{d}r, \tag{4.2}$$

where R^{N} is the length of the serving link between the UE and the closest NLOS BS, $f_{R^{\mathrm{N}}}(r)$ is the PDF of R^{N} and $\mathbb{P}[SIR > T|R^{\mathrm{N}}]$ denotes the coverage probability conditioned on the shortest NLOS link with the length R^{N}.

4.3.1.1 PDF of the Distance between the Closest NLOS BS and the Typical UE

Following the assumption in Section 3.3.1.1, the event E_3 is defined as $E_3 = \{$all the BSs are LOS to the UE in round area $C(O,r)\}$, then the probability of event E_3 conditioned on the event E_1 is computed as

$$\begin{aligned}\mathbb{P}(E_3|E_1) &= \left[\int_0^r P_{\mathrm{L}}(t)\frac{2t}{r^2}\mathrm{d}t\right]^n \\ &= \left[\frac{2M(r)}{r^2}\right]^n.\end{aligned} \tag{4.3}$$

Then, the CCDF of R_N is computed as

$$\mathbb{P}\{R^{\mathrm{N}} > r\} = \mathbb{P}(E_3)$$

$$
\begin{aligned}
&= \sum_{n=0}^{\infty} \mathbb{P}(E_3|E_1)\mathbb{P}(E_1) \\
&= \sum_{n=0}^{\infty} \left[\frac{2M(r)}{r^2}\right]^n \frac{e^{-\pi r^2\mu}(\pi r^2\mu)^n}{n!} \\
&= e^{-\pi r^2\mu} \sum_{n=0}^{\infty} \frac{\left[\frac{2M(r)}{r^2}\pi r^2\mu\right]^n}{n!} \\
&= e^{-\pi r^2\mu\left[1-\frac{2M(r)}{r^2})\right]}, \qquad (4.4)
\end{aligned}
$$

and the PDF of R^{N} can be calculated by differentiating the CDF of it, so the $f_{R^{\mathrm{N}}}(r)$ can be present as

$$
\begin{aligned}
f_{R^{\mathrm{N}}}(r) &= \frac{\mathrm{d}F_{R^{\mathrm{N}}}(r)}{\mathrm{d}r} \\
&= 2\pi r\mu e^{-\pi\mu\left[r^2-2M(r)\right]}(1-e^{-\beta r}). \qquad (4.5)
\end{aligned}
$$

The derivation procedure is omitted here.

4.3.1.2 Coverage Probability

The coverage probability conditioned on the shortest length of NLOS link, $\mathbb{P}\left[SIR > T|R^{\mathrm{N}}\right]$, is given by

$$
\begin{aligned}
&\mathbb{P}\left\{\frac{S_j h_j d_j^{-\alpha}}{I_{\mathrm{L}}+I_{\mathrm{N}}+\frac{N_0}{\eta_0 p_T}} > T \middle| R^{\mathrm{N}} = r\right\} \\
=&\mathbb{P}\left\{h_j > \left(\sum_{m\in\Phi_{\mathrm{L}},d_m\in(0,D)} h_m S_m d_m^{-\alpha} + \sum_{n\in\Phi_{\mathrm{N}}/j,d_n\in(r,D)} h_n S_n d_n^{-\alpha} + \frac{N_0}{\eta_0 p_T}\right) T r^{\alpha} S_j^{-1}\right\} \\
=&\mathbb{E}\left[\exp\left(-\left(\sum_{m\in\Phi_{\mathrm{L}},d_m\in(0,D)} h_m S_m d_m^{-\alpha} + \sum_{n\in\Phi_{\mathrm{N}}/j,d_n\in(r,D)} h_n S_n d_n^{-\alpha} + \frac{N_0}{\eta_0 p_T}\right) T r^{\alpha} S_j^{-1}\right)\right] \\
\overset{(a)}{=}&\mathbb{E}\left[\prod_{m\in\Phi_{\mathrm{L}},d_m\in(0,D)} \mathbb{E}_{h_m}\left[\exp\left(-h_m d_m^{-\alpha} T r^{\alpha}\omega^{-\mathbb{E}[K_j]}\right)\right] \times \right. \\
&\left. \prod_{n\in\Phi_{\mathrm{N}}/j,d_n\in(r,D)} \mathbb{E}_{h_n}\left[\exp\left(-h_n d_n^{-\alpha} T r^{\alpha}\omega^{-\mathbb{E}[K_j]}\omega^{\mathbb{E}[K_n]}\right)\right] \times \exp\left(-\frac{N_0}{\eta_0 p_T} T r^{\alpha}\omega^{-\mathbb{E}[K_j]}\right)\right]
\end{aligned}
$$

$$
\begin{aligned}
=&\mathbb{E}\left[\prod_{m\in\Phi_{\mathrm{L}},d_m\in(0,D)}\frac{d_m^{\alpha}}{d_m^{\alpha}+Tr^{\alpha}\omega^{-\mathbb{E}[K_j]}}\right] \quad \times \\
&\mathbb{E}\left[\prod_{n\in\Phi_{\mathrm{N}}/j,d_n\in(r,D)}\frac{d_n^{\alpha}}{d_n^{\alpha}+Tr^{\alpha}\omega^{-\mathbb{E}[K_j]}\omega^{\mathbb{E}[K_n]}}\right] \quad \times \quad \exp\left(-\frac{N_0}{\eta_0 p_T}Tr^{\alpha}\omega^{-\mathbb{E}[K_j]}\right) \\
\overset{(b)}{=}&\exp\Bigg(-2\pi\left[\int_0^{\infty}\mu P_{\mathrm{L}}(t)\left[1-\frac{t^{\alpha}}{t^{\alpha}+Tr^{\alpha}\omega^{-\beta r}}\right]t\mathrm{d}t \quad + \right. \\
&\left.\int_r^{\infty}\mu P_{\mathrm{N}}(t)\left[1-\frac{t^{\alpha}}{t^{\alpha}+Tr^{\alpha}\omega^{\beta(t-r)}}\right]t\mathrm{d}t\right]\Bigg)\times\exp\left(-\frac{N_0}{\eta_0 p_T}Tr^{\alpha}\omega^{-\beta r}\right) \\
=&\exp\Bigg(-2\pi\mu\left[\int_0^{\infty}e^{-\beta t}\left[1-\frac{t^{\alpha}}{t^{\alpha}+Tr^{\alpha}\omega^{-\beta r}}\right]t\mathrm{d}t \quad + \right. \\
&\left.\int_r^{\infty}(1-e^{-\beta t})\left[1-\frac{t^{\alpha}}{t^{\alpha}+Tr^{\alpha}\omega^{\beta(t-r)}}\right]t\mathrm{d}t\right]\Bigg)\times\exp\left(-\frac{N_0}{\eta_0 p_T}Tr^{\alpha}\omega^{-\beta r}\right),
\end{aligned}
\tag{4.6}
$$

where the steps (a) and (b) have been presented in the (3.19). Besides, $S_j=\omega^{\mathbb{E}[K_j]}=\omega^{\beta r}$.

Thus, the coverage probability under the NLOS UAS is computed by combining (4.5) and (4.6) as

$$
\begin{aligned}
&P_c^{\mathrm{N}}(T) \\
&=\int_0^{D}\left\{\mathbb{P}\left[\frac{S_j h_j d_j^{-\alpha}}{I_{\mathrm{L}}+I_{\mathrm{N}}+\frac{N_0}{\eta_0 p_T}}>T\middle|R^{\mathrm{N}}=r\right]f_{R^{\mathrm{N}}}(r)\right\}\mathrm{d}r \\
&=\int_0^{D}2\pi r\mu e^{-\pi\mu\left[r^2-2M(r)\right]}(1-e^{-\beta r})\exp\Bigg(-2\pi\mu\left[\int_0^{\infty}e^{-\beta t}\left[1-\frac{t^{\alpha}}{t^{\alpha}+Tr^{\alpha}\omega^{-\beta r}}\right]t\mathrm{d}t+\right. \\
&\left.\int_r^{\infty}(1-e^{-\beta t})\left[1-\frac{t^{\alpha}}{t^{\alpha}+Tr^{\alpha}\omega^{\beta(t-r)}}\right]t\mathrm{d}t\right]\Bigg)\exp\left(-\frac{N_0}{\eta_0 p_T}Tr^{\alpha}\omega^{-\beta r}\right)\mathrm{d}r.
\end{aligned}
\tag{4.7}
$$

4.3.2 Simplified NLOS User Association Strategy under a High Density of Interior Walls

In the indoor environment, the presence of interior walls limits the existence of LOS links. In this section, we simplify the analysis by assuming that there are no LOS links under high-density interior walls. This simplification allows us to focus on the performance analysis of the SCN model specifically for NLOS links. Consequently, the coverage probability calculations only consider the NLOS links, and the serving BS is determined as the closest BS. This simplification not only streamlines the performance analysis of the SCN model under high-density interior walls, but also facilitates efficient calculations.

Hence, the SINR can be expressed as

$$\begin{aligned}\mathrm{SINR}_j =& \frac{\eta_0 p_T h_j S_j d_j^{-\alpha}}{\sum\limits_{i\in\Phi/j} \eta_0 p_T h_i S_i d_i^{-\alpha} + N_0} \\ =& \frac{h_j S_j d_j^{-\alpha}}{I_{\mathrm{N}} + \frac{N_0}{\eta_0 p_T}}.\end{aligned} \tag{4.8}$$

4.3.2.1 PDF of the Distance between the Closest BS and the Typical UE

Based on the assumption of a high density of interior walls, we select the closest BS to serve the UE, ensuring that no other link length is shorter than R_s^{N}. The PDF of R_s^{N} can be determined by the null probability of the BSs' PPP, which is given by $\exp(-\mu A)$, where A denotes the size of the indoor area. Consequently, the CCDF of R_s^{N} can be

calculated using the following relationship [100]:

$$\begin{aligned}\mathbb{P}\{R_s^{\mathrm{N}} > r\} =& \mathbb{P}[\text{No length of links shorter than r}] \\ =& \exp(-\mu\pi r^2).\end{aligned} \tag{4.9}$$

Therefore, the CDF of the serving link is $\mathbb{P}[R_s^{\mathrm{N}} \leq r] = F_{R_s^{\mathrm{N}}}(r) = 1 - \exp(-\mu\pi r^2)$ and the PDF of R_s^{N} can be calculated as

$$\begin{aligned}f_{R_s^{\mathrm{N}}}(r) =& \frac{\mathrm{d}F_{R_s^{\mathrm{N}}}(r)}{\mathrm{d}r} \\ =& 2\pi\mu r e^{-\mu\pi r^2}.\end{aligned} \tag{4.10}$$

4.3.2.2 Coverage Probability

The coverage probability conditioned on the shortest length of link $P\left[SIR > T | R_s^{\mathrm{N}}\right]$ can be computed as

$$\begin{aligned}&\mathbb{P}\left\{\frac{S_j h_j d_j^{-\alpha}}{I_{\mathrm{N}} + \frac{N_0}{\eta_0 p_T}} > T | R_s^{\mathrm{N}} = r\right\} \\ =&\mathbb{P}\left\{h_j > \left(\sum_{i\in\Phi/j, d_i\in(0,D)} h_i S_i d_i^{-\alpha} + \frac{N_0}{\eta_0 p_T}\right) T r^{\alpha} S_j^{-1}\right\} \\ =&\mathbb{E}\left[\exp\left(-\left(\sum_{i\in\Phi/j, d_i\in(0,D)} h_i S_i d_i^{-\alpha} + \frac{N_0}{\eta_0 p_T}\right) T r^{\alpha} S_j^{-1}\right)\right] \\ \overset{(a)}{=}&\mathbb{E}\left[\prod_{i\in\Phi/j, d_i\in(0,D)} \mathbb{E}_{h_i}\left[\exp\left(-h_i \omega^{\mathbb{E}[K_i]} d_i^{-\alpha} T r^{\alpha} \omega^{-\mathbb{E}[K_j]}\right)\right]\right] \times \exp\left(-\frac{N_0}{\eta_0 p_T} T r^{\alpha} \omega^{-\mathbb{E}[K_j]}\right) \\ =&\mathbb{E}\left[\prod_{i\in\Phi/j, d_i\in(0,D)} \frac{d_i^{\alpha}}{d_i^{\alpha} + T r^{\alpha} \omega^{-\mathbb{E}[K_j]} \omega^{\mathbb{E}[K_i]}}\right] \times \exp\left(-\frac{N_0}{\eta_0 p_T} T r^{\alpha} \omega^{-\mathbb{E}[K_j]}\right) \\ \overset{(b)}{=}&\exp\left(-2\pi\mu \int_r^D \left[1 - \frac{t^{\alpha}}{t^{\alpha} + T r^{\alpha} \omega^{\beta(t-r)}}\right] t\mathrm{d}t\right) \times \exp\left(-\frac{N_0}{\eta_0 p_T} T r^{\alpha} \omega^{-\beta r}\right) \\ =&\exp\left(-2\pi\mu \int_r^D \left[\frac{T r^{\alpha} \omega^{\beta(t-r)}}{t^{\alpha} + T r^{\alpha} \omega^{\beta(t-r)}}\right] t\mathrm{d}t\right) \times \exp\left(-\frac{N_0}{\eta_0 p_T} T r^{\alpha} \omega^{-\beta r}\right),\end{aligned} \tag{4.11}$$

where the steps (a) and (b) have been presented in the (3.19). Besides, $S_j = \omega^{\mathbb{E}[K_j]} = \omega^{\beta r}$ and $S_i = \omega^{\mathbb{E}[K_i]} = \omega^{\beta t}$.

Therefore, based on (4.10) and (4.11), the unconditional coverage probability $P_{c,s}^{\mathrm{N}}(T)$ for the case, which the NLOS UAS under a high density of interior walls, can be calculated as

$$
\begin{aligned}
&P_{c,s}^{\mathrm{N}}(T) \\
&= \int_0^D \left\{ \mathbb{P}\left[\frac{S_j h_j d_j^{-\alpha}}{I_{\mathrm{N}} + \frac{N_0}{\eta_0 p_T}} > T \middle| R_s^{\mathrm{N}} = r \right] f_{R_s^{\mathrm{N}}}(r) \right\} \mathrm{d}r \\
&= \int_0^D 2\pi\mu r e^{-\mu\pi r^2} \exp\left(-2\pi\mu \int_r^D \left[\frac{T r^{\alpha} \omega^{\beta(t-r)}}{t^{\alpha} + T r^{\alpha} \omega^{\beta(t-r)}} \right] t \mathrm{d}t \right) \exp\left(-\frac{N_0}{\eta_0 p_T} T r^{\alpha} \omega^{-\beta r} \right) \mathrm{d}r.
\end{aligned}
\tag{4.12}
$$

4.4 Numerical Results and Analysis

In this wok, in order to verify the accuracy of the analytical results obtained from our proposed model, we conducted Monte Carlo simulations for two UAS scenarios with different wall attenuation. The simulation parameters used in these experiments are summarized in Table I, which provides important information regarding the simulation setup and system parameters [106]. By comparing the simulation results with the analytical results, we can assess the validity of our proposed model and evaluate its performance in practical scenarios.

A. The Nearest NLOS Connectivity

Figure 4.2 presents the results of coverage probability for the NLOS BS UAS scenario with different wall attenuations, based on the derived expression (4.2). The coverage

Table 4.1: Parameters for Numerical Simulations and Analysis in Chapter 4

Parameter	**Value**
maximum link length	20 m
Transmit power	$p_T = 24$ dBm
AWNG power	$N_0 = -95$ dBm
Path loss at reference distance	$\eta_0 = -38.5$ dB
BSs density	$\mu = 0.01$ m^{-2}
Wall density	$\lambda = 0.05$ m^{-2}
Wall Orientation	$\psi_k \in [0, \pi)$
Wall attenuation	$\omega = 3, 7, 10$ dB
Average width of walls	$L = 3$ m
Path-loss exponent	$\alpha = 2$
Simulation times	10^5

probability is influenced by the wall attenuation, as it affects the interference levels in the network. The curves in Figure 4.2 demonstrate a strong agreement between the analytical results and the Monte Carlo simulations, validating the accuracy of our proposed model. It is interesting to note that the NLOS BS UAS is particularly suitable for scenarios with low wall attenuation, such as 5 dB or smaller as mentioned in [110]. This indicates that the performance of the NLOS BS UAS is more sensitive to the wall attenuation compared to the LOS BS UAS scenario discussed in Chapter 3. The influence of wall attenuation is more pronounced in this connectivity due to the NLOS nature of the links. These findings highlight the significance of considering wall attenuation in the analysis and optimization of indoor SCNs, especially when employing NLOS BS UAS.

Figure 4.3 illustrates the comparison between the analytical and simulation results of coverage probability with wall attenuation under the nearest NLOS BS connectivity. The curves representing the analytical results align closely with the Monte Carlo simulation results, indicating the accuracy of our derived expression for coverage probability. It is observed that the coverage probability exhibits a decrease with the increase in

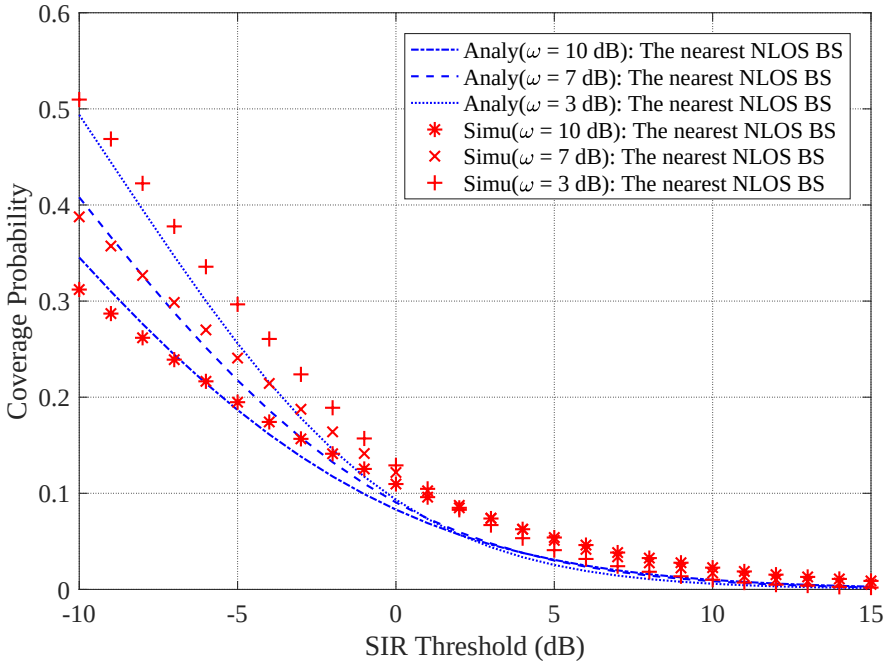

Figure 4.2: The analytical and simulation results of coverage probability under the nearest NLOS BS connectivity with different wall attenuation taken as 10 dB, 7 dB and 3 dB, respectively.

wall attenuation, while maintaining the same SINR threshold. This trend suggests that higher wall attenuation can reduce the coverage probability in the nearest NLOS BS connectivity scenario. The reduction in interference from NLOS links and the decrease in received signal due to increased wall attenuation contribute to this reduction in coverage probability. The results presented in Figure 4.3 highlight the importance of considering wall attenuation in indoor SCN design and analysis, as it can have a significant impact on network performance, especially in scenarios with NLOS BS connectivity.

Figure 4.4 presents the comparison between the analytical and simulation results of the coverage probability with a SINR threshold under the three typical layout, considering different wall attenuations (ω) of 3 and 10 dB. The analytical results are obtained using (4.7), while the simulation results are based on 10^5 Monte Carlo repetitions. From the figure, we can observe a small gap between the two sets of results for random layout and binary orientation layout. This indicates that the analytical model provides a reasonably

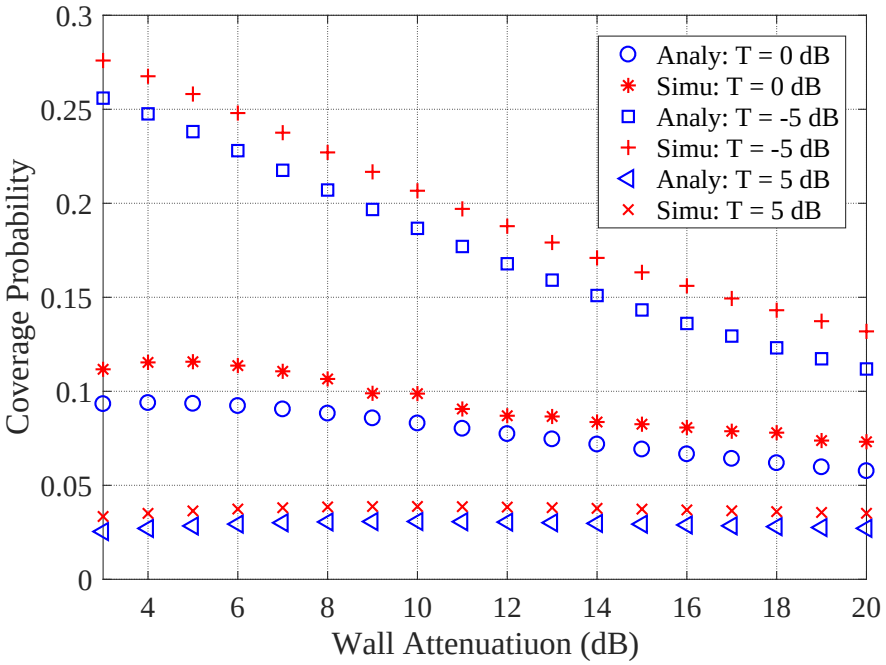

Figure 4.3: The analytical and simulation results of coverage probability under nearest NLOS connectivity case with wall attenuations, for SIR threshold $T = -5, 0, 5$ dB.

accurate estimation of the coverage probability for these two layouts. However, there is a bigger disparity in the analytical results for the Manhattan grid layout. This suggests that the analytical model may have some limitations or approximations when it comes to accurately capturing the performance of the Manhattan grid layout. The difference between the analytical and simulation results could be attributed to the complexity of the Manhattan grid layout and the interactions between walls and links. Furthermore, it is evident that the coverage probability of these three interior wall layouts is influenced by the wall attenuation. A larger wall attenuation leads to a bigger difference between the analytical and simulation results, especially for the Manhattan grid layout. This highlights the importance of considering the impact of wall attenuation in indoor SCN design and analysis, as it can significantly affect the network performance and coverage probability. Careful consideration of wall attenuation can lead to more accurate and reliable results in practical scenarios.

Figure 4.5 shows the analytical results of coverage probability with varying threshold

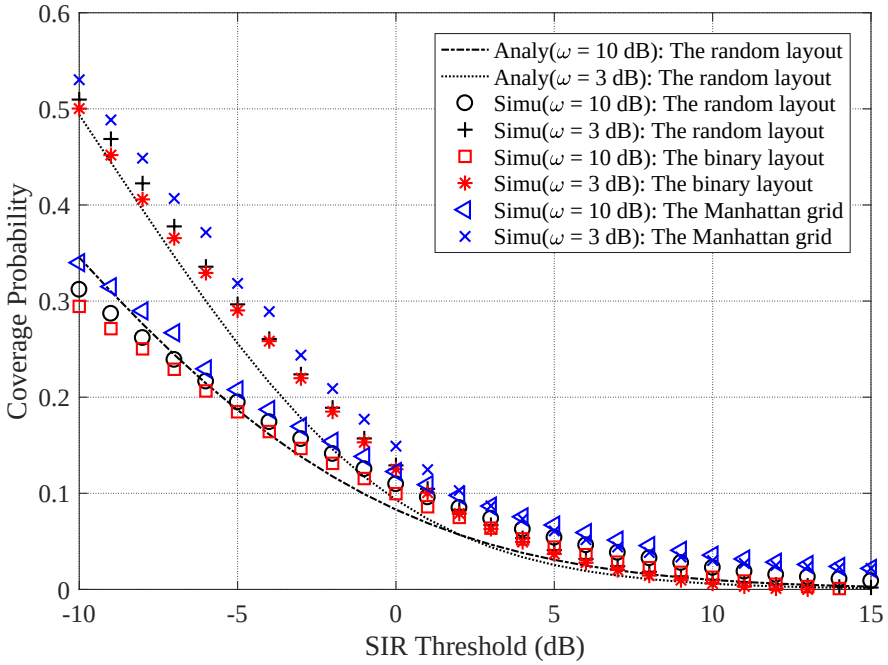

Figure 4.4: The analytical and simulation results of coverage probability for the nearest LOS connectivity case with the SINR Threshold under the three typical interior wall layout, for different wall attenuation taken as 10 dB and 3 dB, respectively.

for different SC densities $\mu = 0.001, 0.01, 0.1$ m^{-2}, under the nearest LOS BS connectivity scenario in chapter 3 and NLOS BS connectivity scenario in chapter 4. Comparing the results among different BS densities, it can be observed that the coverage probability of NLOS connectivity is higher than that of LOS connectivity at a low BS density. This is because at low BS densities, the typical UE is more likely to be served by NLOS BSs, which have lower path losses due to interior wall penetration losses. As a result, the coverage probability under NLOS connectivity is higher than that under LOS connectivity. However, as the small-cell density increases, the coverage probability of LOS connectivity becomes much larger than that of NLOS connectivity. This is because at higher BS densities, the typical UE is more likely to be served by LOS BSs, which have higher path losses due to the presence of more interfering walls. Despite the higher path losses, the stronger received signals from LOS BSs lead to improved coverage probability under LOS connectivity. Therefore, the UAS (LOS or NLOS) is

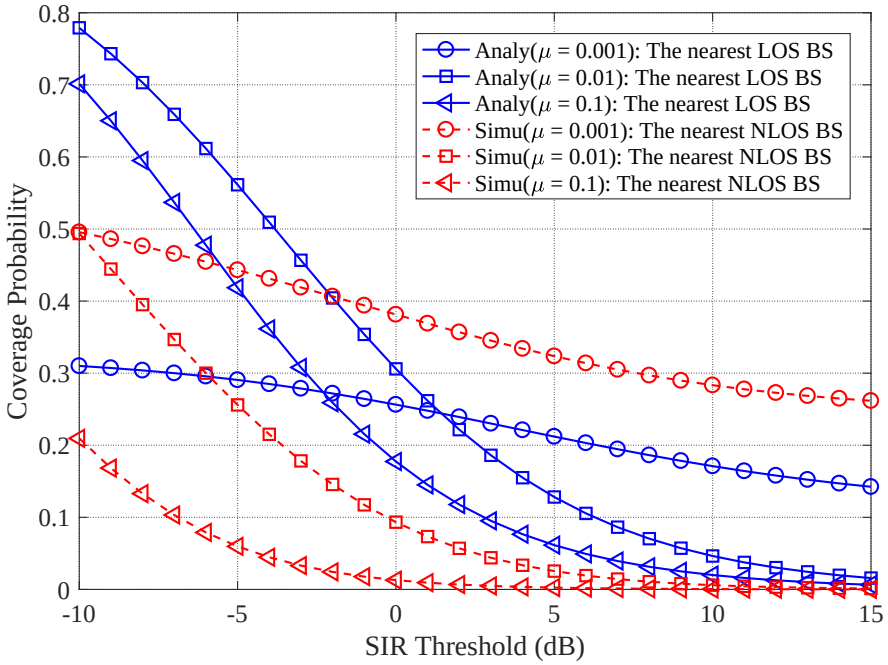

Figure 4.5: The analytical results of coverage probability under the nearest LOS BS connectivity scenario in chapter 3 and NLOS BS connectivity scenario in chapter 4, for different BS density taken as $0.001, 0.01, 0.1$ m^{-2}, respectively.

important factors that influence the network performance and coverage probability in indoor SCNs. The results in Figure 4.5 highlight the significance of considering these factors when designing and analyzing indoor SCNs.

Figure 4.6 displays the analytical results of coverage probability with varying BS densities for different wall attenuations $\omega = 3, 5, 7, 10, 15$ dB, under the nearest NLOS BS connectivity scenario. It is observed that the gaps between the curves representing different wall attenuations are relatively small, indicating that wall attenuation has a limited influence on the performance of the SCN model with dense BSs under NLOS BS UAS. The coverage probability does not exhibit a strict proportionality to the BS density when the UE is served by the closest NLOS transmitter. Instead, there exists an optimal BS density that maximizes the coverage probability. The initial rapid increase in coverage probability with increasing BS density is due to the availability of more LOS interference-free links. However, as the BS density continues to increase, the cov-

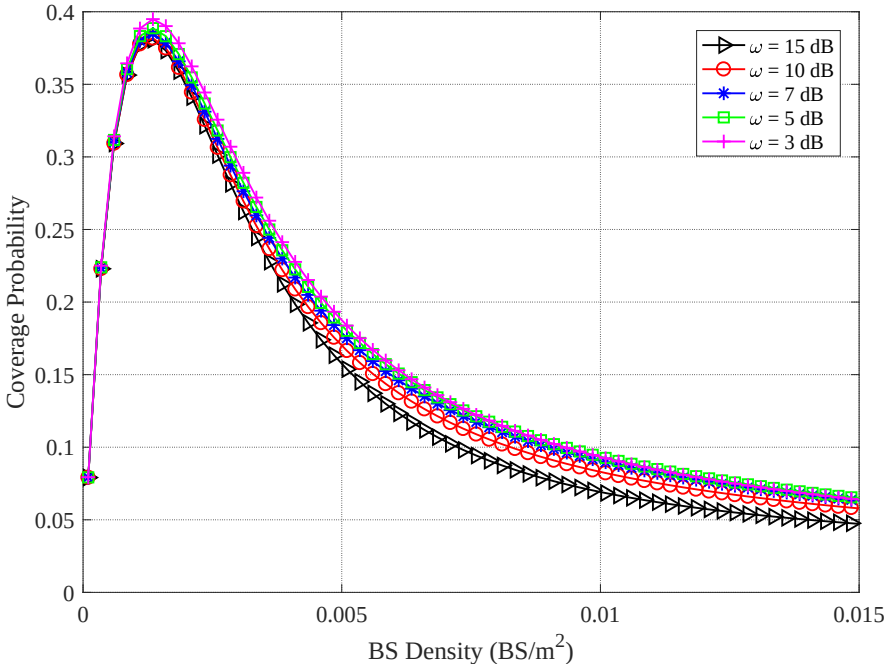

Figure 4.6: The analytical results of coverage probability under nearest NLOS connectivity case with BS densities, for wall attenuations $\omega = 3, 5, 7, 10, 15$ dB and SIR threshold $T = 0$ dB.

erage probability experiences a rapid decline. This behaviour can be attributed to the dominant effect of LOS interferences in densely populated networks. It is worth noting that the coverage probability tends to be lower in scenarios with a sufficient number of BSs. This is because in such cases, the interference from LOS links becomes the limiting factor for achieving higher coverage probability under NLOS BS UAS.

Figure 4.7 presents the analytical results of coverage probability under nearest NLOS BS connectivity with varying BS densities for different wall attenuations $\omega = 3, 5, 7, 10,$ 15 dB. The figure illustrates that the coverage probability initially increases to a maximum value as the wall density increases. However, with a further increase in wall density, the coverage probability starts to decline. The initial increase in coverage probability can be attributed to the decrease in the power of both serving and interfering links. As the wall density increases, the penetration loss caused by interior walls leads to a reduction in the power of the interfering links, resulting in improved coverage

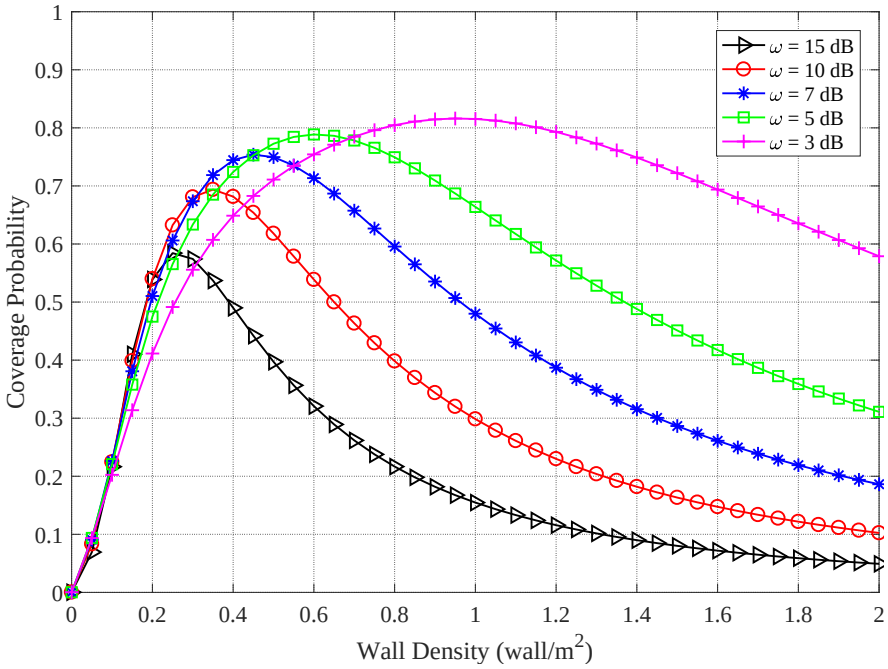

Figure 4.7: The analytical results of coverage probability under nearest NLOS connectivity case with different wall density, for wall attenuations $\omega = 3, 5, 7, 10, 15$ dB and SINR threshold $T = 0$ dB.

probability. However, as the wall density continues to increase, the power of the serving link also decreases. This decrease in power, combined with the increasing noise power, leads to a gradual decline in coverage probability. At high wall densities, the coverage probability is primarily influenced by the power of the AWGN since the power of the serving link becomes comparable to the AWGN power. Under this conditions, further increasing the wall density has a limited impact on the coverage probability, as the noise power dominates the received signal power.

Figure 4.8 illustrates the analytical results of coverage probability under nearest NLOS BS connectivity with varying BS densities for different average wall lengths $L = 1, 3, 5, 7, 9$ m, assuming a fixed wall attenuation of $\omega = 10$ dB. The figure reveals several important observations. Firstly, the coverage probability initially increases rapidly as the BS density grows. This is because the denser BS deployment leads to a higher likelihood of having a closer NLOS BS to serve the UE, resulting in improved coverage.

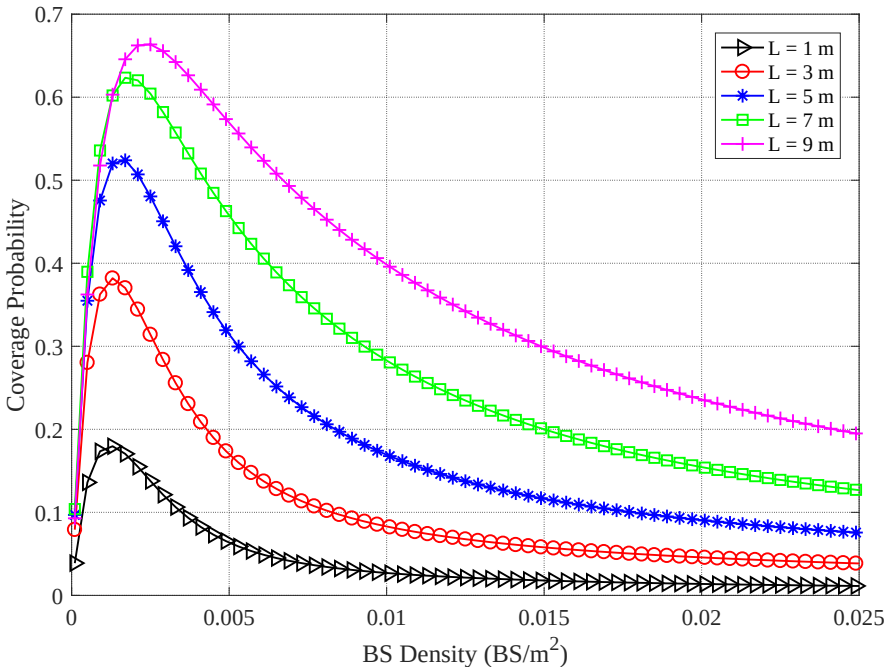

Figure 4.8: The analytical results of coverage probability under nearest NLOS connectivity with different BS density, for the average wall length $L = 1, 3, 5, 7, 9$ m, SINR threshold $T = 0$ dB and wall attenuation $\omega = 10$ dB.

However, after reaching a turning point, the coverage probability starts to decline with further increases in BS density. This decline is due to the increasing interference caused by the higher density of neighbouring BSs. Secondly, among the different average wall lengths, it is evident that the coverage probability exhibits more pronounced fluctuations for smaller average wall lengths. This is because a lower average wall length implies a higher likelihood of having more intersecting walls along the link, which leads to more variations in the received signal power and interference levels. Furthermore, the variance in coverage probability among different average wall lengths highlights the significant impact of average wall length on the performance of the proposed SCN model under nearest NLOS BS connectivity. The average wall length plays a crucial role in determining the LOS and NLOS probabilities, which in turn affect the coverage probability. Lastly, it is worth noting that for each average wall length, there exists an optimal BS density that maximizes the coverage probability. This optimal density rep-

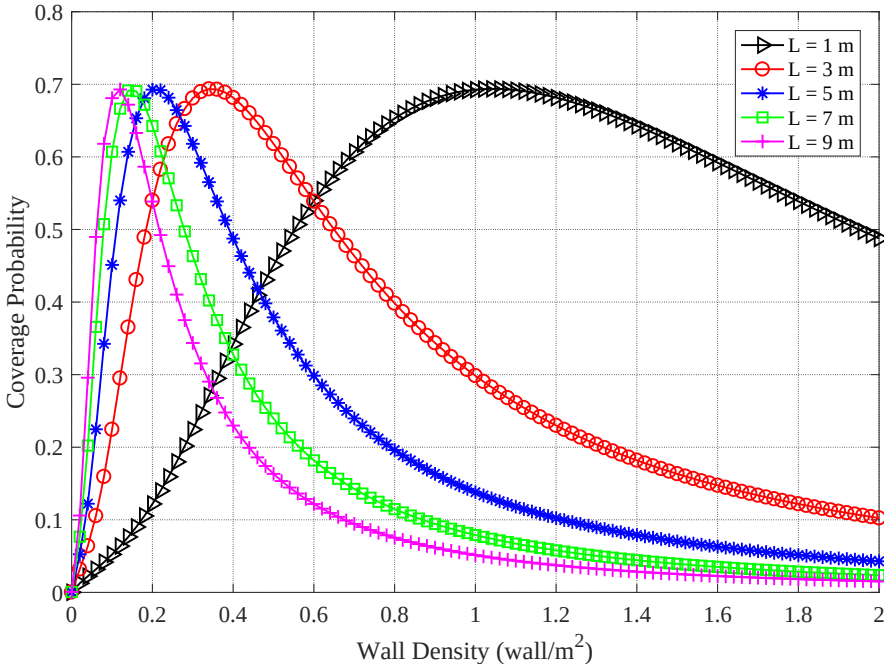

Figure 4.9: The analytical results of coverage probability under nearest NLOS connectivity with different wall density, for the average wall length $L = 1$, 3, 5, 7, 9 m, SINR threshold $T = 0$ dB and wall attenuation $\omega = 10$ dB.

resents a trade-off between having sufficient BSs to improve coverage and minimizing interference from neighboring BSs.

Figure 4.9 depicts the analytical results of coverage probability under nearest NLOS BS UAS connectivity for varying wall densities, considering different average wall lengths $L = 1, 3, 5, 7, 9$ m and a fixed wall attenuation of $\omega = 10$ dB. The figure reveals several important trends. Firstly, the coverage probability initially increases as the wall density increases, reaching a peak value. This behavior is due to the fact that as the wall density rises, the likelihood of having more interior walls intersecting with the links increases. This leads to a reduction in interference from NLOS links and an improvement in coverage probability. However, beyond a certain threshold of wall density, the coverage probability starts to decline. This decline can be attributed to the increasing attenuation caused by a higher density of interior walls, which reduces the received signal power and impacts the coverage. Secondly, among the different average wall lengths, it is

evident that the coverage probability exhibits a more significant change for higher average wall lengths. This indicates that the average wall length has a pronounced effect on the coverage probability. A higher average wall length results in a larger number of intersecting walls along the links, leading to more substantial variations in received signal power and interference levels, thereby influencing the coverage probability.

B. Simplified The Nearest NLOS Connectivity under Dense Interior Wall

For numerical analyses and simulations in this section, the default values for the parameters are listed in Table I. The density of interior walls is chosen as $\lambda = 1\text{m}^{-2}$ for the dense interior wall scenario. These parameter values provide a baseline for evaluating the performance of the proposed SCN model under the nearest NLOS BS UAS connectivity. It is important to note that these values can be adjusted according to specific indoor environments and deployment scenarios to accurately reflect the characteristics of the network being studied.

Figure 4.10 presents the results of coverage probability with different wall attenuations based on the expression of coverage probability (4.12). The curves show a good agreement between the analytical results and simulations, indicating the accuracy of the derived expression. The coverage probability increases with the increase of wall attenuation, which is consistent with the intuition that higher wall attenuation reduces interference and improves coverage. The close match between the analytical and simulation results further validates the effectiveness of the proposed SCN model under the nearest NLOS BS UAS connectivity with a dense interior wall. The analytical expression captures the impact of wall attenuation on the coverage probability, allowing for a better understanding of the trade-offs between wall attenuation and network performance. The agreement between the analytical and simulation results also highlights the

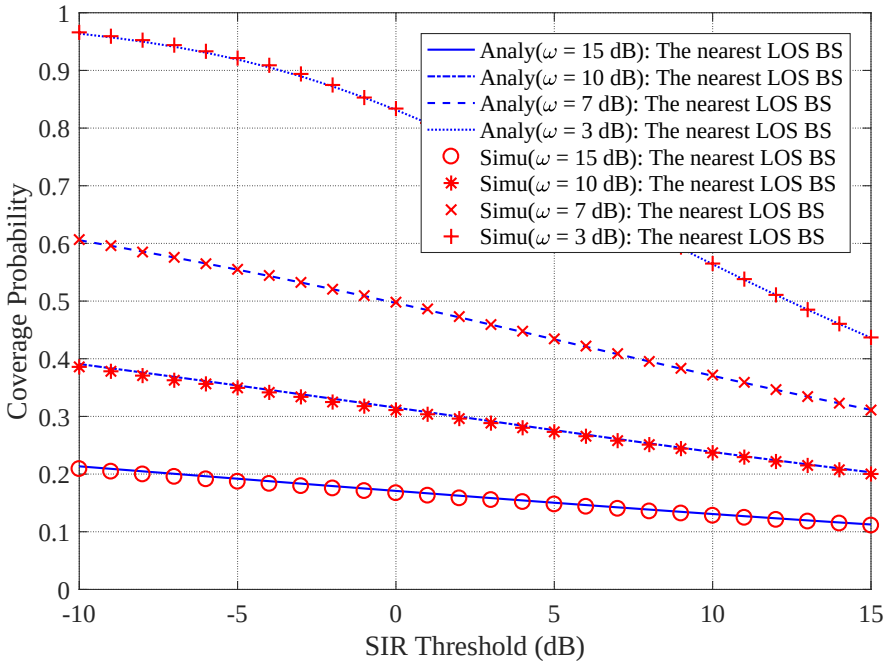

Figure 4.10: The analytical and simulation results of coverage probability under the nearest NLOS BS connectivity with a dense interior wall, for different wall attenuation taken as 3 dB, 7 dB, 10 dB and 15 dB, respectively.

robustness of the proposed model in predicting the coverage probability in real-world indoor SCN scenarios.

Figure 4.11 illustrates the comparison between the analytical and simulation results of coverage probability for wall attenuation under the nearest NLOS BS connectivity with a dense interior wall. The curves representing the analytical results align closely with the Monte Carlo simulation results, indicating the accuracy of our derived expression for coverage probability. It is observed that the coverage probability exhibits a significant decrease with the increase in wall attenuation while maintaining the same SINR threshold. This observation confirms the impact of wall attenuation on the network performance and coverage probability, especially in scenarios with dense interior walls. As the wall attenuation increases, the interior walls become more effective at reducing interference and received signal. The agreement between the analytical and simulation results demonstrates the reliability of our proposed model in analysing in-

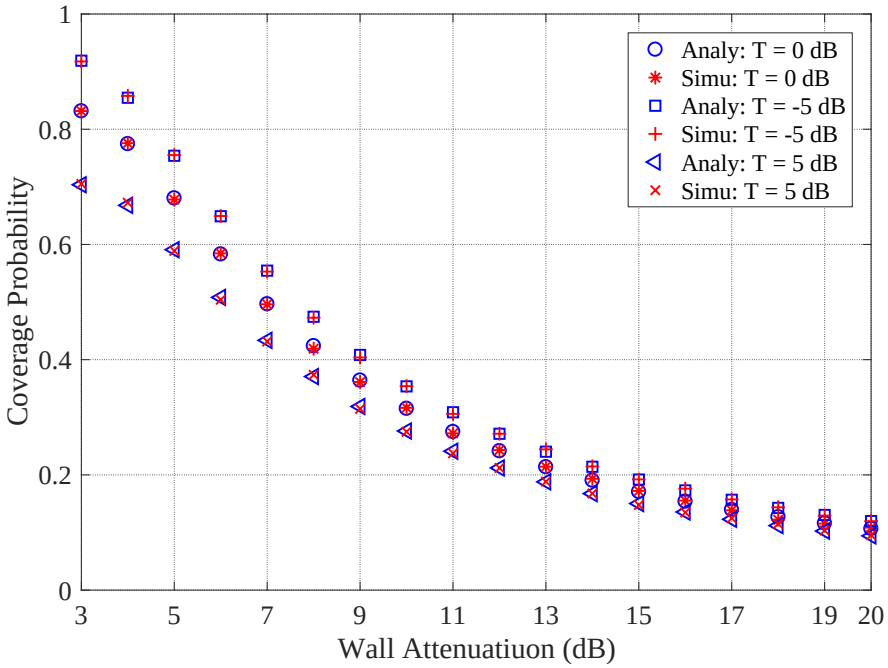

Figure 4.11: The analytical and simulation results of coverage probability under nearest NLOS connectivity case with a dense interior wall for wall attenuations, for SIR threshold $T = -5, 0, 5$ dB.

door SCN performance under the nearest NLOS BS UAS connectivity with a dense interior wall. The derived expression for coverage probability provides valuable insights into the trade-offs between wall attenuation, interior wall density, and network coverage.

Figure 4.12 shows the analytical results of coverage probability with varying threshold for different wall attenuations $\omega = 3, 7, 10, 15$ dB, under the nearest NLOS BS connectivity scenario and simplified the nearest NLOS BS connectivity scenario with a dense interior wall. The curves in the figure show the coverage probability for the two different mathematical framework. It can be observed that there is a minor gap between the curves, indicating that the simplified nearest NLOS BS connectivity scenario can be a good approximation for the nearest NLOS BS connectivity scenario with a dense interior wall. The simplified scenario involves assuming a high density of interior walls, which results in a large number of walls intersecting with each link. This simplifi-

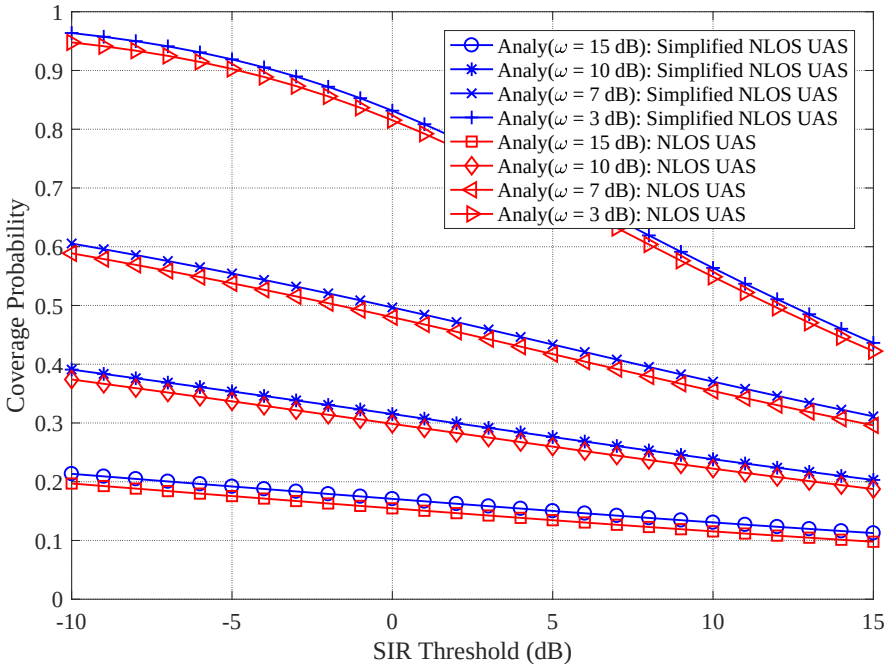

Figure 4.12: The analytical and simulation results of coverage probability under the two types nearest NLOS BS connectivity with a dense interior wall, for different wall attenuation taken as 3 dB, 7 dB, 10 dB and 15 dB, respectively.

cation allows for a more straightforward calculation of the coverage probability. The results in the figure suggest that the simplified scenario captures the essential characteristics of the coverage probability under the nearest NLOS BS connectivity with a dense interior wall. By using the simplified scenario, network designers and analysts can simplify their calculations while still obtaining reasonably accurate results. This provides a practical and efficient approach for evaluating the coverage performance of indoor SCNs under the nearest NLOS BS connectivity with a dense interior wall.

Overall, the results presented in Figures emphasize the importance of considering wall attenuation in indoor SCN design and optimization, as it can significantly affect the network performance and coverage probability in scenarios with dense interior walls.

4.5 Conclusion

In this chapter, the incorporation of interior wall penetration losses into the path loss model under the nearest NLOS BS UAS has been presented. The derived expression of downlink coverage probability based on the nearest NLOS BS connectivity provides valuable insights into the performance analysis of indoor SC networks. The results emphasize the significance of considering wall attenuation in the analysis of indoor SCNs, particularly under the nearest NLOS BS UAS scenario.

Comparing the results with the nearest LOS BS UAS in Chapter 3, it is evident that the coverage probability under the nearest NLOS BS UAS is more influenced by wall attenuation. The denser wall scenarios have a more pronounced impact on the performance of the nearest NLOS BS UAS. Thus, careful consideration and accurate modeling of wall attenuation are crucial for accurately assessing the performance of SCN under the nearest NLOS BS UAS. The numerical results highlight the sensitivity of the nearest NLOS BS UAS to BS density. There exists an optimal BS density that maximizes the coverage probability, considering a given wall density and different wall attenuations and average wall length. These findings provide valuable guidelines for network planning and optimization, emphasizing the importance of balancing BS density and wall density to achieve optimal coverage probability.

In conclusion, this chapter's analysis significantly enhances our understanding of how interior wall blockages and wall attenuation affect the performance of small-cell networks under the nearest NLOS BS UAS. The derived expressions and numerical results offer valuable insights for network designers and researchers to optimize indoor SCN deployments and improve coverage performance. By considering the impact of interior walls and wall attenuation, network planners can make informed decisions to maximize coverage and enhance the overall performance of indoor small-cell networks. The find-

ings of this chapter provide a solid foundation for further research and advancements in indoor network design and optimization, ultimately leading to more efficient and reliable indoor wireless communication systems.

Chapter 5

The Effect of Interior Wall Penetration Losses on Indoor Small-Cell Networks under the Strongest Received Signal User Association Strategy

5.1 Introduction

In this chapter, the effect of interior wall penetration losses on the downlink coverage probability of an indoor SCN under the smallest path-loss user association is investigated.

The indoor SCN consists of small-cell BSs distributed according to an HPPP, and the interior walls are modelled using the random shape theory. The channel model incorporates various factors such as distance-dependent path loss, LOS probability, Rayleigh

fading, and wall penetration loss to capture the impact of interior wall blockages. The LOS probability follows an exponential model that decays exponentially with distance. The interior walls are randomly generated as lines on the ground plane, and their centers are distributed according to an HPPP. Using the constructed system model, the PDF of the distance between a typical user and its serving BS under the smallest path-loss UAS is derived. This PDF allows for the calculation of the downlink coverage probability, taking into account the interior wall penetration losses. The derived expression for coverage probability is validated through Monte Carlo simulations, considering different interior wall penetration losses, BS densities, and wall densities.

Additionally, the coverage probability of SCNs under three typical interior wall layouts (random layout, binary orientation, and Manhattan grid) is compared using simulations. These comparisons provide insights into the impact of interior wall penetration losses on the downlink coverage probability, offering valuable guidance for network planning and optimization.

Overall, this chapter contributes to a comprehensive understanding of the influence of interior wall penetration losses on the performance of indoor SCNs under the smallest path-loss UAS. The derived expressions and simulation results provide valuable insights for the design and optimization of indoor SCNs, considering the effects of interior wall blockages on coverage probability.

This chapter is organised along these lines. In Section 5.2, the system model and path-loss model are introduced. This model captures the key characteristics of an indoor small-cell network and provides a framework for analyzing the downlink coverage probability. The analytical expressions of downlink coverage probability under the smallest path-loss UAS are derived in Section 5.3. The derived expression considers the impact of interior wall penetration losses, enabling a quantification of the effect of wall

blockages on the coverage performance of the indoor small-cell network. In Section 5.4, numerical and simulation results are presented, and some discussions are drawn. The results provide insights into the effect of interior wall blockages on the downlink coverage probability and emphasize the significance of considering these blockages in the design and analysis of indoor small-cell networks. Finally, Section 5.5 summarizes the key findings of this chapter and draws conclusions regarding the impact of interior wall penetration losses on the downlink coverage probability of indoor small-cell networks.

5.2 System Model

In this section, an indoor SCN model is presented, where the BSs are generated by an HPPP and three typical layouts of the interior walls are considered. We propose a path-loss model comprised of the LOS probability, the large-scale path loss, small-scale fading, and interior wall penetration losses.

In this section, we introduce an indoor SCN model that incorporates the effects of interior walls. The BSs in the network are distributed according to an HPPP, which provides a random and realistic deployment pattern. To capture the diversity of indoor environments, we consider three typical layouts of the interior walls: random layout, binary orientation, and Manhattan grid. These layouts represent different levels of complexity and wall density in indoor spaces.

In our proposed path-loss model, we take into account several key factors. First, we consider the LOS probability, which determines the likelihood of a direct LOS link between a user and a BS. The LOS probability can decay with increasing distance due to obstacles such as walls and furniture in the environment.

Next, we incorporate the large-scale path loss, which accounts for the signal attenuation over distance. This path loss factor accounts for the decrease in signal power as the distance between the user and the BS increases. It is typically characterized by a distance-dependent exponent that determines the rate of power decay.

In addition, we consider small-scale fading, which captures the rapid fluctuations in signal strength due to multipath propagation and interference effects. Small-scale fading is commonly modelled as Rayleigh fading, which follows a complex Gaussian distribution.

Finally, we include the interior wall penetration losses in our path-loss model. These losses account for the additional signal attenuation caused by the presence of interior walls. The wall penetration losses depend on factors such as the number of walls intersecting the link, the length and orientation of the walls, and the material properties of the walls.

By incorporating these factors into our path-loss model, we aim to provide a comprehensive and accurate representation of the signal propagation characteristics in indoor SCNs. This model enables us to analyse and evaluate the performance of indoor SCN deployments under different interior wall layouts and wall penetration losses.

5.2.1 Path-Loss Model

In the considered indoor SCN model, the indoor area is represented as a 2-D plane. The typical UE is located at the center of the area, while the BSs are randomly distributed throughout the area according to an HPPP denoted by Φ. The density of the HPPP is represented by μ, which determines the average number of BSs per unit area.

In this chapter, we consider the use of the smallest path-loss UAS. Under this strategy,

each UE connects to the BS that provides the strongest downlink received signal, regardless of whether it is an LOS or NLOS link for the typical UE. The path loss in our system model can be expressed as

$$L(d_i) = \begin{cases} \eta_0 d_i^{-\alpha}, & \text{if the link is LOS} \\ S_i^{\mathrm{N}} \eta_0 d_i^{-\alpha}, & \text{if the link is NLOS} \end{cases}, \tag{5.1}$$

where η_0 is the path loss at the reference distance of 1 m, d_i represents the length of the i-th link, $i \in \Phi$, α is the path-loss exponent and S_i^{N} is the wall penetration loss for the NLOS link. Although LOS and NLOS links typically have different path-loss exponents, the introduction of the penetration loss of walls into the path-loss model allows the same distance-based path-loss exponent α for LOS and NLOS links. The wall penetration loss for the i-th NLOS link is $S_i^{\mathrm{N}} = \prod_{k=0}^{K_i} \omega = \omega^{K_i}$, where K_i is the number of walls intersecting with the i-th link and the attenuation of each wall is denoted by ω. The number of walls intersecting with the i-link is essential for deriving the wall penetration loss of NLOS links, and is affiliated with the layout of wall blockages. When considering the wall orientation as $\psi_k \in [0, \pi)$, the average number of interior walls intersecting with the i-th link can be calculated using Equation (3.4).

5.3 Downlink Coverage Probability

In this section, the downlink coverage probability is derived for the random layout with wall orientations $\psi_k \in [0, \pi)$, while considering tractability. The scenario assumes that the typical UE is served by the BS providing the strongest downlink received signal, which corresponds to the link with the smallest path loss. Additionally, the locations of wall blockages are assumed to be independent in this chapter, without considering correlation among wall blockages.

For the random layout with wall orientation $\psi_k \in [0, \pi)$, the probability of a link being LOS or NLOS is presented in 3.2.4. The probability that the i-th link is in the LOS condition is (3.11), and the probability that the i-th link is in the NLOS condition is (3.12). Therefore, the path loss model is expressed as

$$L_{\mathrm{R}}(d_i) \overset{(a)}{\approx} \begin{cases} \eta_0 d_i^{-\alpha}, & \text{with probability } P_{\mathrm{L}}(d_i) \\ \omega^{E[K_i]} \eta_0 d_i^{-\alpha}, & \text{with probability } P_{\mathrm{N}}(d_i) \end{cases}, \tag{5.2}$$

where step (a) is that the actual number of interior wall K_i is replaced by the average number of interior wall $E[K_i]$ for the purpose of mathematical tractability. Thus, the wall penetration loss for the i-th NLOS link can be derived as $S_i^{\mathrm{N}} = \omega^{E[K_i]}$. This means that the wall penetration loss of NLOS links can be characterized by the length of links.

Besides, the expression of SINR is expressed as

$$\begin{aligned} \mathrm{SINR} &= \frac{p_T h_j L(d_j)}{\sum\limits_{i \in \Phi / j, d_i \in (0,D)} p_T h_i L(d_i) + N_0} \\ &\approx \frac{p_T h_j L_{\mathrm{R}}(d_j)}{\sum\limits_{i \in \Phi_{\mathrm{L}} / j} p_T h_i L_{\mathrm{R}}(d_i) + \sum\limits_{i \in \Phi_{\mathrm{N}} / j} p_T h_i L_{\mathrm{R}}(d_i) + N_0} \\ &= \frac{p_T h_j L_{\mathrm{R}}(d_j)}{I_{\mathrm{L}} + I_{\mathrm{N}} + N_0}, \end{aligned} \tag{5.3}$$

where p_T represents the transmission power of a BS assuming all BSs have the same transmission power, D is the maximum length of links in the considered indoor scenario, N_0 is the power of AWGN, d_j represents the length of j-th link between the typical UE and its serving BS, h_i and h_j denote the power gains of Rayleigh fading for the j-th link and the i-th link, respectively, I_{L} and I_{N} denote the total interference powers received by the typical UE from LOS and NLOS interference links, respectively. Φ_{L} denotes the set of LOS BSs and Φ_{N} denotes the set of NLOS BSs.

The coverage probability represents the probability that the SINR of the typical UE is higher than a given threshold and is computed by

$$\begin{aligned} P_c(T) &= \mathbb{P}(\text{SINR} > T) \\ &= \hat{P_c^{\text{L}}}(T) + \hat{P_c^{\text{N}}}(T) \\ &= \int_0^D \mathbb{P}\left[\frac{p_T h_j L_{\text{R}}(d_{\text{LOS}_j})}{I_{\text{L}} + I_{\text{N}} + N_0} > T\right] \hat{f}_{\text{L}}(r)\mathrm{d}r + \int_0^D \mathbb{P}\left[\frac{p_T h_j L_{\text{R}}(d_{\text{NLOS}_j})}{I_{\text{L}} + I_{\text{N}} + N_0} > T\right] \hat{f}_{\text{N}}(r)\mathrm{d}r, \end{aligned} \tag{5.4}$$

where T is the threshold of SINR, d_{LOS_j} and d_{NLOS_j} are the length of the LOS and NLOS serving links, respectively, r is the length of the serving link, $\hat{f}_{\text{L}}(r)$ and $\hat{f}_{\text{N}}(r)$ are the PDFs of the distance r from the typical UE to its serving BS, when the serving BS is LOS or NLOS conditions, respectively.

5.3.1 PDF of the Distance between Typical UE and the BS with Smallest Path Loss

In this subsection, we analyze the distribution of the serving link in the smallest path-loss UAS scenario. In this scenario, the typical UE is served by the BS that provides the strongest downlink received signal. Therefore, the serving link corresponds to the link with the largest value of $L_{\text{R}}(d_i)$.

5.3.1.1 LOS Case

If the smallest path-loss link is LOS, the event E_4 can be defined as $E_4 = \{$The nearest BS located at the distance r has a LOS path to the typical UE$\}$. According to [34], the

CDF of event E_4 is

$$\begin{aligned} F_{\mathrm{L}}(r) &= 1 - e^{-\int_0^r P_{\mathrm{L}} 2\pi\mu t \mathrm{d}t} \\ &= 1 - e^{-\int_0^r e^{-\beta t} 2\pi\mu t \mathrm{d}t} \\ &= 1 - e^{-\frac{2\pi\mu[1-e^{-\beta r}(1+\beta r)]}{\beta^2}}, \end{aligned} \tag{5.5}$$

and the PDF of event E_4 is the derivative of CDF, derived as

$$\begin{aligned} f_{\mathrm{L}}(r) &= \frac{\mathrm{d}F_{\mathrm{L}}(r)}{\mathrm{d}r} \\ &= e^{-\int_0^r P_{\mathrm{L}} 2\pi\mu t \mathrm{d}t} \times P_{\mathrm{L}} 2\pi\mu r \\ &= 2\pi\mu r e^{-\beta r} e^{-\frac{2\pi\mu[1-e^{-\beta r}(1+\beta r)]}{\beta^2}}. \end{aligned} \tag{5.6}$$

Furthermore, the event E_5 is defined as $E_5 = \{$the UE is associated with a BS at distance $d_{\mathrm{LOS}_j}\}$. Specifically, the serving BS is assumed as the closest LOS BS to the UE, the event E_5 is conditioned on event E_1: $d_{\mathrm{LOS}_j} = r$. This assumption means there are no NLOS BSs outperforming the LOS BSs within distance r. The path-loss function of NLOS links $L_{\mathrm{R}}(d_{\mathrm{NLOS}_i})$ are always smaller than the path-loss function of the serving LOS link $L(r)$. Therefore, the minimum distance r_1 between the UE and the NLOS BSs can be computed by

$$r_1 = r\omega^{\frac{E[K_i]}{\alpha}}. \tag{5.7}$$

According to [34], the probability of E_5 conditioned on $d_{\mathrm{LOS}_j} = r$ can be computed by

$$\begin{aligned} \mathbb{P}[E_5 | d_{\mathrm{LOS}_j} = r] &= e^{-\int_0^{r_1} P_{\mathrm{N}} 2\pi\mu r \mathrm{d}r} \\ &= e^{-\int_0^{r_1} \left(1-e^{-\beta r}\right) 2\pi\mu r \mathrm{d}r} \\ &= e^{-2\pi\mu\left(\frac{r_1^2}{2} + \frac{e^{-\beta r_1}(1+\beta r_1)-1}{\beta^2}\right)}. \end{aligned} \tag{5.8}$$

Denoting C^{L} as the distance between the UE and its serving LOS BS, the CDF of C^{L} can be derived as

$$\begin{aligned}\overline{F}_{d_{\mathrm{LOS}_j}}(r) &= \mathbb{P}[C^{\mathrm{L}} > r] \\ &= \int_0^D \mathbb{P}[C^{\mathrm{L}} > r | d_{\mathrm{LOS}_j} = x] f_{\mathrm{L}}(x)\mathrm{d}x \\ &\overset{(a)}{=} \int_0^r 0 \times f_{\mathrm{L}}(x)\mathrm{d}x + \int_r^D \mathbb{P}[E_5 | d_{\mathrm{LOS}_j} = x] f_{\mathrm{L}}(x)\mathrm{d}x \\ &= \int_r^D \mathbb{P}[E_5 | d_{\mathrm{LOS}_j} = x] f_{\mathrm{L}}(x)\mathrm{d}x, \end{aligned} \tag{5.9}$$

in step (a), when $x \in (0, r]$, $\mathbb{P}[C^{\mathrm{L}} > r | d_{\mathrm{LOS}_j} = x] = 0$; when $x \in (r, D)$, $\mathbb{P}[C^{\mathrm{L}} > r | d_{\mathrm{LOS}_j} = x]$ equals to the probability of conditional event E_5, i.e., $\mathbb{P}[C^{\mathrm{L}} > r | d_{\mathrm{LOS}_j} = x] = \mathbb{P}[E_5 | d_{\mathrm{LOS}_j} = x]$.

Thus, the PDF of d_{LOS_j} is derived as

$$\begin{aligned}\hat{f}_{\mathrm{L}}(r) &= \mathbb{P}[E_5 | d_{\mathrm{LOS}_j} = r] f_{\mathrm{L}}(r) \\ &= e^{-\int_0^{r_1} P_{\mathrm{N}} 2\pi\mu t \mathrm{d}t} \times e^{-\int_0^{r} P_{\mathrm{L}} 2\pi\mu t \mathrm{d}t} \times P_{\mathrm{L}} 2\pi\mu r, \end{aligned} \tag{5.10}$$

using (3.11), the PDF can be rewritten as

$$\hat{f}_{\mathrm{L}}(r) = 2\pi\mu r e^{-\beta r} \times e^{-2\pi\mu\left(\frac{1-e^{-\beta r}(1+\beta r)}{\beta^2}\right)} \times e^{-2\pi\mu\left(\frac{r_1^2}{2} + \frac{e^{-\beta r_1}(1+\beta r_1)-1}{\beta^2}\right)}. \tag{5.11}$$

5.3.1.2 NLOS Case

For the smallest path-loss NLOS connectivity, the event E_6 is defined as $E_6 = \{$The nearest BS located at the distance r has an NLOS path to the typical UE$\}$. Similar to

(5.6), the PDF of event E_6 is obtained as

$$f_{\mathrm{N}}(r) = e^{-\int_0^r P_{\mathrm{N}} 2\pi\mu t \mathrm{d}t} \times P_{\mathrm{N}} 2\pi\mu r. \tag{5.12}$$

The event E_7 is defined as $E_7 = \{$the UE is associated with a BS at distance d_{NLOS_j}, where $d_{NLOS_j} = r\}$, which means the UE is served by the closest NLOS BS, i.e., the path-loss function of a LOS link $L(d_{LOS_i})$ is always smaller than the path-loss function of the NLOS serving link $L(r)$. Therefore, the minimum distance r_2 between the UE and the LOS BSs can be computed by

$$r_2 = r\omega^{-\frac{E[K_i]}{\alpha}}. \tag{5.13}$$

Then, the probability of event E_7 conditioned on $d_{NLOS_j} = r$ can be derived as

$$\mathbb{P}[E_7 | d_{\mathrm{NLOS}_j} = r] = e^{-\int_0^{r_2} P_{\mathrm{L}} 2\pi\mu t \mathrm{d}t}. \tag{5.14}$$

Denoting C^{N} as the distance between the typical UE and its serving NLOS BS, the CDF of C^{N} can be derived as

$$\begin{aligned}
\overline{F}_{d_{\mathrm{NLOS}_j}}(r) &= \mathbb{P}[C^{\mathrm{N}} > r] \\
&= \int_0^D \mathbb{P}[C^{\mathrm{N}} > r | d_{\mathrm{NLOS}_j} = x] f_{\mathrm{N}}(x) \mathrm{d}x \\
&\overset{(a)}{=} \int_0^r 0 \times f_{\mathrm{N}}(x) \mathrm{d}x + \int_r^D \mathbb{P}[E_7 | d_{\mathrm{NLOS}_j} = x] f_{\mathrm{N}}(x) \mathrm{d}x \\
&= \int_r^D \mathbb{P}[E_7 | d_{\mathrm{NLOS}_j} = x] f_{\mathrm{N}}(x) \mathrm{d}x,
\end{aligned} \tag{5.15}$$

in step (a), when $x \in (0, r]$, $\mathbb{P}[C^{\mathrm{N}} > r | d_{\mathrm{NLOS}_j} = x] = 0$; when $x \in (r, D)$, $\mathbb{P}[C^{\mathrm{N}} > r | d_{\mathrm{NLOS}_j} = x]$ equals to the probability of conditional event E_5, i.e., $\mathbb{P}[C^{\mathrm{N}} > r | d_{\mathrm{NLOS}_j} =$

$x] = \mathbb{P}[E_5 | d_{\mathrm{NLOS}_j} = x]$.

Thus, the PDF of d_{NLOS_j} is derived as

$$\begin{aligned} \hat{f}_{\mathrm{N}}(r) &= \mathbb{P}[E_7 | d_{\mathrm{NLOS}_j} = r] f_{\mathrm{N}}(r) \\ &= e^{-\int_0^{r_2} P_{\mathrm{L}} 2\pi\mu t \mathrm{d}t} \times e^{-\int_0^{r} P_{\mathrm{N}} 2\pi\mu t \mathrm{d}t} \times P_{\mathrm{N}} 2\pi\mu r. \end{aligned} \tag{5.16}$$

Due to the penetration losses of interior walls, the path loss of an NLOS link is generally smaller than that of a LOS link with the same link length. Therefore, the calculation of (5.16) should be discussed by the numerical relationship among r, r_2 and the maximum link length D.

If the length range of the NLOS serving link r is $(0, r_D]$, the length range of NLOS interferences would accordingly be $[r, r_D]$ and the length range of LOS interferences would accordingly be $[r_2, D)$. Specifically, the value of r_D is delimited by D and r_2, where the possible maximum length of LOS links is D. Within the length range of the NLOS serving link, the LOS and NLOS interferences both exist. Substituting (3.11) and (3.12) into (5.16), the PDF of the typical UE connecting to nearest NLOS BS at distance r, where its range is within $(0, r_D]$, is rewritten as

$$\begin{aligned} \hat{f}^a_{\mathrm{N}}(r) &= \{\mathbb{P}[E_7 | d_{\mathrm{NLOS}_j} = r] f_{\mathrm{N}}(r) \,\big|\, 0 < r \le r_D\} \\ &= e^{(-\int_0^{r_2} P_{\mathrm{L}} 2\pi\mu t \mathrm{d}t)} \times e^{-\int_0^{r} P_{\mathrm{N}} 2\pi\mu t \mathrm{d}t} \times P_{\mathrm{N}} 2\pi\mu r \\ &= 2\pi\mu r(1 - e^{-\beta r}) \times e^{-2\pi\mu(\frac{r^2}{2} + \frac{e^{-\beta r}(1+\beta r)-1}{\beta^2})} \times e^{-2\pi\mu(\frac{1-e^{-\beta r_2}(1+\beta r_2)}{\beta^2})}. \end{aligned} \tag{5.17}$$

If the length range of the NLOS serving link r is (r_D, D), the length range of NLOS interferences would accordingly be $[r, D)$ and the possible minimum length of the LOS links r_2 exceeds the boundary of indoor area. Consequently, only the NLOS interfer-

ence exists. Substituting (3.12) into (5.16), the PDF of the typical UE connecting to nearest NLOS BS at distance r, where its range is within (r_D, D), is rewritten as

$$\begin{aligned}\hat{f}_{\mathrm{N}}^{b}(r) &= \{\mathbb{P}[E_7|d_{\mathrm{NLOS}_j}=r]f_{\mathrm{N}}(r)\,\big|\,r_D<r<D\}\\ &= e^{-\int_0^r P_{\mathrm{N}}2\pi\mu t\mathrm{d}t}\times P_{\mathrm{N}}2\pi\mu r\\ &= 2\pi\mu r(1-e^{-\beta r})\times e^{-2\pi\mu(\frac{r^2}{2}+\frac{e^{-\beta r}(1+\beta r)-1}{\beta^2})}. \end{aligned} \tag{5.18}$$

5.3.2 Coverage Probability

In this subsection, I derive the conditional coverage probabilities for the smallest path-loss UAS scenario. In this scenario, the typical UE can be associated with either a LOS BS or an NLOS BS. We analyse the coverage probabilities separately for these two cases.

The conditional coverage probability of the typical UE, when it is connected to a LOS BS, is computed by

$$\begin{aligned}&\mathbb{P}\left\{\frac{p_T h_j L_{\mathrm{R}}(d_{\mathrm{LOS}_j})}{I_{\mathrm{L}}+I_{\mathrm{N}}+N_0}>T|d_{\mathrm{LOS}_j}=r,0<r<D\right\}\\ =&\mathbb{P}\left\{h_j>\left(\sum_{m\in\Phi_{\mathrm{L}}/j,d_m\in[r,D)}p_T h_m L_{\mathrm{R}}(d_m)\quad+\right.\right.\\ &\left.\left.\sum_{n\in\Phi_{\mathrm{N}},d_n\in[r_1,D)}p_T h_n L_{\mathrm{R}}(d_n)+N_0\right)\frac{T}{p_T}L_{\mathrm{R}}(d_j)^{-1}\right\}\\ =&\mathbb{E}\left[\exp\left(-\left(\sum_{m\in\Phi_{\mathrm{L}}/j,d_m\in[r,D)}h_m L_{\mathrm{R}}(d_m)\quad+\right.\right.\right.\\ &\left.\left.\left.\sum_{n\in\Phi_{\mathrm{N}},d_n\in[r_1,D)}h_n L_{\mathrm{R}}(d_n)+\frac{N_0}{p_T}\right)TL_{\mathrm{R}}(d_j)^{-1}\right)\right]\\ =&\mathbb{E}\left[\prod_{m\in\Phi_{\mathrm{L}}/j,d_m\in[r,D)}\mathbb{E}_{h_m}\left[\exp\left(-h_m d_m^{-\alpha}Tr^{\alpha}\right)\right]\quad\times\right.\end{aligned}$$

$$
\begin{aligned}
&\prod_{n\in\Phi_{\mathrm{N}},d_n\in[r_1,D)} \mathbb{E}_{h_n}\left[\exp\left(-h_n d_n^{-\alpha} T r^{\alpha}\omega^{E[K_n]}\right)\right]\times\exp\left(-\frac{N_0}{p_T\eta_0}Tr^{\alpha}\right)\Bigg] \\
=&\mathbb{E}\left[\prod_{m\in\Phi_{\mathrm{L}}/j,d_m\in[r,D)}\frac{d_m^{\alpha}}{d_m^{\alpha}+Tr^{\alpha}}\right] \quad \times \\
&\mathbb{E}\left[\prod_{n\in\Phi_{\mathrm{N}},d_n\in[r_1,D)}\frac{d_n^{\alpha}}{d_n^{\alpha}+Tr^{\alpha}\omega^{E[K_n]}}\right]\times\exp\left(-\frac{N_0}{p_T\eta_0}Tr^{\alpha}\right) \\
\overset{(a)}{=}&\exp\Bigg(-2\pi\Bigg[\int_r^D \mu P_{\mathrm{L}(m)}\left[1-\frac{t^{\alpha}}{t^{\alpha}+Tr^{\alpha}}\right]t\mathrm{d}t \quad + \\
&\qquad\int_{r_1}^D \mu P_{\mathrm{N}(n)}\left[1-\frac{t^{\alpha}}{t^{\alpha}+Tr^{\alpha}\omega^{\beta t}}\right]t\mathrm{d}t\Bigg]\Bigg)\times\exp\left(-\frac{N_0}{p_T\eta_0}Tr^{\alpha}\right) \\
=&\exp\Bigg(-2\pi\mu\Bigg[\int_r^D e^{-\beta t}\left[1-\frac{t^{\alpha}}{t^{\alpha}+Tr^{\alpha}}\right]t\mathrm{d}t \quad + \\
&\qquad\int_{r_1}^D (1-e^{-\beta t})\left[1-\frac{t^{\alpha}}{t^{\alpha}+Tr^{\alpha}\omega^{\beta t}}\right]t\mathrm{d}t\Bigg]\Bigg)\times\exp\left(-\frac{N_0}{p_T\eta_0}Tr^{\alpha}\right),
\end{aligned}
\tag{5.19}
$$

where step (a) is obtained using the PGFL of PPP for the LOS and NLOS transmitters. The PGFL allows us to characterize the distribution of transmitters in the network. I calculate the densities of LOS and NLOS transmitters by incorporating the probabilities of LOS and NLOS links with the overall BS density μ.

Based on (5.10) and (5.19), the unconditional coverage probability of the LOS serving link with the smallest path-loss is computed by

$$
\begin{aligned}
&\hat{P}_c^{\mathrm{L}}(T) \\
&=\int_0^D\left\{\mathbb{P}\left[\frac{p_T h_j L_{\mathrm{R}}(d_{\mathrm{LOS}_j})}{I_{\mathrm{L}}+I_{\mathrm{N}}+N_0}>T\right]\hat{f}_{\mathrm{L}}(r)\middle|0<r<D\right\}\mathrm{d}r \\
&=\int_0^D 2\pi\mu r e^{-\beta r}\times e^{-2\pi\mu\left(\frac{1-e^{-\beta r}(1+\beta r)}{\beta^2}\right)}\times e^{-2\pi\mu\left(\frac{r_1^2}{2}+\frac{e^{-\beta r_1}(1+\beta r_1)-1}{\beta^2}\right)}\times \\
&\qquad\exp\left(-\frac{N_0}{p_T\eta_0}Tr^{\alpha}\right)\times\exp\Bigg[-2\pi\mu\left(\int_r^D e^{-\beta t}\left(1-\frac{t^{\alpha}}{t^{\alpha}+Tr^{\alpha}}\right)t\mathrm{d}t \quad +\right.
\end{aligned}
$$

$$\int_{r_1}^{D}\left(1-e^{-\beta t}\right)\left(1-\frac{t^{\alpha}}{t^{\alpha}+Tr^{\alpha}\omega^{\beta t}}\right)t\mathrm{d}t\Bigg)\Bigg]\mathrm{d}r. \tag{5.20}$$

When the typical UE is associated with an NLOS BS, the conditional coverage probability is influenced by the numerical relationship among r, r_2 and the maximum link length D in an indoor area. According to the discussion of NLOS cases in Section **??**, the range of serving link length is divided into $(0, r_D]$ and (r_D, D), where r_D can be derived by the relationship between r_2 and D.

According to the discussion of r in the NLOS case, the coverage probability conditioned on the length range of the serving NLOS link is $(0, r_D]$, where both the LOS and NLOS interferences exist, is given by

$$\begin{aligned}
&\mathbb{P}\left\{\frac{p_T h_j L_{\mathrm{R}}(d_{\mathrm{NLOS}_j})}{I_{\mathrm{L}}+I_{\mathrm{N}}+N_0} > T | d_{\mathrm{NLOS}_j}=r, 0<r\le r_D\right\}\\
=&\mathbb{P}\Bigg\{h_j > \Bigg(\sum_{m\in\Phi_{\mathrm{L}},d_m\in[r_2,D)} p_T h_m L_{\mathrm{R}}(d_m) \quad +\\
&\qquad\qquad \sum_{n\in\Phi_{\mathrm{N}}/j,d_n\in[r,r_D]} p_T h_n L_{\mathrm{R}}(d_n)+N_0\Bigg)\frac{T}{p_T}L_{\mathrm{R}}(d_j)^{-1}\Bigg\}\\
=&\mathbb{E}\Bigg[\exp\Bigg(-\Bigg(\sum_{m\in\Phi_{\mathrm{L}},d_m\in(r_2,D)} h_m L_{\mathrm{R}}(d_m) \quad +\\
&\qquad\qquad \sum_{n\in\Phi_{\mathrm{N}}/j,d_n\in[r,r_D]} h_n L_{\mathrm{R}}(d_n)+\frac{N_0}{p_T}\Bigg)TL_{\mathrm{R}}(d_j)^{-1}\Bigg)\Bigg]\\
=&\mathbb{E}\Bigg[\prod_{m\in\Phi_{\mathrm{L}},d_m\in[r_2,D)}\mathbb{E}_{h_m}\left[\exp\left(-h_m d_m^{-\alpha}Tr^{\alpha}\omega^{-E[K_j]}\right)\right] \quad\times\\
&\prod_{n\in\Phi_{\mathrm{N}}/j,d_n\in[r,r_D]}\mathbb{E}_{h_n}\left[\exp\left(-h_n d_n^{-\alpha}Tr^{\alpha}\omega^{-E[K_j]}\omega^{E[K_n]}\right)\right] \quad\times\\
&\qquad\qquad \exp\left(-\frac{N_0}{p_T\eta_0}Tr^{\alpha}\omega^{-E[K_j]}\right)\Bigg]
\end{aligned}$$

$$
\begin{aligned}
=&\mathbb{E}\left[\prod_{m\in\Phi_{\mathrm{L}},d_m\in[r_2,D)}\frac{d_m^{\alpha}}{d_m^{\alpha}+Tr^{\alpha}\omega^{-E[K_j]}}\right]\times\\
&\mathbb{E}\left[\prod_{n\in\Phi_{\mathrm{N}}/j,d_n\in[r,r_D]}\frac{d_n^{\alpha}}{d_n^{\alpha}+Tr^{\alpha}\omega^{-E[K_j]}\omega^{E[K_n]}}\right]\times\exp(-\frac{N_0}{p_T\eta_0}Tr^{\alpha}\omega^{-E[K_j]})\\
\overset{(a)}{=}&\exp\Bigg(-2\pi\Bigg[\int_{r_2}^{D}\mu P_{\mathrm{L}(m)}\left[1-\frac{t^{\alpha}}{t^{\alpha}+Tr^{\alpha}\omega^{-\beta r}}\right]t\mathrm{d}t\quad+\\
&\qquad\int_{r}^{r_D}\mu P_{\mathrm{N}(n)}\left[1-\frac{t^{\alpha}}{t^{\alpha}+Tr^{\alpha}\omega^{\beta(t-r)}}\right]t\mathrm{d}t\Bigg]\Bigg)\times\exp(-\frac{N_0}{p_T\eta_0}Tr^{\alpha}\omega^{-\beta r})\\
=&\exp\Bigg(-2\pi\mu\Bigg[\int_{r_2}^{D}e^{-\beta t}\left[1-\frac{t^{\alpha}}{t^{\alpha}+Tr^{\alpha}\omega^{-\beta r}}\right]t\mathrm{d}t\quad+\\
&\qquad\int_{r}^{r_D}(1-e^{-\beta t})\left[1-\frac{t^{\alpha}}{t^{\alpha}+Tr^{\alpha}\omega^{\beta(t-r)}}\right]t\mathrm{d}t\Bigg]\Bigg)\times\exp(-\frac{N_0}{p_T\eta_0}Tr^{\alpha}\omega^{-\beta r}),
\end{aligned}
\tag{5.21}
$$

where step (a) is obtained using the PGF of PPP for the LOS and NLOS transmitters.

Conditioned on the length range of the serving NLOS link being (r_D,D), the coverage probability, where the interferences only come from the NLOS links, is given by

$$
\begin{aligned}
&\mathbb{P}\left\{\frac{p_T h_j L_{\mathrm{R}}(d_{\mathrm{NLOS}_j})}{I_{\mathrm{N}}+N_0}>T|d_{\mathrm{NLOS}_j}=r,r_D<r<D\right\}\\
=&\mathbb{P}\left\{h_j>\left(\sum_{n\in\Phi_{\mathrm{N}}/j,d_n\in(r_D,D)}p_T h_n S_n d_n^{-\alpha}+N_0\right)\frac{T}{p_T}L_{\mathrm{R}}(d_j)^{-1}\right\}\\
=&\mathbb{E}\left[\exp\left(-\left(\sum_{n\in\Phi_{\mathrm{N}}/j,d_n\in(r_D,D)}h_n S_n d_n^{-\alpha}+\frac{N_0}{p_T}\right)TL_{\mathrm{R}}(d_j)^{-1}\right)\right]\\
=&\mathbb{E}\left[\prod_{n\in\Phi_{\mathrm{N}}/j,d_n\in(r_D,D)}\mathbb{E}_{h_n}\left[\exp\left(-h_n d_n^{-\alpha}Tr^{\alpha}\omega^{-E[K_j]}\omega^{E[K_n]}\right)\right]\right.\\
&\qquad\left.\times\quad\exp(-\frac{N_0}{p_T\eta_0}Tr^{\alpha}\omega^{-E[K_j]})\right]\\
=&\mathbb{E}\left[\prod_{n\in\Phi_{\mathrm{N}}/j,d_n\in(r_D,D)}\frac{d_n^{\alpha}}{d_n^{\alpha}+Tr^{\alpha}\omega^{-E[K_j]}\omega^{E[K_n]}}\right]\\
&\times\quad\exp(-\frac{N_0}{p_T\eta_0}Tr^{\alpha}\omega^{-E[K_j]})
\end{aligned}
$$

$$\begin{aligned}
&\overset{(a)}{=}\exp\left(-2\pi\left[\int_r^D \mu P_{\mathrm{N}(n)}\left[1-\frac{t^\alpha}{t^\alpha+Tr^\alpha\omega^{\beta(t-r)}}\right]t\mathrm{d}t\right]\right)\times\exp(-\frac{N_0}{p_T\eta_0}Tr^\alpha\omega^{-\beta r})\\
&=\exp\left(-2\pi\mu\left[\int_r^D (1-e^{-\beta t})\left[1-\frac{t^\alpha}{t^\alpha+Tr^\alpha\omega^{\beta(t-r)}}\right]t\mathrm{d}t\right]\right)\times\exp(-\frac{N_0}{p_T\eta_0}Tr^\alpha\omega^{-\beta r}),
\end{aligned} \tag{5.22}$$

where step (a) is the PGF of PPP for the NLOS transmitters.

Therefore, the unconditional coverage probability $P_c^N(T)$ of the NLOS case is computed by combining (5.17), (5.18), (5.21) and (5.22) as

$$\begin{aligned}
&P_c^{\mathrm{N}}(T)\\
&=\int_0^{r_D}\left\{\mathbb{P}\left[\frac{p_T h_j L_{\mathrm{R}}(d_{\mathrm{NLOS}_j})}{I_{\mathrm{L}}+I_{\mathrm{N}}+N_0}>T\right]\hat{f}_{\mathrm{N}}(r)^a\middle|0<r\le r_D\right\}\mathrm{d}r \quad +\\
&\quad\int_{r_D}^D\left\{\mathbb{P}\left[\frac{p_T h_j L_{\mathrm{R}}(d_{\mathrm{NLOS}_j})}{I_{\mathrm{N}}+N_0}>T\right]\hat{f}_{\mathrm{N}}(r)^b\middle|r_D<r<D\right\}\mathrm{d}r\\
&=\int_0^{r_D}2\pi\mu r(1-e^{-\beta r})\times e^{-2\pi\mu(\frac{r^2}{2}+\frac{e^{-\beta r}(1+\beta r)-1}{\beta^2})}\times e^{-2\pi\mu(\frac{1-e^{-\beta r_2}(1+\beta r_2)}{\beta^2})}\times\\
&\qquad\exp(-\frac{N_0}{p_T\eta_0}Tr^\alpha\omega^{-\beta r})\times\exp\left(-2\pi\mu\left[\int_{r_2}^D e^{-\beta t}\left[1-\frac{t^\alpha}{t^\alpha+Tr^\alpha\omega^{-\beta r}}\right]t\mathrm{d}t+\right.\right.\\
&\qquad\qquad\left.\left.\int_r^{r_D}(1-e^{-\beta t})\left[1-\frac{t^\alpha}{t^\alpha+Tr^\alpha\omega^{\beta(t-r)}}\right]t\mathrm{d}t\right]\right)\mathrm{d}r\\
&\quad+\int_{r_D}^D 2\pi\mu r(1-e^{-\beta r})\times e^{-2\pi\mu(\frac{r^2}{2}+\frac{e^{-\beta r}(1+\beta r)-1}{\beta^2})}\times\exp(-\frac{N_0}{p_T\eta_0}Tr^\alpha\omega^{-\beta r})\times\\
&\qquad\exp\left(-2\pi\mu\left[\int_r^D(1-e^{-\beta t})\left[1-\frac{t^\alpha}{t^\alpha+Tr^\alpha\omega^{\beta(t-r)}}\right]t\mathrm{d}t\right]\right)\mathrm{d}r.
\end{aligned} \tag{5.23}$$

Table 5.1: Parameters for Numerical Simulations and Analysis in Chapter 5

Parameter	**Value**
maximum link length	20 m
Transmit power	$p_T = 24$ dBm
AWNG power	$N_0 = -95$ dBm
Path loss at reference distance	$\eta_0 = -38.5$ dB
BSs density	$\mu = 0.01$ m^{-2}
Wall density	Random and binary orientation layout: $\lambda = 0.05$ m^{-2} Manhattan grid: $\lambda' = \frac{\lambda L}{2} = \frac{3}{40}$ m^{-2}
Wall Orientation	Random layout: $\psi_k \in [0, \pi)$ Binary orientation layout: $\psi_k \in \{0, \frac{\pi}{2}\}$
Average width of walls	$L = 3$ m
Path-loss exponent	$\alpha = 2$
Simulation times	10^5

5.4 Numerical Evaluation

In this section, I present the numerical results of the downlink coverage probability based on the analytical expressions derived in Section 5.3. The numerical results are obtained for different wall attenuations and are validated using Monte Carlo simulations. The simulations consider three typical layouts of walls, namely random layout, binary orientation layout, and Manhattan grid. The default parameter values used for the simulations are provided in Table 5.1 [4]. Furthermore, I analyze the performance of SCNs with different wall attenuations under various densities of BSs and walls.

Figure 5.1 presents the analytical and simulation results of coverage probability for the random layout of interior walls with different wall attenuations. The curves represent the coverage probabilities of the nearest LOS UAS (5.20), the nearest NLOS UAS (5.23), and the smallest path-loss UAS (5.4), respectively. The analytical results

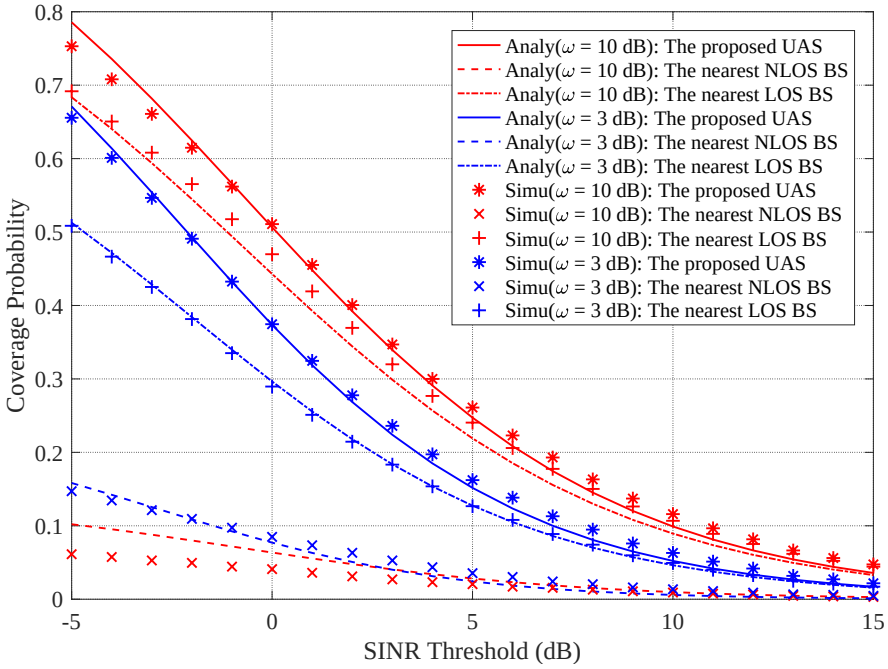

Figure 5.1: The analytical and simulation results under the random layout. The analytical coverage probability for the smallest path-loss LOS BS serving case , the smallest path-loss NLOS BS serving case and the smallest path-loss case UAS is calculated using (5.20), (5.23) and (5.4), respectively.

closely match the simulation results, although a small gap exists between them. This discrepancy can be attributed to the approximation made by replacing the factor of ω^{K_i} with $\omega^{E[K_i]}$ in the derived expressions of coverage probability. By comparing the curves for two different values of wall attenuations (3 and 10 dB), it is observed that a higher wall attenuation leads to a higher coverage probability. This is because a larger wall attenuation reduces inter-cell interference, resulting in improved overall coverage performance of the network. The impact of wall attenuation on coverage probability highlights the importance of carefully considering the wall properties in indoor SCN design and deployment. Additionally, the analysis of different user association strategies (nearest LOS, nearest NLOS, and smallest path-loss UAS) provides valuable insights into the network performance under various scenarios. Overall, the analytical model in this work serves as a powerful tool for understanding and optimizing the coverage probability in indoor SCNs with varying wall attenuations.

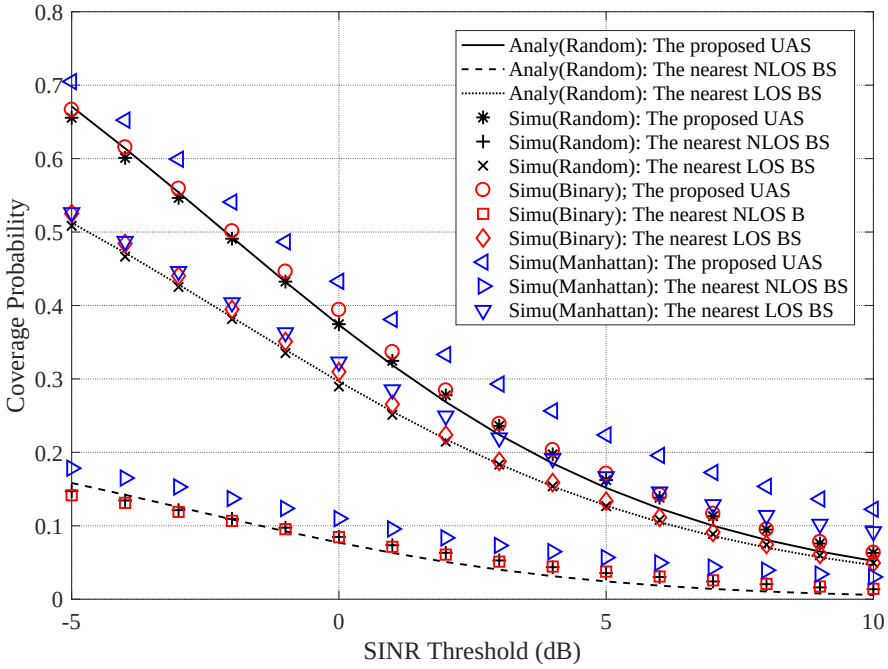

Figure 5.2: The analytical results under the random layout and simulation results under random layout, binary orientation layout and Manhattan grid, for the wall attenuation $\omega = 3\,\text{dB}$.

Figure 5.2 illustrates the analytical and simulation results of coverage probability versus SINR threshold for the random layout of interior walls, as well as the simulation results for the binary orientation layout and Manhattan grid of interior walls. The curves for these three interior wall layouts show small gaps, which are not statistically significant, especially between the random layout and binary orientation layout. This indicates that the choice of interior wall layout does not have a significant impact on the coverage probability under different SINR thresholds. The overall performance of the network remains relatively consistent regardless of the specific arrangement of interior walls. This finding suggests that the proposed analytical model can effectively capture the performance of indoor SCNs for different interior wall layouts, providing valuable insights into network design and optimization.

Figure 5.3 compares the coverage probabilities of the random layout, binary orientation layout, and Manhattan grid. The difference between the random layout and binary ori-

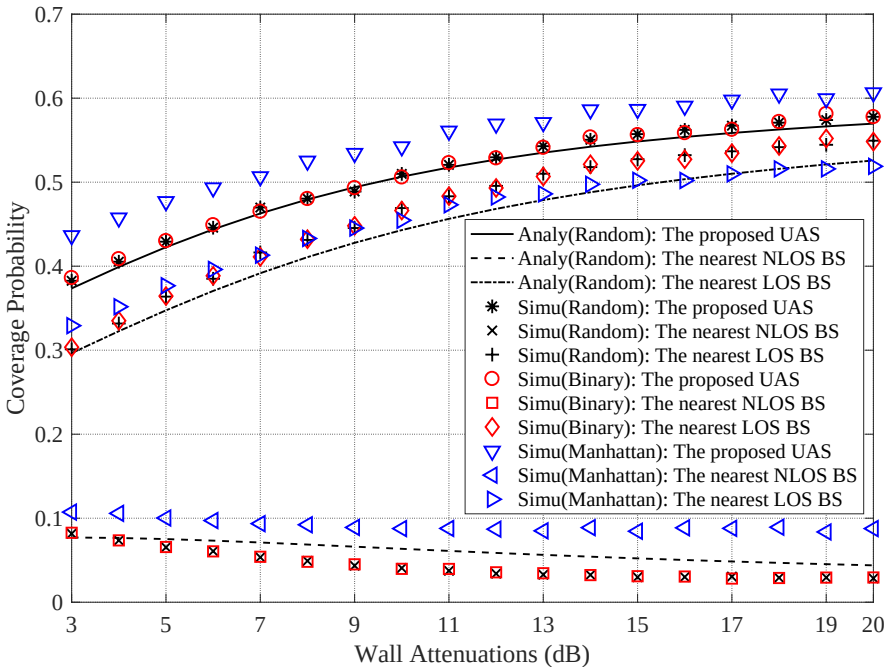

Figure 5.3: The analytical results under the random layout and simulation results under random layout, binary orientation layout and Manhattan grid, for the SINR threshold $T = 0\,\text{dB}$.

entation layout is found to be negligible, indicating that the wall orientation has limited influence on the performance of our proposed SCN model. Furthermore, the simulation results of the Manhattan grid, when compared with the other wall layouts, show similar network performance in terms of coverage probability. These three wall layouts, with corresponding average numbers of interior walls (same average wall volume), result in comparable coverage probabilities. This suggests that the choice of wall layout, as long as it represents a realistic indoor environment, does not significantly impact the overall coverage probability. Notably, the Manhattan grid model is considered a good approximation of practical wall layouts [2]. Therefore, our analytical expression of the coverage probability serves as a tight lower bound for the practical indoor wireless coverage performance.

Figure 5.4 presents the analytical results of coverage probability with different BS densities and wall attenuations (3, 10, and 15 dB). Observing the analytical curves, it is ev-

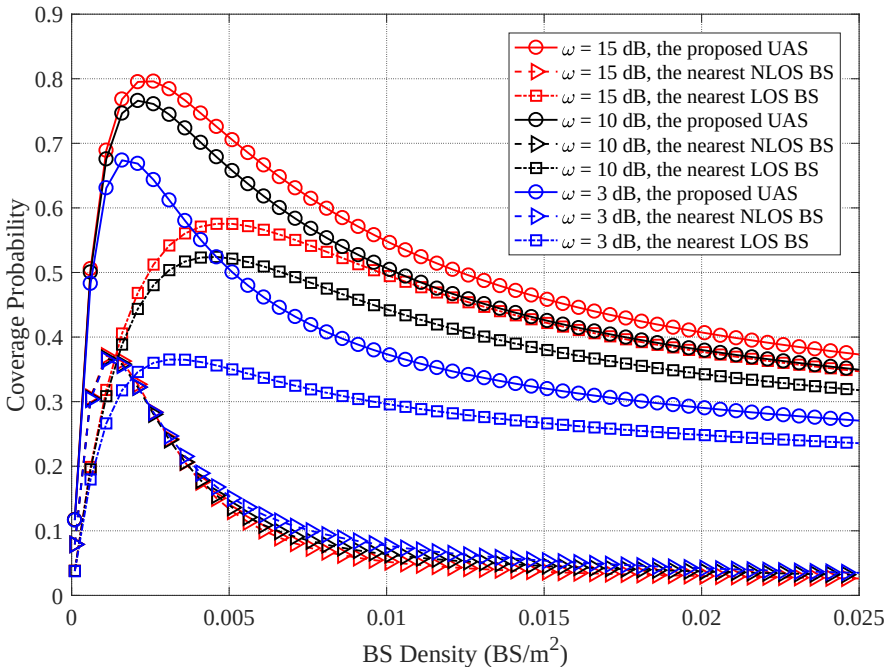

Figure 5.4: The analytical results of coverage probability versus the BS density under the random layout for wall attenuations of 3, 10 and 15 dB and the SINR threshold $T = 0\,\text{dB}$.

ident that the coverage probability of the nearest NLOS UAS initially increases rapidly with the increase in BS density and then declines quickly. In contrast, the coverage probability of the nearest LOS UAS exhibits a smoother variation. This behavior suggests that at low BS densities, the serving BS is predominantly in NLOS conditions. However, as the BS density increases, the LOS BS becomes the dominant serving BS, leading to a smoother increase in coverage probability. Moreover, the results indicate the existence of an optimal BS density that maximizes the coverage probability. The optimal BS density increases with the wall attenuation, indicating that higher wall attenuations benefit from denser BS deployment. Additionally, it is observed that the curves of coverage probability flatten after reaching a sufficiently high density of BSs. This implies that there is a diminishing return in terms of coverage improvement beyond a certain BS density. Furthermore, the analysis of different wall attenuations reveals that larger wall attenuations lead to higher coverage probabilities in dense SCNs. This effect

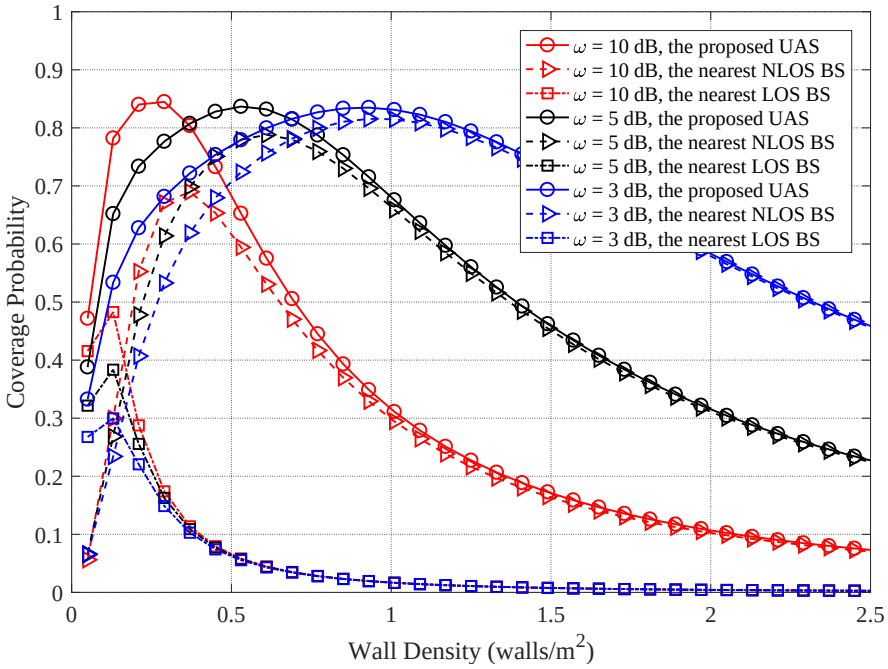

Figure 5.5: The analytical results of coverage probability versus the wall density under the random layout for wall attenuations of 3, 5 and 10 dB and the SINR threshold $T = 0\,\text{dB}$.

can be attributed to the reduction of inter-cell interference with larger wall attenuations, thereby improving the overall coverage probability. These results provide valuable insights into the impact of BS density and wall attenuation on the coverage probability and offer guidance for optimal indoor SCN design and deployment strategies.

Figure 5.5 illustrates the analytical results of coverage probability with different wall densities and wall attenuations (3, 5, and 10 dB). From the curves, it can be observed that the coverage probability for the nearest NLOS BS UAS initially increases with the wall density and then sharply drops after reaching a turning point. This behavior is due to the fact that an appropriate number of walls reduces inter-cell interference, leading to an improvement in coverage probability. However, with a further increase in wall density, the power of both serving and interfering links decreases, resulting in a gradual descent of the coverage probability. In this regime, the coverage probability is mainly affected by the AWGN power, as the power of the serving link is of the same magni-

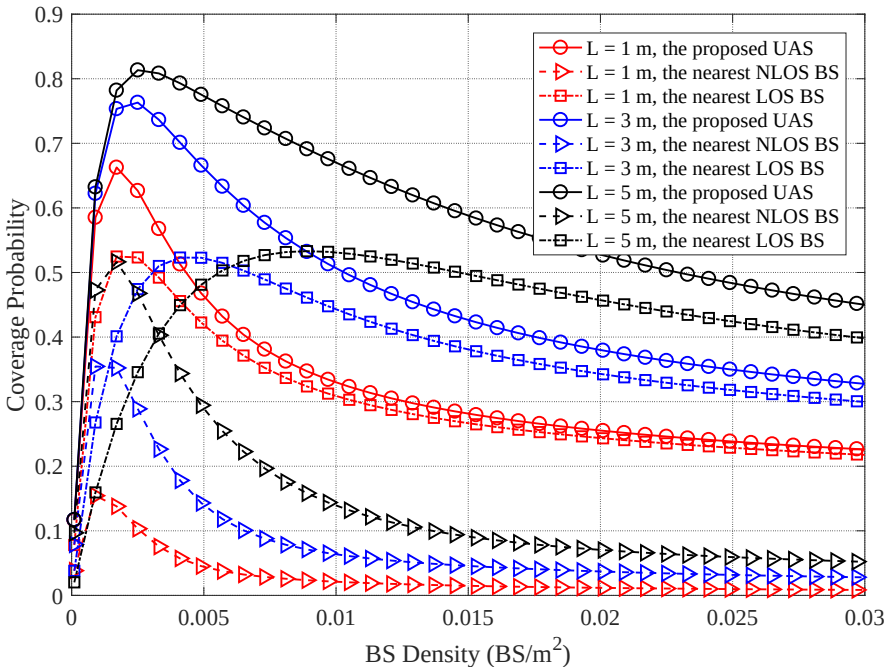

Figure 5.6: The analytical results of coverage probability versus the BS density under the random layout with different average wall length, for the wall attenuation $\omega = 10\,\text{dB}$ and the SINR threshold $T = 0\,\text{dB}$.

tude as the AWGN power. Furthermore, the results reveal the existence of a critical wall density, which corresponds to the wall density that maximizes the coverage probability. This critical wall density decreases with increasing wall attenuation. This means that in scenarios with higher wall attenuations, the optimal wall density for achieving maximum coverage probability is lower. This phenomenon can be attributed to the fact that higher wall attenuations result in stronger attenuation of the interfering links, reducing their impact on the coverage probability. Overall, the results highlight the trade-off between wall density and coverage probability, and the dependence of this trade-off on the wall attenuation. These insights provide valuable guidelines for optimizing indoor SCN performance by carefully selecting the wall density and wall attenuation based on specific deployment scenarios.

Figure 5.6 shows the analytical results of coverage probability versus BS density under the random layout with different average wall lengths (1, 3, and 5 m). The curves

clearly illustrate that the average wall length has a significant influence on the performance of the proposed SCN model. The coverage probability curves initially experience a rapid increase with increasing BS density, indicating improved coverage as more BSs are deployed. However, as the BS density continues to increase, the coverage probability starts to drop, indicating diminishing returns in terms of coverage improvement. Additionally, it is observed that the proportion of LOS/NLOS links in the network is noticeably affected by the average wall length, given a fixed wall density and attenuation. This is because the average wall length directly affects the number of intersecting walls along the links, which in turn affects the LOS probability and the interference levels in the network. Therefore, the choice of average wall length plays a crucial role in determining the coverage probability and the overall performance of the SCN model. The results highlight the trade-off between BS density, average wall length, and coverage probability. A careful selection of these parameters is essential for achieving optimal coverage and network performance in indoor SCN deployments.

Figure 5.7 illustrates the analytical results of the coverage probability versus wall density under the random layout with different average wall lengths (1, 3, and 5 m). The curves demonstrate that the coverage probability experiences a rapid change as the wall density increases, followed by a decline with further increases in the number of interior walls. This behavior can be attributed to the interplay between LOS and NLOS links in the network. Initially, as the wall density increases, the LOS probability decreases, leading to a reduction in the number of LOS links and an increase in the interference levels. Consequently, the coverage probability declines. However, as the wall density continues to increase, the number of intersecting walls along the links also increases. This results in a greater number of NLOS links, which have lower interference levels compared to LOS links. As a result, the coverage probability gradually improves with a denser wall density. It is worth noting that, at a certain point, the NLOS BSs be-

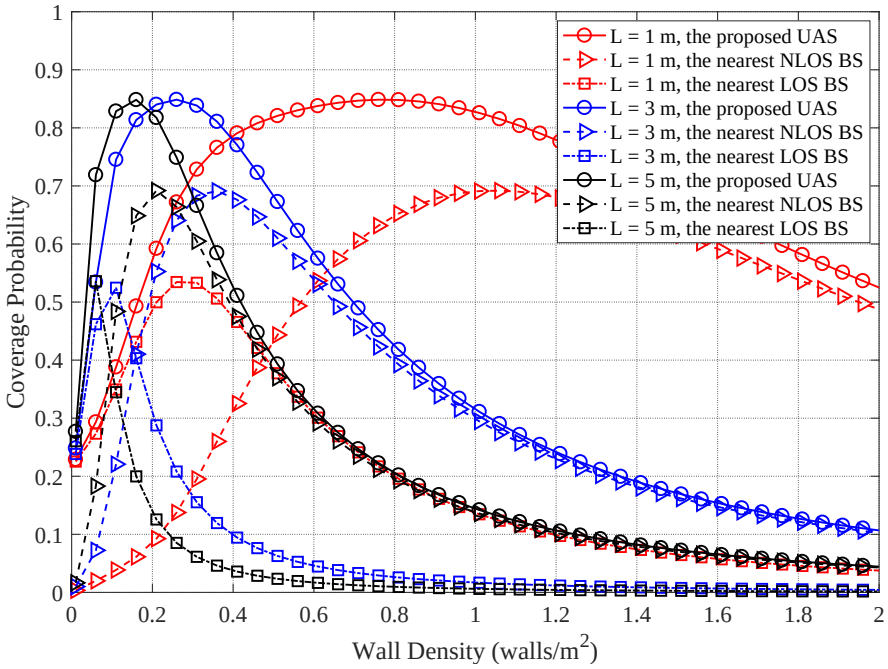

Figure 5.7: The analytical results of coverage probability versus the wall density under the random layout, for with different average wall length, for the wall attenuation $\omega = 10\,\text{dB}$ and the SINR threshold $T = 0\,\text{dB}$.

come the dominant serving BSs in the network due to the high density of interior walls. This transition from LOS to NLOS dominance is reflected in the declining coverage probability. Therefore, the optimal wall density that maximizes the coverage probability lies within the range where LOS and NLOS links coexist. Beyond this range, the dominance of NLOS links leads to a decrease in the coverage probability. These results highlight the importance of carefully selecting the wall density in indoor SCN design to achieve optimal coverage performance. Moreover, the insights gained from this analysis can guide network planners in making informed decisions on the wall density for specific indoor environments and coverage requirements.

5.5 Conclusions

In conclusion, this chapter presents a comprehensive analysis of the performance of indoor small-cell networks considering interior wall penetration losses. The proposed distance-dependent channel model and derived coverage probability expressions provide a solid foundation for evaluating coverage performance under different scenarios, including both LOS and NLOS links. The agreement between analytical and simulation results confirms the accuracy and reliability of the proposed model.

The investigation of different interior wall layouts reveals that the coverage probability is relatively robust to the specific layout as long as the average number of interior walls remains consistent. This finding indicates that the proposed analytical expressions can serve as reliable performance indicators for practical indoor scenarios with various wall arrangements.

Furthermore, the thorough exploration of the impact of BS density and wall density on the coverage probability reveals valuable insights into the design of indoor small-cell networks. The sensitivity of coverage probability to variations in BS density emphasizes the significance of choosing an appropriate density that maximizes coverage performance. Additionally, the non-linear relationship between wall density and coverage probability highlights the complex interplay between LOS and NLOS links and their corresponding interference levels. These findings underscore the critical role of carefully selecting the BS density and wall characteristics in indoor SCN design to achieve optimal coverage performance. The insights gained from this analysis can provide valuable guidance for network planners in making informed decisions on the appropriate BS density and wall characteristics for specific indoor environments and coverage requirements. By leveraging this knowledge, indoor SCN deployments can be optimized to ensure reliable and efficient wireless communication in diverse indoor settings, meeting

the ever-increasing demands for high-data services in modern indoor environments.

Overall, the comprehensive analysis in this chapter significantly contributes to a deeper understanding of the impact of interior wall blockages and wall attenuation on the performance of small-cell networks under the smallest path-loss BS UAS. The derived analytical model provides valuable tools for network planners to make informed decisions and optimize coverage performance in real-world indoor environments. By considering the intricate interplay between interior walls, wall attenuation, and network parameters, the proposed model offers valuable insights into the design and deployment of indoor SCN, leading to improved coverage and network performance in practical scenarios. With the aid of this analytical framework, network planners can efficiently tackle the challenges posed by indoor environments, meeting the growing demands for high-quality and reliable wireless communication services.

Chapter 6

Conclusions and Future Work

In the thesis, the importance of studying stochastic geometry for modelling SCNs is emphasized in the literature review. Stochastic geometry provides a powerful framework for characterizing the randomness and tractability of network deployments, making it a widely adopted approach in both academia and industry.

The literature review highlights the key contributions and advancements in SCN modelling, including the use of stochastic geometry to model the spatial distribution of BSs and users, as well as the modelling of channel characteristics such as path loss, fading, and interference. The review also discusses various mathematical channel models, such as the popular path-loss models, and their applications in SCN analysis.

By leveraging stochastic geometry, researchers are able to capture the spatial distribution of BSs, which is crucial for understanding the network behaviour and performance. This includes analysing key performance metrics such as coverage probability, interference, capacity, and energy efficiency. Stochastic geometry enables the derivation of analytical expressions and provides insights into the fundamental limits and trade-offs of SCNs.

Moreover, the literature review highlights the relevance of mathematical channel models in capturing the propagation characteristics of wireless signals in SCNs. These models take into account factors such as path loss, shadowing, fading, and interference, which play a significant role in determining the network performance. By incorporating these models into the stochastic geometry framework, researchers are able to analyse and optimize the performance of SCNs under various scenarios and deployment configurations.

Overall, the literature review sets the foundation for the thesis by establishing the importance of stochastic geometry and mathematical channel modelling in the study of SCNs. It provides an overview of existing research, identifies gaps and challenges, and motivates the need for further investigation and analysis in the subsequent chapters of the thesis.

6.1 Conclusion

This thesis mainly investigates the effect of the interior wall blockages on the downlink coverage probability of an indoor SCN under the nearest LOS BS UAS, the nearest NLOS BS UAS, and the smallest path-loss UAS. We derive the expressions of PDF with the distance from a typical user to its serving BS, and use the PDF to derive a numerically tractable expression of the downlink coverage probability for the indoor SCN while considering the interior wall penetration losses. Specifically, the indoor small-cell BSs are distributed following an HPPP. The interior walls are modelled by using the random shape theory, where the interior walls are generated as lines on the ground plane with random lengths and orientations, and the centres of interior walls follow a spatial HPPP. The channel model includes the distance-dependent indoor path loss, a LOS probability, Rayleigh fading and interior wall penetration loss.

This thesis focuses on the impact of interior wall blockages on the downlink coverage probability of an indoor SCN under different user association strategies. Specifically, three user association schemes are considered: the nearest LOS BS UAS, the nearest NLOS BS UAS, and the smallest path-loss BS UAS.

To analyse the performance of the indoor SCN, the network is modelled using an HPPP to distribute the small-cell BSs. The interior walls are modelled using the random shape theory, where the walls are represented as lines on the ground plane with random lengths and orientations. The centres of the interior walls follow a spatial HPPP.

The channel model incorporates various factors, including distance-dependent path loss, LOS probability, Rayleigh fading, and interior wall penetration loss. These factors influence the signal propagation and the strength of the received signal at the UE.

To evaluate the downlink coverage probability, the expressions of the PDF of the distance between a typical user and its serving BS are derived. These PDFs are then used to derive numerically tractable expressions for the downlink coverage probability under different user association schemes, accounting for the interior wall penetration losses.

The derived expressions are validated through Monte Carlo simulations, which provide a benchmark for the performance analysis of the indoor SCN. By considering different wall attenuations, BS densities, wall densities, and average wall lengths, the impacts of these parameters on the coverage probability are investigated.

- **Chapter 3**

  An indoor SC network model was proposed, incorporating the effects of blockages and employing the nearest LOS UAS. Using stochastic geometry, an analytical model for the indoor SC network was developed, and the expression for the downlink coverage probability considering interior wall penetration losses was

derived. Monte Carlo simulations were conducted to validate the analytical results and investigate the reasons for any discrepancies between the analytical and simulation results.

The findings of the study highlighted the importance of considering wall attenuation in accurately analysing indoor SC networks. The results showed that the nearest LOS BS connectivity was sensitive to wall attenuation. Furthermore, the analytical results revealed the existence of optimal BS density and wall density values that maximize the coverage probability for different wall attenuations under the nearest LOS BS connectivity. Additionally, the average wall length was found to significantly affect the performance of the proposed SCN model.

The combination of analytical and simulation results provided insights into the behaviour of the indoor SCN model under different scenarios, shedding light on the impact of wall attenuation, BS density, and wall density on coverage probability. These findings can guide the design and optimization of indoor SC networks, leading to improved performance and user experience.

- **Chapter 4**

  An indoor SCN model was developed using stochastic geometry, focusing on the nearest NLOS BS UAS. The model incorporated interior wall penetration losses into the path loss model, considering the effects of wall attenuation. The downlink coverage probability based on the nearest NLOS BS connectivity was derived.

  The results of the study highlighted the significance of wall attenuation in analysing indoor SC networks. It was found that the coverage probability under the nearest NLOS BS UAS was more profoundly influenced by wall attenuation compared to the nearest LOS BS strategy discussed in Chapter 3. Therefore, careful consideration of wall attenuation is necessary when applying the nearest NLOS BS

UAS.

The numerical results revealed that the performance of the nearest NLOS BS UAS was sensitive to the BS density. There existed an optimal BS density that maximized the coverage probability for a given wall density, considering different wall attenuations and average wall lengths.

The findings of this chapter contribute to the understanding of indoor SCN performance under the nearest NLOS BS UAS, shedding light on the impact of wall attenuation and BS density. These insights can aid in the design and optimization of indoor SC networks, improving their coverage and overall performance.

- **Chapter 5**

  A distance-dependent indoor channel model was proposed to account for the differentiation between LOS and NLOS links, as well as the effects of interior wall penetration loss. The downlink coverage probability of an indoor SCN under the smallest path-loss UAS was derived.

  The analytical results obtained from the derived expressions demonstrated a good agreement with the Monte Carlo simulations, validating the accuracy of the analytical model. The simulation results also revealed that, for the same average number of interior walls, the downlink coverage probability of the indoor SCN was nearly identical across three different layouts of interior walls: random layout, binary orientation layout, and Manhattan grid.

  Furthermore, the analytical results provided insights into the behavior of the coverage probability with respect to the BS density. It was observed that the coverage probability exhibited sensitivity to the BS density for low-to-medium densities, and there existed an optimal BS density that maximized the coverage probability. Moreover, for a given BS density, the coverage probability initially increased with the wall density due to reduced inter-cell interference. However, beyond a

certain threshold, the coverage probability started to decline as the SCN became noise-limited with high wall densities.

These findings contribute to a better understanding of the performance characteristics of indoor SCNs and can guide network planning and optimization. The developed analytical framework provides a valuable tool for evaluating the coverage probability and optimizing the deployment of indoor SCNs under the smallest path-loss UAS.

Overall, this thesis focuses on investigating the impact of interior walls on the performance of indoor SCNs. It explores various aspects, such as the spatial distribution of interior walls, the channel model incorporating path loss, fading, and wall penetration losses, and different user association strategies. The thesis also derives the downlink coverage probability as a function of BS density, wall density, and wall penetration loss for different user association scenarios. Through rigorous analysis and simulations, valuable insights into the effects of interior walls on network performance are gained.

The findings of this thesis contribute to the understanding and design of indoor SCNs. By providing accurate analytical expressions and validating them through simulations, the thesis offers valuable tools for network designers and researchers to analyze and optimize indoor wireless communication systems. The insights gained from this work can potentially lead to improved coverage and performance in practical indoor SCN deployments, further advancing the development of wireless communication technologies in urban and indoor environments.

6.2 Future Work

The research conducted in this thesis opens up several potential areas and extensions for future work, which are outlined as follows:

- **Binomial point process:** This thesis focused on the analysis of a typical user located at the centre of the indoor area using HPPP. To provide a more comprehensive evaluation of indoor networks, future work can explore the use of a binomial point process (BPP) instead of HPPP. The BPP can better model finite areas and capture the performance differences of users located at various positions within the building. This will enable a more realistic assessment of indoor SCN performance across the entire indoor environment.

- **Small-scale fading:** While this thesis employed Rayleigh fading to model small-scale fading, future research could consider using Nakagami fading instead. Nakagami fading provides a more flexible fading model that can better capture the characteristics of both LOS and NLOS links, which are prevalent in indoor environments. Moreover, considering the LOS and NLOS links separately in fading models can lead to more accurate results in indoor SCN analysis.

- **Distributions and layouts of walls:** While this thesis considered the random shape theory and HPPP for modelling interior wall blockages, future research can explore other wall distributions and layouts that better represent real-world indoor scenarios. This could involve investigating more exact assumptions for wall distributions, considering specific building layouts, or incorporating architectural floor plans. Different wall layouts may have varying impacts on network performance, and a thorough analysis can provide valuable insights for indoor SCN design and deployment.

- **Material of walls:** The material of walls in indoor environments can have a significant impact on the performance of indoor SCNs. Different materials exhibit varying levels of signal attenuation, reflection, and penetration, which can affect the propagation characteristics of wireless signals. The choice of wall material can also influence the extent of interference between neighbouring cells, as certain materials may reflect or scatter signals, causing interference and degraded network performance. Understanding the effect of wall materials on indoor SCNs is essential for network planning, optimization, and deployment strategies. By considering the specific material properties of walls in the design of indoor SCNs, network engineers can enhance coverage, capacity, and overall network performance, ultimately providing users with reliable and high-quality wireless connectivity in indoor environments.

- **Millimeter-wave communications:** As millimeter-wave (mmWave) frequencies are being explored for indoor wireless communication, future work could extend the proposed indoor SCN model to analyse the performance of indoor mmWave or terahertz networks. This would involve considering the unique propagation characteristics and challenges associated with higher-frequency bands, such as increased susceptibility to blockages and diffraction effects. Understanding the performance of indoor mmWave networks can provide valuable insights into the feasibility and deployment strategies of these emerging technologies.

- **Multi-tier indoor SCN models:** This thesis mainly focused on single-tier indoor SCN models. Future research could explore multi-tier indoor SCN models that incorporate different types of base stations, such as macrocells, small cells, and femtocells. This will allow for a more comprehensive analysis of indoor network performance and the investigation of potential interference management techniques.

- **Energy efficiency and sustainability:** As energy efficiency and sustainability become crucial considerations in wireless communication networks, future work could explore how indoor SCN designs can be optimized to reduce energy consumption and environmental impact. This may involve investigating energy-efficient deployment strategies for small cells, dynamic power management techniques, and renewable energy integration.

By addressing these areas of future research, a more comprehensive understanding of indoor SCN models can be achieved, leading to improved network design, optimization, and performance evaluation in realistic indoor environments. The results and insights obtained from these future investigations will be crucial for the continued development and deployment of indoor wireless communication systems to meet the growing demand for high-data services in urban and indoor settings.

Bibliography

[1] www.cisco.com/c/en/us/solutions/collateral/executive-perspectives/annual-internet-report/white-paper-c11-741490.html.

[2] M. K. Muller, M. Taranetz, and M. Rupp, "Analyzing wireless indoor communications by blockage models," *IEEE Access*, vol. 5, pp. 2172–2186, 2017.

[3] T. Barnett, S. Jain, U. Andra, and T. Khurana, "Cisco visual networking index (vni) complete forecast update, 2017–2022," *Americas/EMEAR CKN Presentation*, 2018.

[4] C. Chen, Y. Zhang, J. Zhang, X. Chu, and J. Zhang, "On the performance of indoor multi-story small-cell networks," *IEEE Trans. Wireless Commun.*, vol. 20, no. 2, pp. 1336–1348, Feb. 2021.

[5] T. Nakamura, S. Nagata, A. Benjebbour, Y. Kishiyama, T. Hai, S. Xiaodong, Y. Ning, and L. Nan, "Trends in small cell enhancements in lte advanced," *IEEE Commun. Mag.*, vol. 51, no. 2, pp. 98–105, 2013.

[6] V. Chandrasekhar, J. G. Andrews, and A. Gatherer, "Femtocell networks: a survey," *IEEE Communications magazine*, vol. 46, no. 9, pp. 59–67, 2008.

[7] J. G. Andrews, S. Buzzi, W. Choi, S. V. Hanly, A. Lozano, A. C. Soong, and J. C. Zhang, "What will 5g be?" *IEEE Journal on selected areas in communications*, vol. 32, no. 6, pp. 1065–1082, 2014.

[8] Huawei, "Five trends to small cell 2020," 2016.

[9] H.-Y. Hsieh, S.-E. Wei, and C.-P. Chien, "Optimizing small cell deployment in arbitrary wireless networks with minimum service rate constraints," *IEEE Transactions on Mobile Computing*, vol. 13, no. 8, pp. 1801–1815, 2013.

[10] K. Pahlavan and A. H. Levesque, *Wireless information networks*. John Wiley & Sons, 2005.

[11] S. Misra, I. Woungang, and S. C. Misra, *Guide to wireless ad hoc networks*. Springer Science & Business Media, 2009.

[12] M. Steinbauer, A. F. Molisch, and E. Bonek, "The double-directional radio channel," *IEEE Antennas and propagation Magazine*, vol. 43, no. 4, pp. 51–63, 2001.

[13] C. A. Balanis, *Advanced engineering electromagnetics*. John Wiley & Sons, 2012.

[14] J. Ling, D. Chizhik, and R. A. Valenzuela, "Predicting multi-element receive & transmit array capacity outdoors with ray tracing," in *IEEE VTS 53rd Vehicular Technology Conference, Spring 2001. Proceedings (Cat. No. 01CH37202)*, vol. 1. IEEE, 2001, pp. 392–394.

[15] A. F. Molisch, "A generic model for mimo wireless propagation channels in macro-and microcells," *IEEE Transactions on Signal Processing*, vol. 52, no. 1, pp. 61–71, 2004.

[16] J. W. Wallace and M. A. Jensen, "Modeling the indoor mimo wireless channel," *IEEE Transactions on Antennas and Propagation*, vol. 50, no. 5, pp. 591–599, 2002.

[17] X. Wang, E. Turgut, and M. C. Gursoy, "Coverage in downlink heterogeneous mmwave cellular networks with user-centric small cell deployment," *IEEE Transactions on Vehicular Technology*, vol. 68, no. 4, pp. 3513–3533, 2019.

[18] G. Miao, J. Zander, K. W. Sung, and S. B. Slimane, *Fundamentals of mobile data networks*. Cambridge University Press, 2016.

[19] A. AlAmmouri, J. G. Andrews, and F. Baccelli, "A unified asymptotic analysis of area spectral efficiency in ultradense cellular networks," *IEEE Transactions on Information Theory*, vol. 65, no. 2, pp. 1236–1248, 2019.

[20] D. P. Kroese, T. J. Brereton, T. Taimre, and Z. I. Botev, "Why the monte carlo method is so important today," *Wiley Interdisciplinary Reviews: Computational Statistics*, vol. 6, 2014.

[21] H. ElSawy, A. Sultan-Salem, M.-S. Alouini, and M. Z. Win, "Modeling and analysis of cellular networks using stochastic geometry: A tutorial," *IEEE Communications Surveys & Tutorials*, vol. 19, no. 1, pp. 167–203, 2016.

[22] D. J. Daley, D. Vere-Jones *et al.*, *An introduction to the theory of point processes: volume I: elementary theory and methods*. Springer, 2003.

[23] J. Zhang and G. De la Roche, *Femtocells: Technologies and Deployment*. John Wiley & Sons, 2011.

[24] T. Q. Duong, X. Chu, and H. A. Suraweera, *Ultra-dense Networks for 5G and Beyond: Modelling, Analysis, and Applications*. John Wiley & Sons, 2019.

[25] C. Forecast, "Cisco visual networking index: Global mobile data traffic forecast update, 2017–2022," *Update*, vol. 2017, pp. 20–22, 2019.

[26] J. G. Andrews, H. Claussen, M. Dohler, S. Rangan, and M. C. Reed, "Femtocells: Past, present, and future," *IEEE Journal on Selected Areas in communications*, vol. 30, no. 3, pp. 497–508, 2012.

[27] J. Hoydis, M. Kobayashi, and M. Debbah, "Green small-cell networks," *IEEE Vehicular Technology Magazine*, vol. 6, no. 1, pp. 37–43, 2011.

[28] M. Win, "A mathematical model for network interference," in *Proc. IEEE Commun. Theory Workshop*, 2007, pp. 99–110.

[29] M. Z. Win, P. C. Pinto, and L. A. Shepp, "A mathematical theory of network interference and its applications," *Proceedings of the IEEE*, vol. 97, no. 2, pp. 205–230, 2009.

[30] M. Haenggi, J. G. Andrews, F. Baccelli, O. Dousse, and M. Franceschetti, "Stochastic geometry and random graphs for the analysis and design of wireless networks," *IEEE journal on selected areas in communications*, vol. 27, no. 7, pp. 1029–1046, 2009.

[31] M. Haenggi, *Stochastic geometry for wireless networks*. Cambridge University Press, 2012.

[32] H. ElSawy, E. Hossain, and M. Haenggi, "Stochastic geometry for modeling, analysis, and design of multi-tier and cognitive cellular wireless networks: A survey," *IEEE Communications Surveys & Tutorials*, vol. 15, no. 3, pp. 996–1019, 2013.

[33] D. Stoyan, W. S. Kendall, S. N. Chiu, and J. Mecke, *Stochastic geometry and its applications*. John Wiley & Sons, 2013.

[34] J. G. Andrews, F. Baccelli, and R. K. Ganti, "A tractable approach to coverage and rate in cellular networks," *IEEE Trans. Wireless Commun.*, vol. 59, no. 11, pp. 3122–3134, Nov. 2011.

[35] F. Baccelli, M. Klein, M. Lebourges, and S. Zuyev, "Stochastic geometry and architecture of communication networks," *Telecommunication Systems*, vol. 7, no. 1, pp. 209–227, 1997.

[36] T. X. Brown, "Cellular performance bounds via shotgun cellular systems," *IEEE Journal on Selected Areas in Communications*, vol. 18, no. 11, pp. 2443–2455, 2000.

[37] A. Guo and M. Haenggi, "Spatial stochastic models and metrics for the structure of base stations in cellular networks," *IEEE Transactions on Wireless Communications*, vol. 12, no. 11, pp. 5800–5812, 2013.

[38] B. Błaszczyszyn, M. K. Karray, and H. P. Keeler, "Using poisson processes to model lattice cellular networks," in *2013 Proceedings IEEE INFOCOM*. IEEE, 2013, pp. 773–781.

[39] M. Di Renzo and P. Guan, "Stochastic geometry modeling of coverage and rate of cellular networks using the gil-pelaez inversion theorem," *IEEE Communications Letters*, vol. 18, no. 9, pp. 1575–1578, 2014.

[40] H. S. Dhillon, R. K. Ganti, F. Baccelli, and J. G. Andrews, "Modeling and analysis of k-tier downlink heterogeneous cellular networks," *IEEE J. Sel. Areas Commun.*, vol. 30, no. 3, pp. 550–560, 2012.

[41] H.-S. Jo, Y. J. Sang, P. Xia, and J. G. Andrews, "Heterogeneous cellular networks with flexible cell association: A comprehensive downlink sinr analysis," *IEEE Trans. Wireless Commun.*, vol. 11, no. 10, pp. 3484–3495, 2012.

[42] H. S. Dhillon, R. K. Ganti, F. Baccelli, and J. G. Andrews, "Coverage and ergodic rate in k-tier downlink heterogeneous cellular networks," in *2011 49th Annual Allerton Conference on Communication, Control, and Computing (Allerton)*. IEEE, 2011, pp. 1627–1632.

[43] M. Di Renzo, A. Guidotti, and G. E. Corazza, "Average rate of downlink heterogeneous cellular networks over generalized fading channels: A stochastic geometry approach," *IEEE Transactions on Communications*, vol. 61, no. 7, pp. 3050–3071, 2013.

[44] H. S. Dhillon and J. G. Andrews, "Downlink rate distribution in heterogeneous cellular networks under generalized cell selection," *IEEE Wireless Communications Letters*, vol. 3, no. 1, pp. 42–45, 2013.

[45] X. Yu, Q. Cui, and M. Haenggi, "Coherent joint transmission in downlink heterogeneous cellular networks," *IEEE Wireless Communications Letters*, vol. 7, no. 2, pp. 274–277, 2017.

[46] J. Zhang and J. G. Andrews, "Distributed antenna systems with randomness," *IEEE Transactions on Wireless Communications*, vol. 7, no. 9, pp. 3636–3646, 2008.

[47] H. S. Dhillon, M. Kountouris, and J. G. Andrews, "Downlink mimo hetnets: Modeling, ordering results and performance analysis," *IEEE Transactions on Wireless Communications*, vol. 12, no. 10, pp. 5208–5222, 2013.

[48] A. K. Gupta, H. S. Dhillon, S. Vishwanath, and J. G. Andrews, "Downlink multi-antenna heterogeneous cellular network with load balancing," *IEEE Transactions on Communications*, vol. 62, no. 11, pp. 4052–4067, 2014.

[49] R. Tanbourgi, H. S. Dhillon, and F. K. Jondral, "Analysis of joint transmit–receive diversity in downlink mimo heterogeneous cellular networks," *IEEE Transactions on Wireless Communications*, vol. 14, no. 12, pp. 6695–6709, 2015.

[50] M. Di Renzo and W. Lu, "Stochastic geometry modeling and performance evaluation of mimo cellular networks using the equivalent-in-distribution (eid)-based approach," *IEEE Transactions on Communications*, vol. 63, no. 3, pp. 977–996, 2015.

[51] A. Adhikary, H. S. Dhillon, and G. Caire, "Massive-mimo meets hetnet: Interference coordination through spatial blanking," *IEEE Journal on Selected Areas in Communications*, vol. 33, no. 6, pp. 1171–1186, 2015.

[52] Q. Zhang, H. H. Yang, T. Q. Quek, and J. Lee, "Heterogeneous cellular networks with los and nlos transmissionsthe role of massive mimo and small cells," *IEEE Transactions on Wireless Communications*, vol. 16, no. 12, pp. 7996–8010, 2017.

[53] T. Bai and R. W. Heath, "Coverage and Rate Analysis for Millimeter-Wave Cellular Networks," *IEEE Trans. Wireless Commun.*, vol. 14, no. 2, pp. 1100–1114, Feb. 2015.

[54] M. Di Renzo, "Stochastic geometry modeling and analysis of multi-tier millimeter wave cellular networks," *IEEE Transactions on Wireless Communications*, vol. 14, no. 9, pp. 5038–5057, 2015.

[55] N. A. Muhammad, P. Wang, Y. Li, and B. Vucetic, "Analytical model for outdoor millimeter wave channels using geometry-based stochastic approach," *IEEE Transactions on Vehicular Technology*, vol. 66, no. 2, pp. 912–926, 2016.

[56] M. Rebato, J. Park, P. Popovski, E. De Carvalho, and M. Zorzi, "Stochastic geometric coverage analysis in mmwave cellular networks with a realistic channel model," in *GLOBECOM 2017-2017 IEEE Global Communications Conference*. IEEE, 2017, pp. 1–6.

[57] C. Chen, J. Zhang, X. Chu, and J. Zhang, "On the optimal base-station height in mmwave small-cell networks considering cylindrical blockage effects," *IEEE Trans. Veh. Technol.*, vol. 70, no. 9, pp. 9588–9592, 2021.

[58] F. Baccelli and A. Giovanidis, "A stochastic geometry framework for analyzing pairwise-cooperative cellular networks," *IEEE Transactions on Wireless Communications*, vol. 14, no. 2, pp. 794–808, 2014.

[59] G. Nigam, P. Minero, and M. Haenggi, "Coordinated multipoint joint transmission in heterogeneous networks," *IEEE Transactions on Communications*, vol. 62, no. 11, pp. 4134–4146, 2014.

[60] ——, "Spatiotemporal cooperation in heterogeneous cellular networks," *IEEE Journal on Selected Areas in Communications*, vol. 33, no. 6, pp. 1253–1265, 2015.

[61] A. Omri and M. O. Hasna, "Modeling and performance analysis of 3-d heterogeneous networks with interference management," *IEEE Communications Letters*, vol. 21, no. 8, pp. 1787–1790, 2017.

[62] J. Yoon and G. Hwang, "Distance-based inter-cell interference coordination in small cell networks: Stochastic geometry modeling and analysis," *IEEE Transactions on Wireless Communications*, vol. 17, no. 6, pp. 4089–4103, 2018.

[63] R. K. Ganti and M. Haenggi, "Spatial analysis of opportunistic downlink relaying in a two-hop cellular system," *IEEE Transactions on Communications*, vol. 60, no. 5, pp. 1443–1450, 2012.

[64] M. Di Renzo and W. Lu, "On the diversity order of selection combining dual-branch dual-hop af relaying in a poisson field of interferers at the destination," *IEEE Transactions on Vehicular Technology*, vol. 64, no. 4, pp. 1620–1628, 2014.

[65] S. Wu, R. Atat, N. Mastronarde, and L. Liu, "Improving the coverage and spectral efficiency of millimeter-wave cellular networks using device-to-device relays," *IEEE Transactions on Communications*, vol. 66, no. 5, pp. 2251–2265, 2017.

[66] K. Belbase, Z. Zhang, H. Jiang, and C. Tellambura, "Coverage analysis of millimeter wave decode-and-forward networks with best relay selection," *IEEE Access*, vol. 6, pp. 22 670–22 683, 2018.

[67] Y. S. Soh, T. Q. Quek, M. Kountouris, and H. Shin, "Energy efficient heterogeneous cellular networks," *IEEE Journal on selected areas in communications*, vol. 31, no. 5, pp. 840–850, 2013.

[68] C. Li, J. Zhang, and K. B. Letaief, "Throughput and energy efficiency analysis of small cell networks with multi-antenna base stations," *IEEE Transactions on Wireless Communications*, vol. 13, no. 5, pp. 2505–2517, 2014.

[69] Z. Chen, L. Qiu, and X. Liang, "Area spectral efficiency analysis and energy consumption minimization in multiantenna poisson distributed networks," *IEEE Transactions on Wireless Communications*, vol. 15, no. 7, pp. 4862–4874, 2016.

[70] H. Jin, X. Wu, H.-s. Kim, and B. C. Jung, "Energy efficiency of ultra-dense small-cell downlink networks with adaptive cell breathing," *IET Communications*, vol. 12, no. 3, pp. 367–372, 2018.

[71] M. Di Renzo, A. Zappone, T. T. Lam, and M. Debbah, "System-level modeling and optimization of the energy efficiency in cellular networksa stochastic geometry framework," *IEEE Transactions on Wireless Communications*, vol. 17, no. 4, pp. 2539–2556, 2018.

[72] H. S. Dhillon, Y. Li, P. Nuggehalli, Z. Pi, and J. G. Andrews, "Fundamentals of heterogeneous cellular networks with energy harvesting," *IEEE Transactions on Wireless Communications*, vol. 13, no. 5, pp. 2782–2797, 2014.

[73] T. A. Khan, P. V. Orlik, K. J. Kim, R. W. Heath, and K. Sawa, "A stochastic geometry analysis of large-scale cooperative wireless networks powered by energy harvesting," *IEEE Transactions on Communications*, vol. 65, no. 8, pp. 3343–3358, 2016.

[74] J. Ye, H. Lei, Y. Liu, G. Pan, D. B. da Costa, Q. Ni, and Z. Ding, "Cooperative communications with wireless energy harvesting over nakagami-*m* fading channels," *IEEE Transactions on Communications*, vol. 65, no. 12, pp. 5149–5164, 2017.

[75] H. S. Dhillon, R. K. Ganti, F. Baccelli, and J. G. Andrews, "Modeling and analysis of k-tier downlink heterogeneous cellular networks," *IEEE Journal on Selected Areas in Communications*, vol. 30, no. 3, pp. 550–560, 2012.

[76] S. Singh, H. S. Dhillon, and J. G. Andrews, "Offloading in heterogeneous networks: Modeling, analysis, and design insights," *IEEE transactions on wireless communications*, vol. 12, no. 5, pp. 2484–2497, 2013.

[77] W. C. Jakes and D. C. Cox, *Microwave mobile communications*. Wiley-IEEE press, 1994.

[78] T. Bai, R. Vaze, and R. W. Heath, "Analysis of blockage effects on urban cellular networks," *IEEE Trans. Wireless Commun.*, vol. 13, no. 9, pp. 5070–5083, Spet. 2014.

[79] M. Di Renzo, "Stochastic geometry modeling and analysis of multi-tier millimeter wave cellular networks," *IEEE Trans. Wireless Commun.*, vol. 14, no. 9, pp. 5038–5057, 2015.

[80] C. Galiotto, N. K. Pratas, N. Marchetti, and L. Doyle, "A stochastic geometry framework for los/nlos propagation in dense small cell networks," in *2015 IEEE International Conference on Communications (ICC)*. IEEE, 2015, pp. 2851–2856.

[81] M. Ding, P. Wang, D. Lpez-Prez, G. Mao, and Z. Lin, "Performance impact of LoS and NLoS transmissions in dense cellular networks," *IEEE Trans. Wireless Commun.*, vol. 15, no. 3, pp. 2365–2380, Mar. 2016.

[82] J. Arnau, I. Atzeni, and M. Kountouris, "Impact of los/nlos propagation and path loss in ultra-dense cellular networks," in *2016 IEEE international conference on communications (ICC)*. IEEE, 2016, pp. 1–6.

[83] I. Atzeni, J. Arnau, and M. Kountouris, "Downlink cellular network analysis with los/nlos propagation and elevated base stations," *IEEE Trans. Wireless Commun.*, vol. 17, no. 1, pp. 142–156, 2018.

[84] M. Ding and D. Lopez-Perez, "Performance impact of base station antenna heights in dense cellular networks," *IEEE Transactions on Wireless Communications*, vol. 16, no. 12, pp. 8147–8161, 2017.

[85] M. Ding, D. Lopez-Perez, G. Mao, and Z. Lin, "Performance impact of idle mode capability on dense small cell networks," *IEEE Transactions on Vehicular Technology*, vol. 66, no. 11, pp. 10 446–10 460, 2017.

[86] Z. Pi and F. Khan, "An introduction to millimeter-wave mobile broadband systems," *IEEE communications magazine*, vol. 49, no. 6, pp. 101–107, 2011.

[87] J. Zhang, Y. Wang, J. Zhang, and L. Ding, "Performance of spatial modulation with constant transmitted power under los and nlos scenarios," in *2015 IEEE International Conference on Communications (ICC)*. IEEE, 2015, pp. 2750–2755.

[88] J. Ikuno, M. Wrulich, and M. Rupp, "3gpp tr 36.814 v9. 0.0-evolved universal terrestrial radio access (e-utra); further advancements for e-utra physical layer aspects," *Tech. Rep.*, pp. 90–103, 2010.

[89] B. Mondal, T. A. Thomas, E. Visotsky, F. W. Vook, A. Ghosh, Y.-H. Nam, Y. Li, J. Zhang, M. Zhang, Q. Luo *et al.*, "3d channel model in 3gpp," *IEEE Communications Magazine*, vol. 53, no. 3, pp. 16–23, 2015.

[90] S. Sun, T. A. Thomas, T. S. Rappaport, H. Nguyen, I. Z. Kovacs, and I. Rodriguez, "Path loss, shadow fading, and line-of-sight probability models for 5g urban macro-cellular scenarios," in *2015 IEEE Globecom Workshops (GC Wkshps)*. IEEE, 2015, pp. 1–7.

[91] R. Mathur, M. Klepal, A. McGibney, and D. Pesch, "Influence of people shadowing on bit error rate of ieee802. 11 2.4 ghz channel," in *1st International Symposium onWireless Communication Systems, 2004.* IEEE, 2004, pp. 448–452.

[92] A. Goldsmith, *Wireless communications*. Cambridge university press, 2005.

[93] J. Salo, L. Vuokko, H. M. El-Sallabi, and P. Vainikainen, "An additive model as a physical basis for shadow fading," *IEEE Transactions on Vehicular Technology*, vol. 56, no. 1, pp. 13–26, 2007.

[94] T. Chrysikos and S. Kotsopoulos, "Characterization of large-scale fading for the 2.4 ghz channel in obstacle-dense indoor propagation topologies," in *2012 IEEE Vehicular Technology Conference (VTC Fall)*. IEEE, 2012, pp. 1–5.

[95] K. R. Schaubach, N. J. Davis, and T. S. Rappaport, "A ray tracing method for predicting path loss and delay spread in microcellular environments," in *[1992 Proceedings] Vehicular Technology Society 42nd VTS Conference-Frontiers of Technology*. IEEE, 1992, pp. 932–935.

[96] K. Rizk, J.-F. Wagen, and F. Gardiol, "Two-dimensional ray-tracing modeling for propagation prediction in microcellular environments," *IEEE Transactions on Vehicular Technology*, vol. 46, no. 2, pp. 508–518, 1997.

[97] K. Haneda, J. Jarvelainen, A. Khatun, and K.-i. Takizawa, "Spatial coexistence of millimeter-wave distributed indoor channels," in *2015 IEEE 81st Vehicular Technology Conference (VTC Spring)*. IEEE, 2015, pp. 1–5.

[98] T. Hashimoto, Y. Nishioka, Y. Inasawa, and H. Miyashita, "Indoor propagation estimation combining statistical models with ray-tracing," in *2015 International Symposium on Antennas and Propagation (ISAP)*. IEEE, 2015, pp. 1–3.

[99] S. R. Lamas, D. Gonzalez, and J. Hamalainen, "Indoor planning optimization of ultra-dense cellular networks at high carrier frequencies," in *2015 IEEE Wireless Communications and Networking Conference Workshops (WCNCW)*. IEEE, 2015, pp. 23–28.

[100] F. Baccelli, B. Blaszczyszyn, S. Geometry, W. Networks, and I. Volume, *Stochastic Geometry and Wireless Networks , Vol. I - Theory*, 2009.

[101] T. Bai, R. Vaze, and R. W. Heath, "Using random shape theory to model blockage in random cellular networks," in *SPCOM*, 2012, pp. 1–5.

[102] J. Lee, X. Zhang, and F. Baccelli, "A 3-D spatial model for in-building wireless networks with correlated shadowing," *IEEE Trans. Wireless Commun.*, vol. 15, no. 11, pp. 7778–7793, Nov. 2016.

[103] W. Yang, J. Zhang, A. A. Glazunov, and J. Zhang, "Line-of-sight probability for channel modeling in 3-d indoor environments," *IEEE Antennas Wirel. Propag. Lett.*, vol. 19, no. 7, pp. 1182–1186, 2020.

[104] L. Zhang, X. Gu, Z. Liu, L. Zhang, and H. Moon, "Modeling and analysis of indoor coverage probability for future 3d dense mobile networks," in *WPMC*, 2017, pp. 247–252.

[105] M. K. Mller, M. Taranetz, and M. Rupp, "Effects of wall-angle distributions in indoor wireless communications," in *SPAWC*, 2016, pp. 1–5.

[106] H. Zheng, J. Zhang, H. Hu, and J. Zhang, "The analysis of indoor wireless communications by a blockage model in ultra-dense networks," in *IEEE VTC-Fall*, 2018, pp. 1–6.

[107] Z. Li, H. Hu, J. Zhang, and J. Zhang, "Impact of wall penetration loss on indoor wireless networks," *IEEE Antennas Wirel. Propag. Lett.*, vol. 20, no. 10, pp. 1888–1892, 2021.

[108] Y. Wang, H. Zheng, and X. Chu, "Impact of wall blockage on los user association strategy in indoor small cell networks," in *IEEE ISAP*, 2020, pp. 579–580.

[109] Y. Wang, H. Zheng, C. Chen, and X. Chu, "The effect of wall blockages on indoor small cell networks with los/nlos user association strategies," in *IEEE VTC-Spring*, 2021, pp. 1–6.

[110] 3rd Generation Partnership Project (3GPP), *Evolved Universal Terrestrial Radio Access (E-UTRA); Further advancements for E-UTRA physical layer aspects*, Mar. 2010, vol. TR 36.814.